INFORMATION TO USERS

This material was produced from a microfilm copy of the original document. While the most advanced technological means to photograph and reproduce this document have been used, the quality is heavily dependent upon the quality of the original submitted.

The following explanation of techniques is provided to help you understand markings or patterns which may appear on this reproduction.

1. The sign or "target" for pages apparently lacking from the document photographed is "Missing Page(s)". If it was possible to obtain the missing page(s) or section, they are spliced into the film along with adjacent pages. This may have necessitated cutting thru an image and duplicating adjacent pages to insure you complete continuity.

2. When an image on the film is obliterated with a large round black mark, it is an indication that the photographer suspected that the copy may have moved during exposure and thus cause a blurred image. You will find a good image of the page in the adjacent frame.

3. When a map, drawing or chart, etc., was part of the material being photographed the photographer followed a definite method in "sectioning" the material. It is customary to begin photoing at the upper left hand corner of a large sheet and to continue photoing from left to right in equal sections with a small overlap. If necessary, sectioning is continued again — beginning below the first row and continuing on until complete.

4. The majority of users indicate that the textual content is of greatest value, however, a somewhat higher quality reproduction could be made from "photographs" if essential to the understanding of the dissertation. Silver prints of "photographs" may be ordered at additional charge by writing the Order Department, giving the catalog number, title, author and specific pages you wish reproduced.

5. PLEASE NOTE: Some pages may have indistinct print. Filmed as received.

Xerox University Microfilms
300 North Zeeb Road
Ann Arbor, Michigan 48106

Downloaded from SHAREOK. Persistent Handle URL: https://hdl.handle.net/11244/3888

75-11,245

FINKE, William Carl, 1932-
A STUDY OF THE DEHYDRATION OF POTASSIUM TRICHLOROCOBALTATE(II) TETRAHYDRATE AND DEHYDRATION OF $[Cr(H_2O)_6]Cl_3$ WITH LIGAND FIELD TREATMENT OF $[Cr(H_2O)_6]Cl_3$ AND trans $[Cr(H_2O)_4Cl_2]Cl$.

The University of Oklahoma, Ph.D., 1974
Chemistry, inorganic

Xerox University Microfilms, Ann Arbor, Michigan 48106

THIS DISSERTATION HAS BEEN MICROFILMED EXACTLY AS RECEIVED.

THE UNIVERSITY OF OKLAHOMA

GRADUATE COLLEGE

A STUDY OF THE DEHYDRATION OF POTASSIUM TRICHLOROCOBALTATE(II) TETRAHYDRATE

and

DEHYDRATION OF $[Cr(H_2O)_6]Cl_3$ WITH LIGAND FIELD TREATMENT OF $[Cr(H_2O)_6]Cl_3$ AND trans $[Cr(H_2O)_4Cl_2]Cl$

A DISSERTATION

SUBMITTED TO THE GRADUATE FACULTY

in partial fulfillment of the requirements for the

degree of

DOCTOR OF PHILOSOPHY

BY

WILLIAM C. FINKE

Norman, Oklahoma

1974

A STUDY OF THE DEHYDRATION OF POTASSIUM TRICHLOROCOBALTATE(II) TETRAHYDRATE

and

DEHYDRATION OF $[Cr(H_2O)_6]Cl_3$ WITH LIGAND FIELD TREATMENT OF $[Cr(H_2O)_6]Cl_3$

AND trans $[Cr(H_2O)_4Cl_2]Cl$

APPROVED BY

Norman Fogel

Bernard O. Heston

Antone L. Lott II

Stanley C. Neely

John W. Renner

DISSERTATION COMMITTEE

ACKNOWLEDGEMENTS

The author wishes to express his gratitude to Dr. Norman Fogel for suggesting the research topic and the many hours of careful guidance during this period of study.

The author is most grateful to Dr. B. O. Heston, Dr. A. L. Lott and fellow graduate students who have made many timely suggestions.

The author wishes to thank Mrs. Betty Rupp for typing the manuscript.

The author wishes to thank the Department of Chemistry, University of Oklahoma, for financial aid and computer time. Also, many thanks are in order for Dr. B. G. Vowell, Chairman of Chemistry Department at Cameron University for obtaining financial assistance and time off from work so this study could be made.

Finally the author wishes to thank his loving wife Velda and three children, Carla, Charles, and Brian for their patience and understanding during the five years of advanced study.

TABLE OF CONTENTS

	Page
LIST OF TABLES	ii
LIST OF FIGURES	iv
PART I A STUDY OF THE DEHYDRATION OF POTASSIUM TRICHLOROCOBALTATE (II) TETRAHYDRATE	1
Chapter	
1. INTRODUCTION	2
2. COMPOUND FORMATION AND ANALYSIS	6
3. DISSOCIATION PRESSURE	9
4. SPECTRA	39
5. MAGNETIC MOMENTS	82
6. RESULTS AND CONCLUSIONS	110
PART II THE DEHYDRATION OF $[Cr(H_2O)_6]Cl_3$ WITH LIGAND FIELD TREATMENT OF $[Cr(H_2O)_2]Cl_3$ AND TRANS $[Cr(H_2O)_4Cl_2]Cl$	117
Chapter	
1. DEHYDRATION OF $[Cr(H_2O)_6]$ WITH LIGAND FIELD TREATMENT OF $[Cr(H_2O_5]Cl_3$ AND TRANS $[Cr(H_2O).Cl_2]Cl$	118
REFERENCES	133

LIST OF TABLES

Table		Page
1.	Compound Analysis	8
2.	Spring Standardization Data	13
3.	"f" Factors of Stable Potassium Trichlorocobaltate(II) Hydrates Complexes	16
4.	Vapor Pressure Data: $KCoCl_3 \cdot 4H_2O_{(s)} = KCoCl_3 \cdot 3H_2O_{(s)} + H_2O_{(g)}$	21
5.	Vapor Pressure Data: $KCoCl_3 \cdot 3H_2O_{(s)} = KCoCl_3 \cdot 2H_2O_{(s)} + H_2O_{(g)}$	22
6.	Vapor Pressure Data: $KCoCl_3 \cdot 2H_2O_{(s)} = KCoCl_3 \cdot H_2O_{(s)} + H_2O_{(g)}$	23
7.	Vapor Pressure Data: $KCoCl_3 \cdot H_2O_{(s)} = KCoCl_{3(s)} + H_2O_{(g)}$	24
8.	Pressure - Temperature Data for Log P vs 1/T $KCoCl_3 \cdot 4H_2O_{(s)} = KCoCl_3 \cdot 3H_2O_{(s)} + H_2O_{(g)}$	30
9.	Pressure - Temperature Data for Log P vs. 1/T $KCoCl_3 \cdot 3H_2O_{(s)} = KCoCl_3 \cdot 2H_2O_{(s)} + H_2O_{(g)}$	31
10.	Pressure - Temperature Data for Log P vs 1/T $KCoCl_3 \cdot 2H_2O_{(s)} = KCoCl_3 \cdot H_2O_{(s)} + H_2O_{(g)}$	32
11.	Pressure - Temperature Data for Log P vs 1/T $KCoCl_3 \cdot H_2O_{(s)} = KCoCl_{3(s)} + H_2O_{(g)}$	33
12.	Thermodynamic Constants from Equilibrium Data at 25°C	34
13.	Calculated Standard Enthalpies and Entropies of Formation	35

Table		Page
14.	The Terms Energies for A d^7 Configuration	43
15.	Energy Difference Between d^7 Terms	44
16.	Effects of $\hat{V}_o$ on the "d" Orbitals	45
17.	Effects of $\hat{V}_t$ on the "d" orbitals	46
18.	Ground State Dependence on the Sign of D_s and Dt	47
19.	Correlation of Oh to Lower Symmetries	48
20.	Values of the Parameters Alpha (α)	51
21.	Wave Functions of Weak Field Terms Arising From F and P Terms of Maximum Multiplicity For d^7 Electron Configuration	54
22.	Non Zero Elements For Secular Determinant in Figure 11	56
23.	Non Zero Elements For The Secular Determinant in Figure 12	58
24.	Collected Spectral Data	77
25.	Spectral Fitting Parameters	81
26.	Magnetic Susceptibility Data	105
27.	Magnetic Data Summary	106
28.	Calculated Magnetic Susceptibilities for $KCoCl_3 \cdot H_2O$	109
29.	Enthalpy and Entropy Values for Reations $KCoCl_3 nH_2O_{(s)} = KCoCl_3 \cdot mH_2O_{(s)} + (n-m)H_2O_{(g)}$ $K_2CoCl_4 \cdot nH_2O_{(s)} = K_2CoCl_4 \cdot mH_2O_{(s)} + (n-m)H_2O_{(g)}$	117
30.	Vapor Pressure Data: $[Cr(H_2O)_6]Cl_{(s)} = [Cr(H_2O)_4Cl_2]Cl_{(s)} + 2H_2O_{(g)}$	125
31.	Pressure-Temperature Data for Log P vs 1/T: $[Cr(H_2O)_6]Cl_{3(s)} = [Cr(H_2O)_4CL_2]Cl_{(s)} + 2H_2O_{(g)}$	126
32.	Collected Spectral Data for $[Cr(H_2O)_6]Cl_3$ and $[Cr(H_2O)_4Cl_2]Cl$	129
33.	Summary of Fitting Parameters For $[Cr(H_2O)_6]Cl_3$ and $[Cr(H_2O)_4Cl_2]Cl$	131

LIST OF FIGURES

Figure		Page
1.	Vapor Pressure Apparatus	12
2.	Spring Extension vs Spring Load	14
3.	Vapor Pressure vis (f) for KCoCl3 $4H_2O_{(s)} = KCoCl_3 \cdot 3H_2O_{(s)}$ $H_2O_{(g)}$ and $KCoCl_3 \cdot 3H_2O_{(s)} = KCoCl_3 \cdot 2H_2O_{(s)} + H_2O_{(g)}$ at 31.2°	18
4.	Vapor Pressue vs (f) For $KCoCl_3 \cdot 2H_2O_{(s)} = KCoCl_3 \cdot H_2O_{(s)} + H_2O_{(g)}$ above 55.4°C	19
5.	Vapor Pressue vs (f) for $KCoCl_3 \cdot 2H_2O_{(s)} = KCoCl_3 \cdot H_2O_{(s)} + H_2O_{(g)}$ at 45°C and $KCoCl_3 \cdot H_2O_{(s)} = KCoCl_{3(s)} + H_2O_{(g)}$ at 70.4°C	20
6.	Log P(atm) vs 1/T (A°) for $KCoCl_3 \cdot 4H_2O_{(s)} = KCoCl_3 \cdot 3H_2O_{(s)} + H_2O_{(g)}$	26
7.	Log P(atm) vs 1/T (A°) for $KCoCl_3 \cdot 3H_2O_{(s)} = KCoCl_3 \cdot 2H_2O_{(s)} + H_2O_{(g)}$	27
8.	Log P(atm) vs 1/T (A°) for $KCoCl_3 \cdot 2H_2O_{(s)} = KCoCl_3 \cdot H_2O_{(s)} + H_2O_{(g)}$	28
9.	Log P(atm) vs 1/T (A°) $KCoCl_3 \cdot H_2O_{(s)} = KCoCl_{3(s)} + H_2O_{(g)}$	29
10.	Effects of Various Perturbations on "d" Orbitals	41
11.	Secular Determinant for High Spin States Under Oh and D_4h Symmetry	55
12.	Secular Determinant for High Spin States Under Oh and D_3d Symmetry	57

Figure Page

13. Attachment Used to Obtain Low Temperature Spectra 63

14. Tanabe-Sugano Diagram for Cr(III) d^3 65

15. Energy Diagram for Tetrahedral d^7 Configuration Sping Allowed with Tetragonal Distortion 66

16. Energy Diagram for Tetrahedral d^7 Configuration Spin Allowed with Trigonal Distortion 69

17. Tanabe-Sugano Diagram For Co(II) d^7 70

18. Crystal Spectrum of $KCoCl_3 \cdot 4H_2O$ 71

19. Reflectance Spectrum of $KCoCl_3 \cdot 4H_2O$ 72

20. Reflectance Spectrum of $KCoCl_3 \cdot 3H_2O$ 73

21. Reflectance Spectrum of $KCoCl_3 \cdot 2H_2O$ 74

22. Reflectance Spectrum of $KCoCl_3 \cdot H_2O$ 75

23. Reflectance Spectrum of $KCoCl_3$ 76

24. Diagram of Faraday - Type Magnetic Balance 91

25. T(°A) vs $1/X_m^c$ for $KCoCl_3 \cdot 4H_2O$ 95

26. T (A°) vs $1/X_m^c$ for $KCoCl_3 \cdot 3H_2O$ 96

27. T (A°) vs $1/X_m^c$ for $KCoCl_3 \cdot 2H_2O$ 97

28. T (A°) vs L/X_m^c for $KCoCl_3 \cdot H_2O$ 98

29. T (A°) vs $1/X_m^c$ for $KCoCl_3$ 99

30. X_m^c vs $\frac{1}{T+}$ for $KCoCl_3 \cdot 4H_2O$ 100

31. X_m^c vs 1/T+ for $KCoCl_3 \cdot 3H_2O$ 101

32. X_m^c vs 1/T+ for $KCoCl_3 2H_2O$ 102

33. X_m^c vs 1/T+ for $KCoCl_3 \cdot H_2O$ 103

34. X_m^c vs 1/T+ for $KCoCl_3$ 104

35. Log P(atm vs $\frac{1}{T}$ (A°)
$[Cr(H_2O)_6]Cl_{3(s)} = [Cr(H_2O)_4Cl_2]\ Cl_{(s)} + 2H_2O_{(g)}$ 124

36. Vapor Pressure vs (f) For
$[Cr(H_2O)_6]Cl_{3(s)} = [Cr(H_2O)_4Cl_2]Cl_{(s)} + 2H_2O_{(g)}$ 127
37. Reflectance Spectra of $[Cr(H_2O)_6]Cl_3$ and $[Cr(H_2O)_4Cl_2]Cl$ . . 128

PART I

A STUDY OF THE DEHYDRATION OF POTASSIUM TRICHLOROCOBALTATE (II) TETRAHYDRATE

A STUDY OF THE DEHYDRATION OF POTASSIUM TRICHLOROCOBALTATE (II) TETRAHYDRATE

CHAPTER I

INTRODUCTION

Purpose

Divalent cobalt forms complexes of various stereochemistry, the most common of which are octahedral and tetrahedral. Cobalt (II) complexes also change configuration from one stereochemistry to the other during reactions. The study of the energies and conditions which accompany these reactions is useful in understanding the causes of these configurational changes. The purpose of this research was to study the configurational changes of potassium trichlorocobaltate (II) tetrahydrate upon dehydration. To accomplish this the research was performed in three separate parts.

The first investigation is the determination of the number, compostion, and stability of the complex hydrates. The number and composition of the complex hydrate species were determined by the step-wise relationship of the dissociation vapor pressure as a function of the sample mass at constant temperature. The stabilities of the complex hydrates were determined by a study of the dissociation pressure as a function of temperature at a constant composition. The stability

measurments were made at a composition where the ratio of the two solid phases is approximately equal. The enthalpy and entropy of the dehydration reactions obtained from these studies will give a clearer understanding of the energies and conditions promoting the changes in configuration.

The second part of the study is the fitting and interpretation of the diffused reflectance spectra of each pure crystalline complex hydrate identified. This was accomplished by using a computer program developed by H. Joy. (1) The program iterates assignments obtained from the experimental specta to obtain the best fit of the complex to a ligand field model. The ligand field parameters used were Dq, B, C, Ds, Dt, or ($D\sigma$ and $D\tau$), and λ, where Dq is the splitting of the "d" orbital degeneracy by the ligand field, B and C are inter-electronic repulsions of the "d" electrons, Ds and Dt or $D\sigma$, and $D\tau$, are perturbations upon the energies of the "d" orbitals due to distortion from the major symmetry, and λ is the spin-orbit coupling perturbation. The program takes into account configuration interaction between terms having the same symmetry and spin values. These parameters will be discussed more fully in Chapter Four.

The third part of the study is the determination of the magnetic moments of each complex hydrate species identified in part one. There is a relationship between the magnitude of the magnetic moment and the stereochemistry of the complex hydrate. Magnetic moments for octahedral Co(II) complexes have higher values than those for tetrahedral complexes. Theoretical aspects for this will be discussed in Chapter Five.

Of additional interest is the comparison of the energies and

conditions accompanying the changes in configuration during dehydration of $KCoCl_3 \cdot 4H_2O$ with those obtained for $CoCl_2 \cdot 6H_2O$ and $K_2CoCl_4 \cdot 2H_2O$ from a previous study of this type. (2,3)

Survey of Previous Work

Complex halides with the general formula, $ACoX_3$, in which A is ammonium or an alkali-metal ion and X is fluoride or chloride ions have been reported by several investigators during the past 47 years. The preparation of these complex halides can be divided into two methods, wet and dry. The dry method usually involves the fusion of the ammonium or alkali-metal halide with the corresponding cobalt(II)halide in an atmosphere of hydrogen chloride or nitrogen. (4,5) H. Seifert (5) prepared $KCoCl_3$ by differential thermal analysis of the $KCl-CoCl_2$ system and found an incongruent melting point. The peritectic was 362°C and eutectic was 351°C. Wet methods were first used by Benrath (6) to prepare trichlorocobaltates of lithium, rubdium, and cesium by a study of the solubility data of cobalt (II) chloride and the alkali-metal chlorides. Hydrated $KCoCl_3$ was prepared by this same method in a later study by Benrath (7) and is the method used in this study. The dihydrate is reported by Benrath, however, a tetrahydrate, trihydrate, and monohydrate are identified in this study.

The magnetic susceptibilities of $KCoF_3$(8) and $CsCoCl_3$ (9) have been measured. Both are in the range (4.80-5.20 B.M.) expected for octahedral complexes. In both studies the complexes become antiferromagnetic at low temperatures.

The absorption spectra of $KCoF_3$ was interpretated by Ferguson et. al. (10) using the four parameter crystal field theory. A Dq value of 770cm^{-1} places it well within the range of octahedrally coordinated complexes. The absorption spectra of $CsCoCl_3$ and $RbCoCl_3$ were both interpretated by Gilmore (11) as distorted octahedral molecules using crystal field treatment. Gilmore used the dry method to prepare the crystalline samples of $CsCoCl_3$ and $RbCoCl_3$ for spectra determination.

The crystal structures of $KCoF_3$, $CsCoCl_3$, and $RbCoCl_3$ have been determined by X-ray crystallography to be octahedrally coordinated. (12,13,9) The crystal structure of the dihydrate of $CsCoCl_3$ had been determined by Thorup (14) to be a distorted octahedron. The Co (II) ion is octahedrally surrounded with Cl ions and water molecules with the two water molecules cis to each other.

Little information is found in the literature about $KCoCl_3$ hydrates except the basic work performed by Benrath. (7) A study of the configurational changes occurring during dehydration of trichlorocobaltate (II) hydrates have not been undertaken. This study will therefore add new information to the chemistry of trichlorocobaltates.

CHAPTER II

COMPOUND FORMATION AND ANALYSIS

Compound Formation

Potassium trichlorocobaltate (II) has been prepared by Seifert (5) by differential thermal analysis of the KCl-$CoCl_2$ system. Benrath (7) has reported that potassium trichlorocobalt (II) dihydrate can be prepared from the KCl-$CoCl_2$-H_2O system between 40°-50°C. This latter method was used in this study.

Six tenths (0.6) mole of hexaaquocobal (II) chloride (Analytical Grade) and four tenths (0.4) mole of potassium chloride (Analytical Grade) were dissolved in a minimum amount of distilled water. The resulting solution was placed in a covered 50 x 300 mm test tube and suspended in a constant temperature water bath at 44°C. After 10 to 14 days, large, violet crystalline plates were formed which deliquesced upon exposure to the atmosphere.

Dehydration of a sample of this violet crystalline complex in a drying oven indicated, by mass loss, that four moles of water was lost. The color changed from the violet of the tetrahydrate to a light blue for the anhydrous sample. Next a sample of the anhydrous complex was placed in a desiccator over wet calcium nitrate reforming the violet colored tetrahydrate. The absorption spectra and magnetic moment data

of the crystalline tetrahydrate and the powdered tetrahydrate sample formed over wet calcium nitrate indicated the two samples were the same within experimental error and there were no changes in the two forms.

A sample of the tetrahydrate was placed in an evacuated system equipped with a calibrated quartz spring. The water vapor removed by evacuating the system was collected in a cold trap and tested for chloride ion giving a negative test. A negative test indicated that the dehydration of the tetrahydrate was the only reaction occurring.

Analysis

Since the potassium trichlorocobaltate (II) tetrahydrate loses only water of hydration and only the anhydrous salt is the final product, analysis for the elements were performed on the anhydrous salt. The complex hydrate was placed in a drying oven at 120°C for 24 hours. Cobalt analysis was carried out by weighing a 0.5 gram sample of the dried complex salt and dissolving it in a 500 ml volumetric flask. Fifty (50) milliliter aliquots of the dilute solution were then taken for the final analysis. The aliquots were treated with pH 6 buffer, murexide indicator, and titrated directly with 0.01 N standardized EDTA solution to the first appearance of the purple end-point. (15)

Chloride analysis was performed by standard gravimetric procedures. (16) Due to the pink color of the cobalt solution, precipitation titration methods were rendered ineffective for chloride analysis.

The potassium concentration was found by difference. The concentration of the water in the hydrates were determined by dehydrating a

sample of the tetrahydrate to dryness in a tube described on page 12, Chapter Three. The mass of the sample was measured by changes in the extension of a calibrated quartz spring by use of a cathetometer. The water concentration was found from the mass loss for each identified hydrate species and the initial sample weight.

All analysis were performed in triplicate on two different samples of potassium trichlorocobaltate (II) prepared by the described method. The results of the elemental analysis are given in Table 1.

TABLE 1

COMPOUND ANALYSIS

Compound	K		Co		Cl		H_2O	
	Theo.	Exp.	Theo.	Exp.	Theo.	Exp.	Theo.	Exp.
$KCoCl_3$	19.13	19.30	28.83	28.88	52.04	51.78		
$KCoCl_3 \cdot 4H_2O$							35.23	35.30
$KCoCl_3 \cdot 3H_2O$							26.42	25.88
$KCoCl_3 \cdot 2H_2O$							17.61	17.52
$KCoCl_3 \cdot H_2O$							8.81	8.57

CHAPTER 3

DISSOCIATION VAPOR PRESSURE

Discussion

The dehydration study of $KCoCl_3 \cdot 4H_2O$ was carried out by placing a weighed sample in a vacuum system and the water vapor removed slowly by evacuation. The final product of this controlled evacuation was $KCoCl_3$.

The number and compostion of the stable potassium trichlorocobaltate (II) hydrate complexes were determined from a study of the equilibrium vapor pressure of the system as a function of the composition. The behavior of the system is described by the phase rule, F=C-P+2, where F is the number of degrees of freedom, C is the number of components, and P is the number of phases. The degrees of freedom of a two component system ($KCoCl_3$ and H_2O) and three phases (two solids and one gas) is one. By fixing the temperature, a constant vapor pressure occurs when both solid species are present corresponding to the reaction of a higher hydrate to the next lower complex hydrate. The generalized equation for the species studied here would be:

$$KCoCl_3 \cdot nH_2O_{(s)} = KCoCl_3 \cdot mH_2O_{(s)} + (n-m)nH_2O_{(g)} \qquad (1)$$

where "n" is 4,3,2,1, and "m" is 3,2,1,0.

The equilibrium constant for the above reaction is

$$K_{eq} = \frac{[KCoCl_3 \cdot nH_2O]\ P_{H_2O}^{(n-m)}}{[KCoCl_3 \cdot (m)H_2O]} \qquad (2)$$

Both of the complex hydrates are solids and are at unit activity, therefore, the equilibrium constant is a function of the equilibrium vapor pressure alone. This can be expressed by

$$K_{eq} = K_p = P_{H_2O}^{(n-m)} \qquad (3)$$

where P is the equilibrium vapor pressure in atmospheres.

The thermodynamic values for the formation of each hydrate species was found by measuring the equilibrium vapor pressure versus the temperature.

Experimental

The equilibrium vapor pressures were measured with an apparatus previously descibed by Fogel and Lewis (17) with modifications shown in Figure 1.

A weighed sample of the tetrahydrate was suspended from a quartz spring (A) [having a total load capacity of one gram and a total extension of ten (10) centimeters] in a glass bucket (B) inside a sealed glass chamber (C). The extension of the quartz spring varies linearly with the load permitting the mass of the sample inside the tube to be measured directly from outside using a cathetometer. The quartz spring had been previously calibrated by loading the glass bucket with standard weights (Class S, National Bureau of Standards) and measuring the extension using the cathetometer. Five (5) different loads and extensions

were measured and plotted. The data for this standarization is given in Table 2 and the graph of mass versus extension is given in Figure 2. The slope of the line through these data points gave the force constant of the quartz spring. The quartz spring used in this study has a force constant of 0.6657 grams per centimeter of extension. The system contained a mercury manometer (D) for measuring the equilibrium vapor pressure and a Teflon stopcock (E) for evacuation of the system.

For temperature measurements between 30° and 50°C, the sample chamber of the apparatus was submerged in a constant temperature water bath so that the sample bucket was below the level of the water. A long fiber hook between the quartz spring and the sample bucket permitted the extension to be measured without interference from the liquid in the bath. For temperature studies above 50°C an oil bath was used.

The temperature of both bath's was regulated by an electric resistance heater and a bimetallic sensor connected through an electronic relay. The water bath was stirred with a small circulating pump and the oil bath was stirred with a stirring motor equipped with a screw-type propeller.

The temperature of the bath was several degrees above the ambient temperature, therefore, considerable amounts of water was last to the surroundings by evaporation. The water level was maintained by a reservior and siphon system. In this way the temperature could be maintained to approximately ± 0.1°C.

Using the apparatus described in Figure 1, the temperature and composition of the hydrates could be controlled. By evacuating the system, water vapor was evaporated and removed with a vacuum pump. When

FIGURE 1

VAPOR PRESSURE APPARATUS

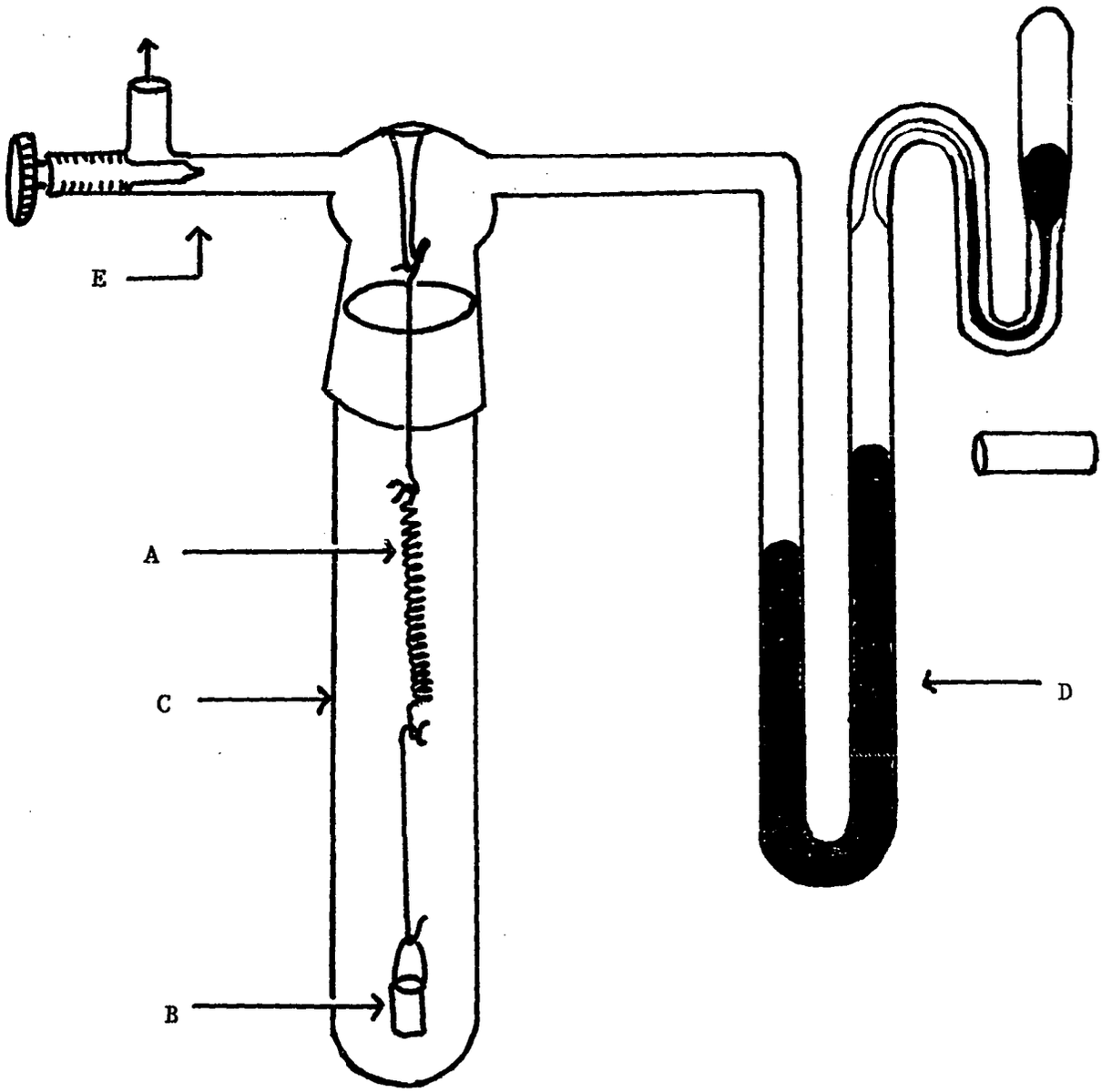

TABLE 2

SPRING STANDARDIZATION DATA

Mass (grams)	X_d (cm)	ΔX_d (cm)	Mass/ X_d (g/cm)
1. no load	3.115	0	0
2. .4135	9.345	6.230	.06637
3. .5130	10.905	7.790	.06585
4. .6129	12.345	9.230	.06640
5. .7135	13.810	10.695	.06671
6. .9239	16.800	13.685	.06751
			Ave. 0.06657

Mass of Sample = X_d(0.06657 g/cm) - mass intercept -(mass of bucket + fibers)

FIGURE 2 -

SPRING EXTENSION VERSUS SPRING LOAD

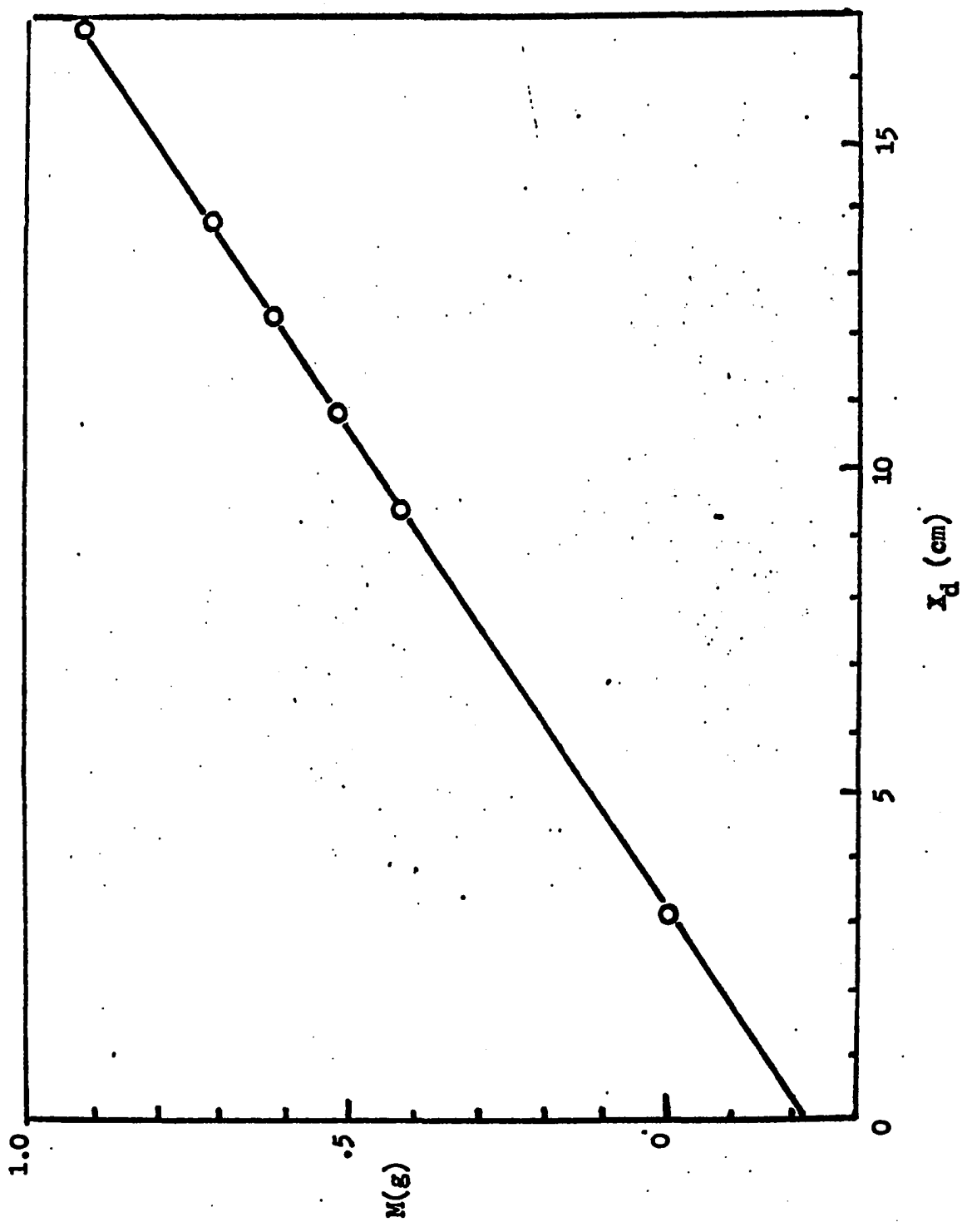

the desired amount was removed the evacuating was stopped and the system was allowed to re-equilibrate. In this way the pressure and composition of each of the hydrates could be studied. At constant composition, the temperature could be varied permitting the pressure-temperature relationships to be studied. The composition chosen was the mid-point of each plateau where equal amounts of the two solid phases exist.

Experimental Results

The pressure as a function of composition of the complex hydrates was studied by placing a sample in the system and evacuating with a vacuum pump until all the air in the system was removed. A constant temperature, (31.2°C), was maintained while the vapor pressure of the tetrahydrate was equilibrating. After several hours, a constant equilibrium vapor pressure was reached as indicated by a constant manometer reading. The system was evacuated again removing the accumulated pressure and again allowed to re-equilibrate, as indicated by the same constant pressure reading. The equilibrium pressure remained constant until the trihydrate was reached, then a slight drop in pressure was observed. After obtaining a hydrate composition equal to that of the dihydrate, the pressure dropped to such a low reading, that the temperature was raised to 45°C. At 45°C, a constant pressure plateau was again obtained until the composition of the monohydrate was reached. At this composition the pressure dropped to a very low reading and the temperature was raised to 70°C. This temperature was impossible to maintain with a water bath due to the large heat loss to the surroundings,

therefore, the apparatus was transferred to an oil bath. A constant pressure was again obtained until the composition of pure $KCoCl_3$ was reached, when the pressure dropped to zero.

The pressure versus composition analysis is shown in Figures 3-5. The plot of the pressure versus composition where the composition is expressed as a factor "f" which is the ratio of the sample weight to the anhydrous $KCoCl_3$ sample weight. The value of "f" for each hydrate species is shown in Table 3.

TABLE 3

"f" FACTORS OF STABLE POTASSIUM TRICHLOROCOBALTATE(II) HYDRATE COMPLEXES

Compound	*f Values
$KCoCl_3 \cdot 4H_2O$	1.352
$KCoCl_3 \cdot 3H_2O$	1.264
$KCoCl_3 \cdot 2H_2O$	1.176
$KCoCl_3 \cdot H_2O$	1.088
$KCoCl_3$	1.000

*f = Sample Weight/Anhydrous $KCoCl_3$ Weight

The equilibrium vapor pressures for each of the temperatures studied are given in Tables 4-7.

On the flat portion of the curves, an equilibrium exists between the two solid species, i.e. $KCoCl_3 \cdot nH_2O$ and $KCoCl_3 \cdot (n-1)H_2O$,

making two solid phases while the water vapor constitutes the third phase. The two components are $KCoCl_3$ and H_2O. According to the phase rule, one degree of freedom exists which is the temperature. By fixing the temperature, the system can be described by the constant equilibrium vapor pressure.

Where "f" is equal to one of the complex hydrate species, only two phases exist, (one solid and a gas) and the system becomes bivariant. The system can no longer be described by its vapor pressure alone. This condition was also found to exist for the dehydration of the dihydrate above 55.4°C as noted by the plot in Figure 4, page 19. The one solid phase which exist above 55.4°C is a solution of the two hydrates and is therefore represented as a solid solution.

The pressure-temperature data was taken at the mid-point of the equilibrium plateau region where the concentration of each of the two species was approximately equal. The temperature of the water bath was raised and a new equilibrium was established. The pressure was noted at this higher temperature and this procedure was repeated for a 10° to 20° range or until the pressure reached 25.75 mm Hg. [The maximum pressure that can be studied with an exposed manometer is the equilibrium vapor pressure of water at room temperature.] The temperature of the water bath was then lowered to each of the same temperatures previously studied. In this way the equilibrium was approached from both directions and the attainment of the same pressure indicated that a true equilibrium was obtained.

The thermodynamic expression used for the pressure-temperature study was derived from the following equations:

FIGURE 3

$KCoCl_3 \cdot 4H_2O(s) = KCoCl_3 \cdot 3H_2O(s) + H_2O(g)$

$KCoCl_3 \cdot 3H_2O(s) = KCoCl_3 \cdot 2H_2O(s) + H_2O(g)$

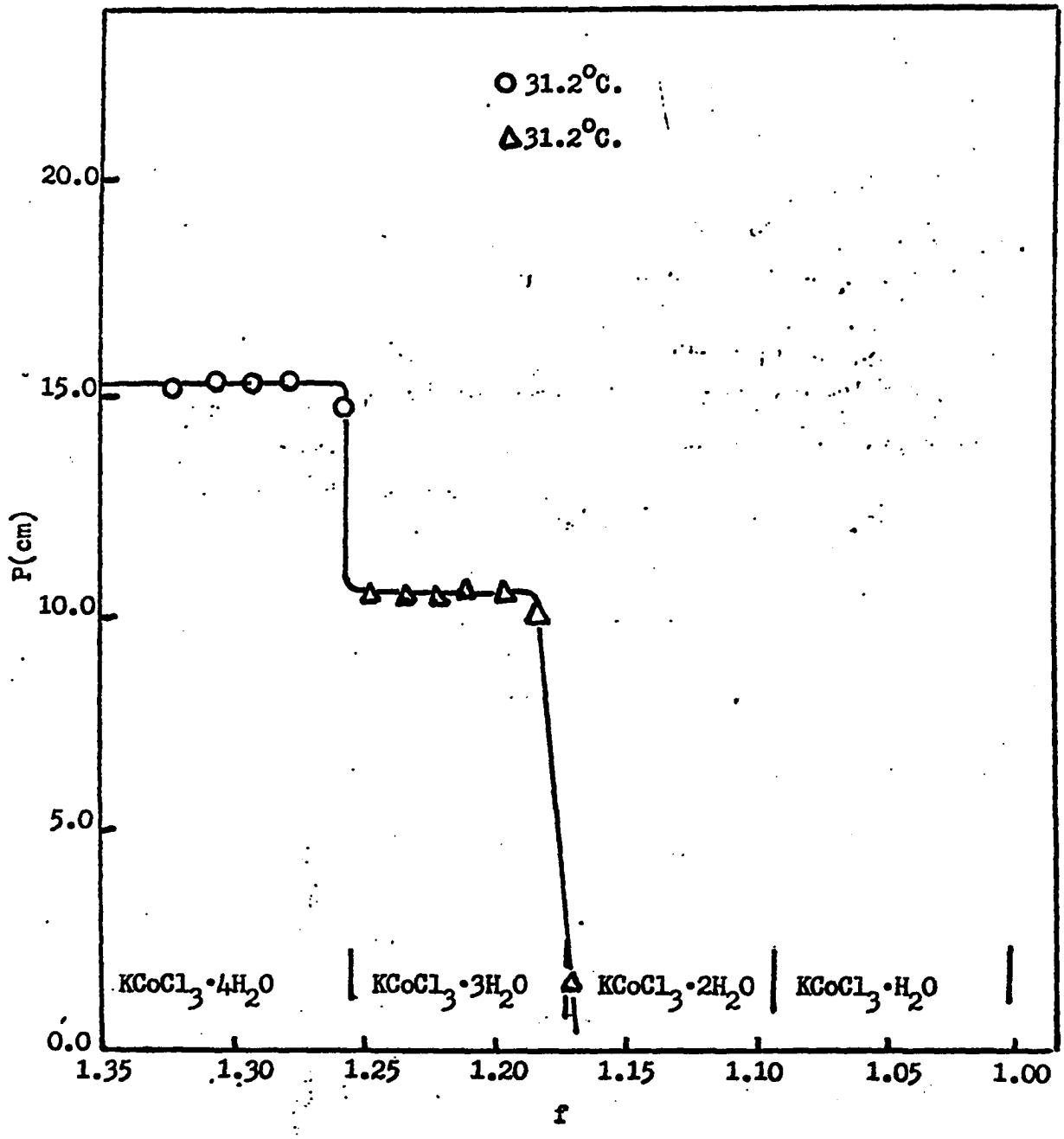

FIGURE 4

$KCoCl_3 \cdot 2H_2O_{(s)} = KCoCl_3 \cdot H_2O_{(s)} + H_2O_{(g)}$

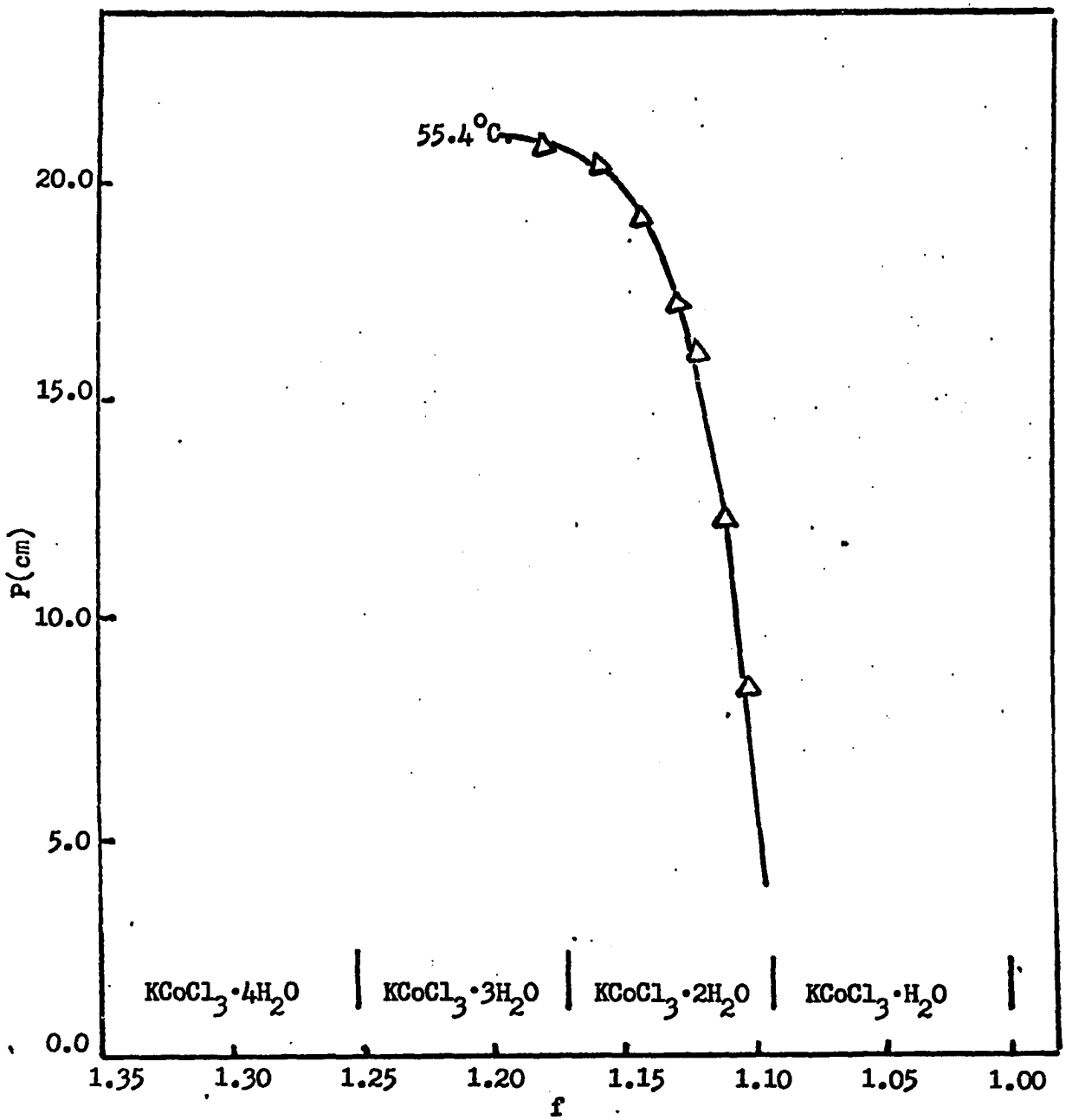

FIGURE 5

$KCoCl_3 \cdot 2H_2O(s) = KCoCl_3 \cdot H_2O(s) + H_2O(g)$

$KCoCl_3 \cdot H_2O(s) = KCoCl_3(s) + H_2O(g)$

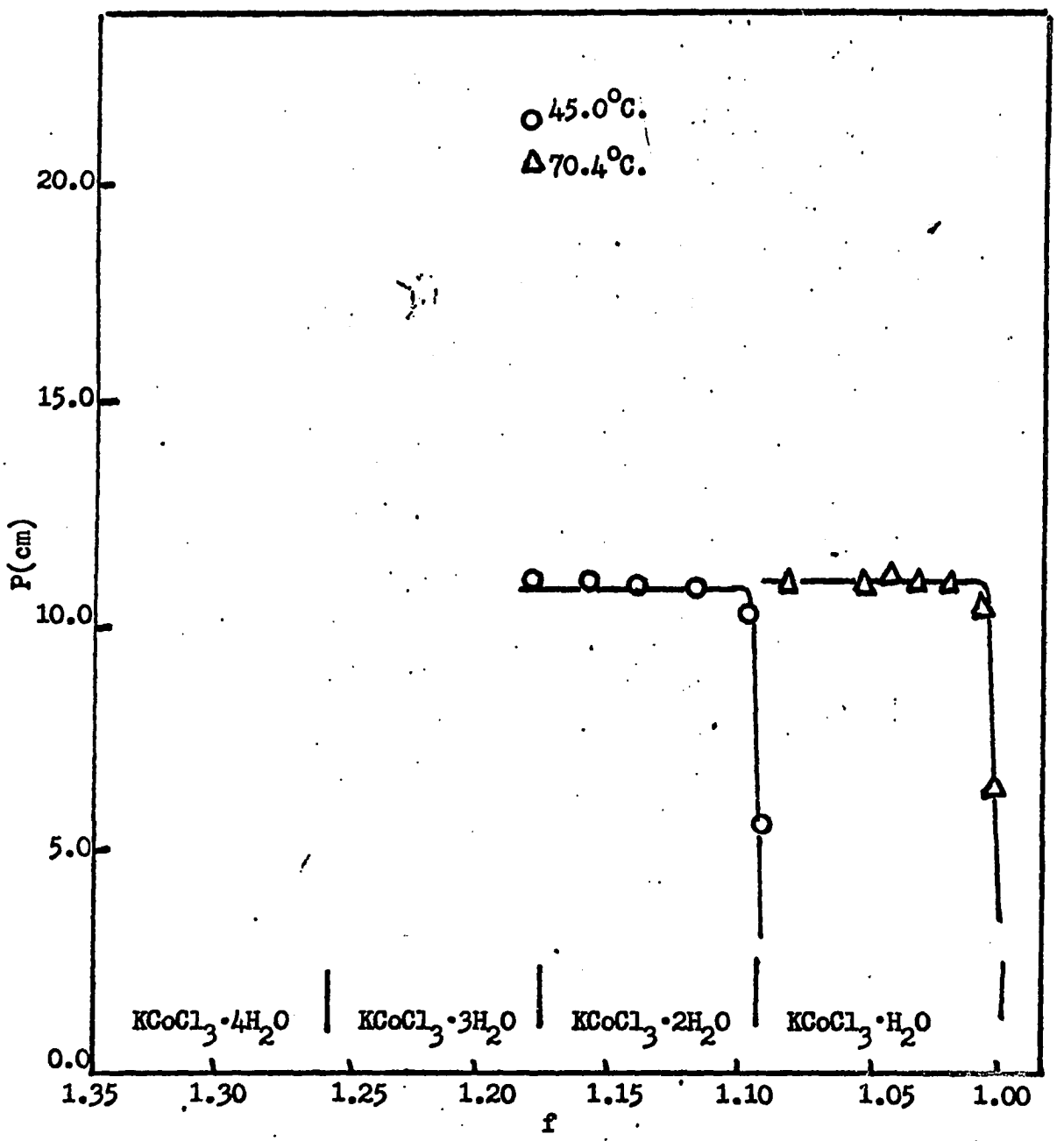

TABLE 4

VAPOR PRESSURE DATA

$KCoCl_3 \cdot 4H_2O_{(s)} = KCoCl_3 \cdot 3H_2O_{(s)} + H_2O_{(g)}$

T°C	P(mm)	f
31.2	15.10	1.327
	15.15	1.306
	15.15	1.281
	15.10	1.272
	14.90	1.261

TABLE 5

VAPOR PRESSURE DATA

$$KCoCl_3 \cdot 3H_2O_{(s)} = KCoCl_3 \cdot 2H_2O_{(s)} + H_2O_{(g)}$$

T°C	P(mm)	f
31.2	11.70	1.257
	11.70	1.246
	11.60	1.230
	11.50	1.218
	11.60	1.198
	11.55	1.190
	11.60	1.183
	10.90	1.179
	1.65	1.176

TABLE 6

VAPOR PRESSURE DATA

$KCoCl_3 \cdot 2H_2O_{(s)} = KCoCl_3 \cdot H_2O_{(s)} + H_2O_{(g)}$

T^oC	P(mm)	f	T^oC	P(mm)	f
45.0	11.80	1.146	55.4	21.30	1.176
	11.80	1.134		20.50	1.143
	11.70	1.126		18.95	1.130
	11.70	1.100		16.90	1.120
	10.20	1.098		16.00	1.110
	6.20	1.091		12.10	1.098
				8.35	1.093

TABLE 7

VAPOR PRESSURE DATA

$$KCoCl_3 \cdot H_2O_{(s)} = KCoCl_{3(s)} + H_2O_{(g)}$$

T°C	P(mm)	f
70.4	12.80	1.074
	12.80	1.058
	12.85	1.044
	12.80	1.033
	12.80	1.025
	11.90	1.016
	6.40	1.001
	0.00	1.000

$$\Delta G^{o} = -2.303RT \log K_{eq} = \Delta H^{o} - T\Delta S^{o} \quad (4)$$

The equilibrium vapor pressure, $P_{H_2O}^{(n-m)}$, is equal to the equilibrium constant. Making this substitution and rearranging equation (4) to give

$$\log P_{H_2O}^{(n-m)} = -\Delta H°/2.303\ (n-m)RT + \Delta S°/2.303\ (n-m)R \quad (5)$$

where P is the experimental equilibrium vapor pressure in atmospheres, ΔH^{o} is the standard enthalpy of reaction in calories $mole^{-1}$, ΔS^{o} is the standard entropy of reaction in entropy units $mole^{-1}$, and (n-m) is the number of moles of water lost. The enthalpy and entropy of reaction can be calculated from the best fit of the logarithm of the equilibrium vapor pressure as an inverse function of the absolute temperature. The linearity of the plots are indicated in Figures 6-9 for the temperature changes of approximately 20°. The linearity of these plots indicate ΔC_p is relatively small and the enthalpy and entropy can be considered to be constant over a temperature range of 10 to 20° degrees. The pressure-temperature data was treated with a least square analysis. Tables 8-11 show the data obtained from these studies.

The thermodynamic constants for the dehydration reactions are given in Table 12.

Once the thermodynamic constants for each dehydration step are obtained the standard enthalpies of formation for each hydrate can be calculated by using the standard enthalpy for the formation of solid $KCoCl_3$, -1.6 kcal $mole^{-1}$ (18) and that for the formation of water vapor, -57.8 kcal $mole^{-1}$. (19) This calculation is made by use of the equation

$$\Delta H_f^{o}\ KCoCl_3 \cdot nH_2O_{(s)} = \Delta H_f^{o}\ KCoCl_3 \cdot mH_2O_{(s)} + (n-m)\Delta H_f^{o}\ H_2O_{(v)} - \Delta H_r^{o} \quad (6)$$

where ΔH_r^{o} is the energy of the dehydration for reation (1).

FIGURE 6

Log P(Atm) vs 1/T(A°)

$KCoCl_3 \cdot 4H_2O_{(s)} = KCoCl_3 \cdot 3H_2O_{(s)} + H_2O_{(g)}$

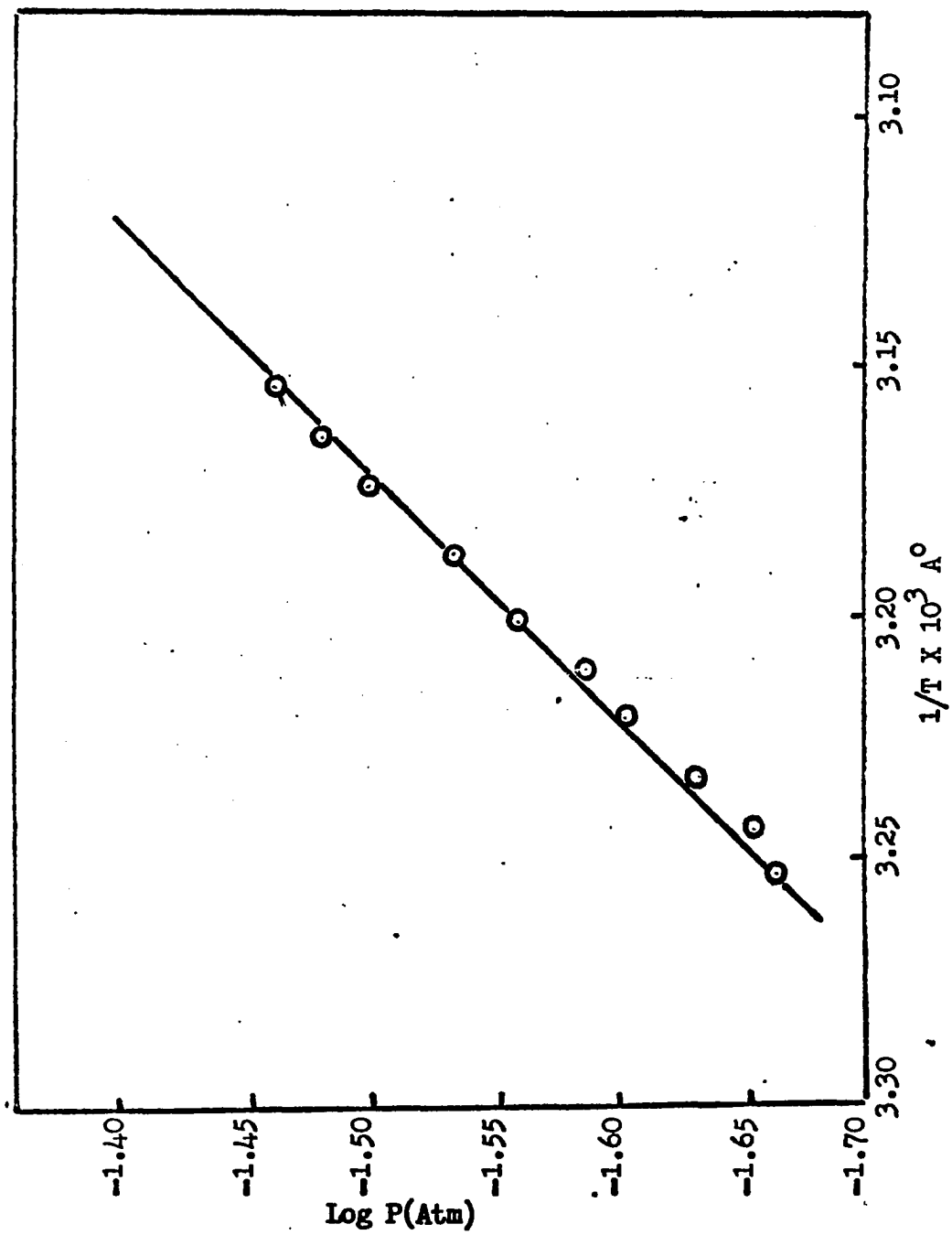

FIGURE 7

Log P(Atm) vs $1/T(A^{\circ})$

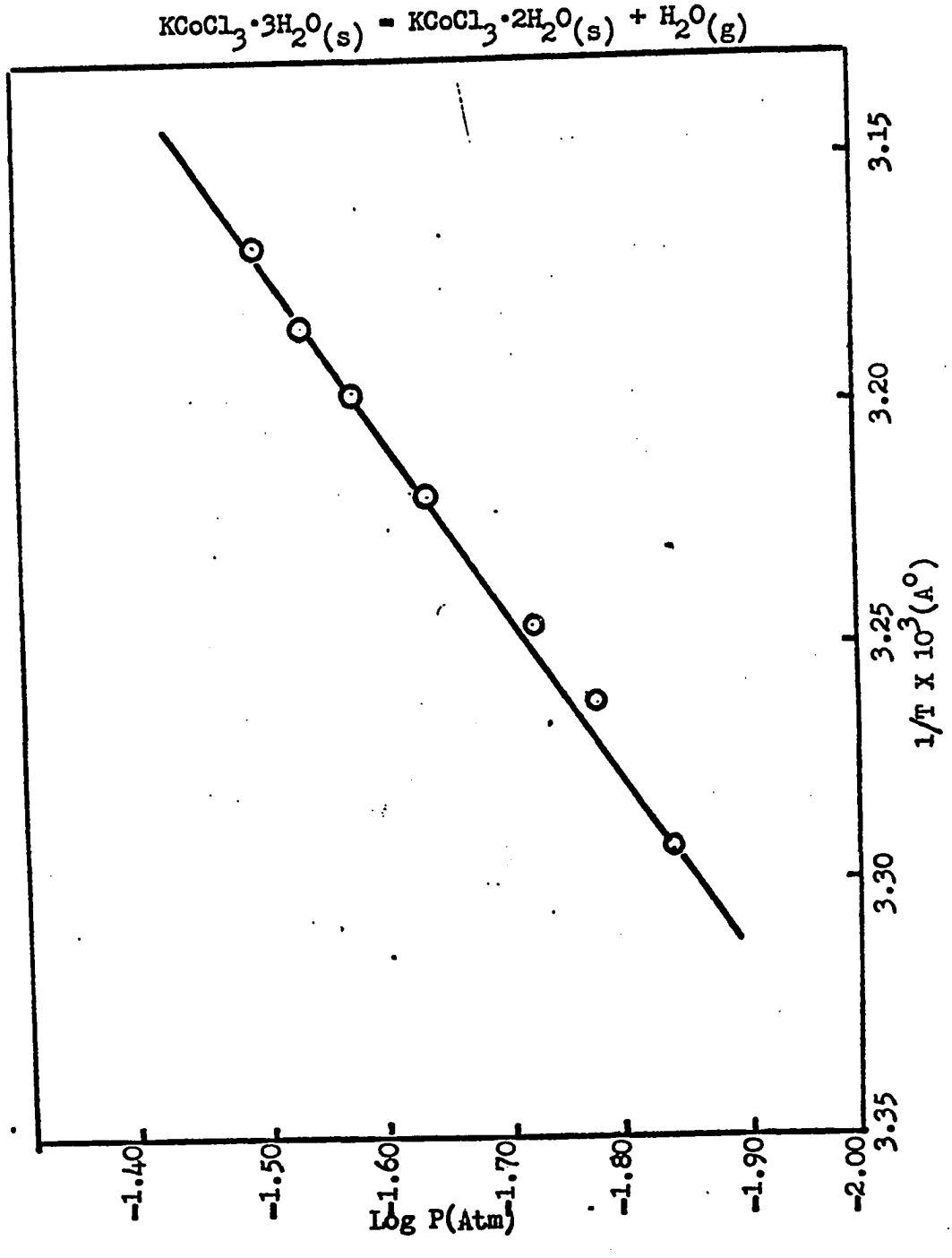

FIGURE 8

Log P(Atm) vs 1/T (A^{o})

$KCoCl_3 \cdot 2H_2O_{(s)} = KCoCl_3 \cdot H_2O_{(s)} + H_2O_{(g)}$

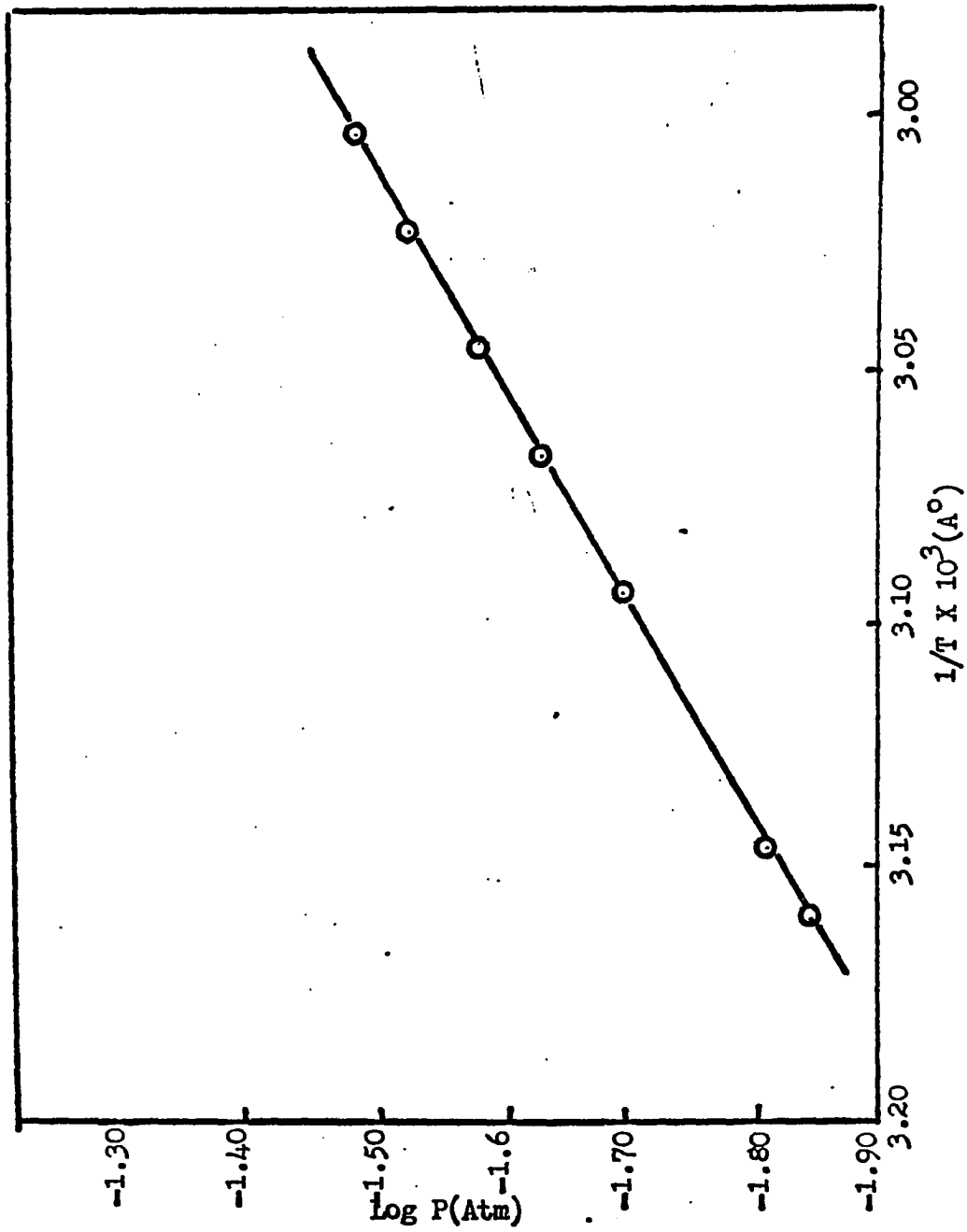

FIGURE 9

Log P(Atm) vs 1/T (A^{o})

$KCoCl_3 \cdot H_2O_{(s)} = KCoCl_{3(s)} + H_2O_{(g)}$

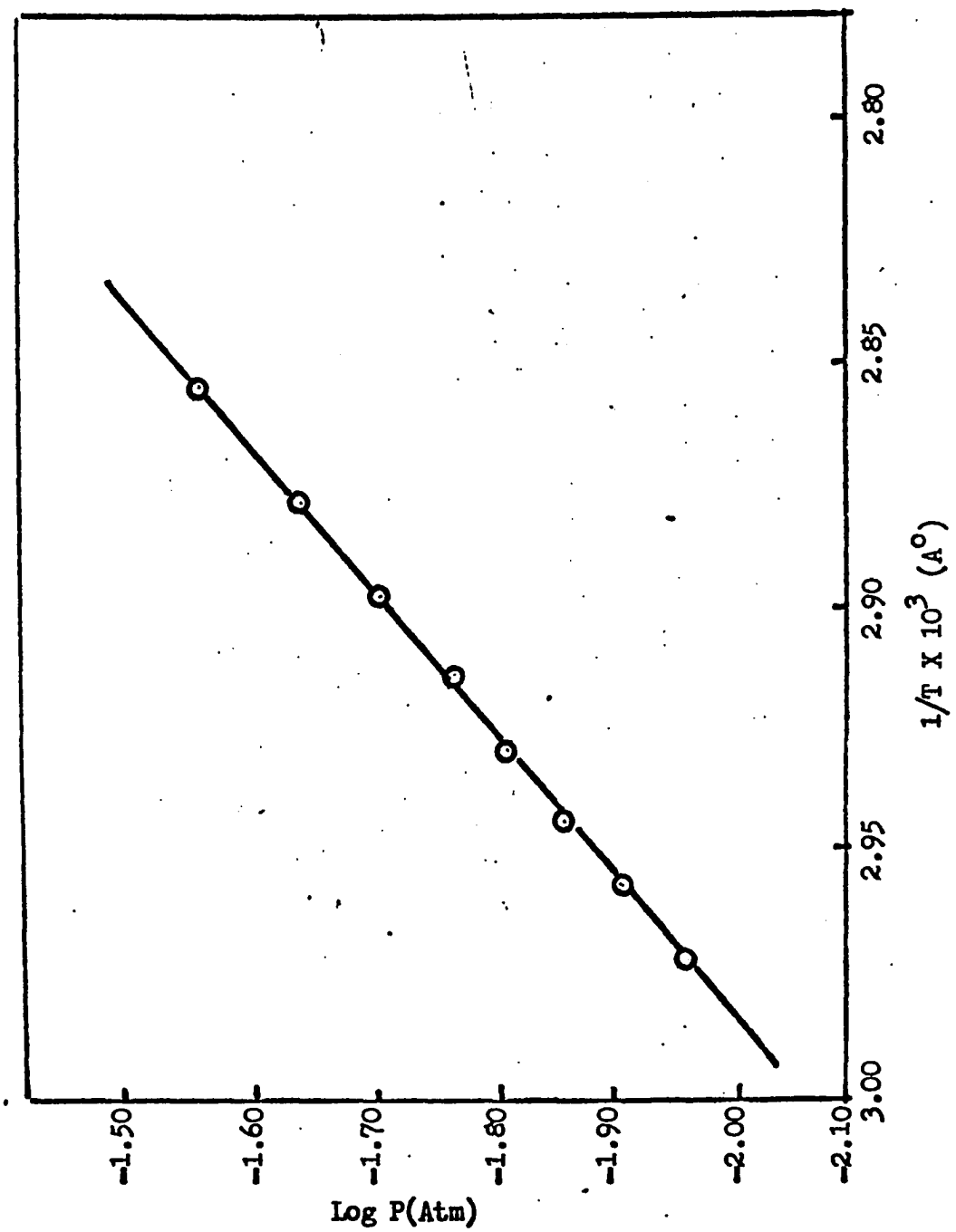

TABLE 8

PRESSURE-TEMPERATURE DATA FOR LOG P VERSUS 1/T

$$KCoCl_3 \cdot 4H_2O_{(s)} = KCoCl_3 \cdot 3H_2O_{(s)} + H_2O_{(g)}$$

P(mm)	P X 10^3(Atm)	Log P(Atm)	T(A^o)	1/T X 10^3(A^o)
15.95	20.987	-1.6780	307.4	3.253
16.35	21.513	-1.6673	308.4	3.243
17.40	22.895	-1.6403	309.4	3.232
18.85	24.803	-1.6055	310.4	3.222
20.00	26.316	-1.5798	311.6	3.209
21.30	28.026	-1.5524	312.4	3.201
22.60	29.737	-1.5268	313.4	3.191
23.70	31.184	-1.5060	314.4	3.181
25.05	32.961	-1.4820	315.4	3.171
26.15	34.408	-1.4633	316.4	3.161

Least Squares Analysis

Slope = -2361.4

Intercept = 6.006

TABLE 9

PRESSURE-TEMPERATURE DATA FOR LOG P VERSUS 1/T

$$KCoCl_3 \cdot 3H_2O_{(s)} = KCoCl_3 \cdot 2H_2O_{(s)} + H_2O_{(g)}$$

P(mm)	P X 10^3(Atm)	Log P(Atm)	T(A^o)	1/T X 10^3(A^o)
10.90	14.342	-1.8434	304.6	3.283
12.10	15.921	-1.7980	306.4	3.264
14.15	18.618	-1.7301	308.4	3.243
16.65	21.908	-1.6594	310.4	3.222
19.20	25.263	-1.5975	312.4	3.201
21.35	28.092	-1.5514	314.4	3.181
23.30	30.653	-1.5134	316.4	3.161

Least Squares Analysis

Slope = -2762.0

Intercept = 7.236

TABLE 10

PRESSURE-TEMPERATURE DATA FOR LOG P VERSUS 1/T

$$KCoCl_3 \cdot 2H_2O_{(s)} = KCoCl_3 \cdot H_2O_{(s)} + H_2O_{(g)}$$

P(mm)	P X 10^3(Atm)	Log P(Atm)	T(A^o)	1/T X 10^3(A^o)
11.00	14.474	-1.8394	316.0	3.165
11.80	15.526	-1.8089	318.0	3.145
14.20	18.684	-1.7285	323.0	3.096
15.30	20.132	-1.6961	325.4	3.073
16.90	22.237	-1.6529	328.4	3.045
19.00	25.000	-1.6021	330.4	3.027
20.05	26.382	-1.5787	333.3	3.000

Least Squares Analysis

Slope = -1631.9

Intercept = 3.321

TABLE 11

PRESSURE-TEMPERATURE DATA FOR LOG P VERSUS 1/T

$$KCoCl_3 \cdot H_2O_{(s)} = KCoCl_{3(s)} + H_2O_{(g)}$$

P(mm)	P X 10^3(Atm)	Log P(Atm)	T(A^o)	1/T X 10^3(A^o)
6.65	8.750	-2.9579	334.0	2.994
8.50	11.184	-1.9514	336.2	2.974
9.30	12.237	-1.9123	338.2	2.957
10.50	13.816	-1.8596	340.0	2.941
11.60	15.263	-1.8164	341.2	2.931
12.85	16.908	-1.7719	343.4	2.912
14.70	19.342	-1.7135	345.4	2.895
17.55	23.092	-1.6365	348.2	2.872
20.60	27.105	-1.5669	351.0	2.849

Least Squares Analysis

Slope = -3208.6

Intercept = 7.573

TABLE 12

THERMODYNAMIC CONSTANTS FROM EQUILIBRIUM DATA AT 25°C

Reactions	ΔH^{o} kcal mole^{-1}	ΔS^{o} e.u. mole^{-1}	ΔG^{o} kcal mole^{-1}
$KCoCl_3 \cdot 4H_2O = KCoCl_3 \cdot 3H_2O + H_2O$	10.81±.2	27.48±.3	2.62±.2
$KCoCl_3 \cdot 3H_2O = KCoCl_3 \cdot 2H_2O + H_2O$	12.64±.2	33.11±.3	2.77±.2
$KCoCl_3 \cdot 2H_2O = KcoCl_3 \cdot H_2O + H_2O$	7.47±.2	15.20±.3	2.94±.2
$KCoCl_3 \cdot H_2O = KCoCl_3 + H_2O$	14.68±.2	34.65±.3	4.35±.2

The standard entropies of formation can be calculated in the same way with the estimated entropy of formation of $KCoCl_3$ using Latimer's Rules (20), 44.1 e.u. mole^{-1}, and the entropy of water vapor, 45.11 e.u. mole^{-1}, (19). The calculated standard enthalpies and entropies are given in Table 13.

TABLE 13

CALCULATED STANDARD ENTHALPIES AND ENTROPIES OF FORMATION

Compound	ΔH_f^o kcal mole^{-1}	$(\Delta H_{f\ m}^o - \Delta H_{f\ n}^o)$ kcal mole^{-1}	ΔS_f^o e.u. mole^{-1}	$-(\Delta S_{f\ m}^o - \Delta S_{f\ n}^o)$ e.u. mole^{-1}
$KCoCl_3$	-1.6		44.1	
		72.48		10.46
$KCoCl_3 \cdot H_2O$	-74.08		54.56	
		65.27		29.91
$KCoCl_3 \cdot 2H_2O$	-139.35		84.47	
		70.44		12.00
$KCoCl_3\ 3H_2O$	-209.79		96.47	
		68.40		17.63
$KCoCl_3 \cdot 4H_2O$	-278.39		114.10	

The average change in the enthalpy and entropy for the dehydration reaction of many hydrates between adjacent solid hydrates is 72.0 kcal mole^{-1} and 9.4 e.u. mole^{-1}, respectively. (3) This can be interpreted by comparing the values of the dehydration reaction with the solid-vapor equilibrium in water and other hydrate systems. The ΔH_r^o and ΔS_r^o from

equation (6) can be written as

$$\Delta H_r^o = (\Delta H_{f\ m}^o - \Delta H_{f\ n}^o) + (n-m)\Delta H_f^o(H_2O)_{(g)} \qquad (7)$$

and

$$\Delta S_r^o = (S_{f\ m}^o - S_{f\ n}^o) + (n-m)\ S_f^o\ (H_2O)_{(g)} \qquad (8)$$

If the structure of the two adjacent hydrates are the same, then the difference in ΔH_f^o of adjacent hydrates ($\Delta H_{f\ m}^o - \Delta H_{f\ n}^o$) should be constant and the enthalpy of reaction (ΔH_r^o) is the ΔH_{sub}^o of the ice-vapor reaction. The ΔH_{sub}^o of the ice-vapor reaction at 25°C is 12.4 kcal mole^{-1} (see page 37). Where a structure change occurs there will be a change in the ΔH_f^o of the next species giving the value considerably different from 72.0 kcal mole^{-1},(3) The same reasoning can be used in interpretating the ΔS_r^o of adjacent hydrates species. The ΔS_{sub}^o of the ice-vapor reaction at 25°C is 35.2 e.v. mole^{-1} (see page 37). If the water lost is held only in a ice-like structure the difference in entropy of formation of adjacent hydrates should be 9.4 e.u. mole^{-1},(3) If however a structure change occurs a value considerably different from this is obtained.

Summary and Conclusions

The pressure-composition data showed there to be four distinct hydrate species during the dehydration, each involving a loss of one mole of water. The dehydration of the dihydrate below 55.4°C gave a constant vapor pressure indicating the formation of a distinct new solid phase. Above 55.4°C the vapor pressue was not constant as shown by Figure 4. The withdrawal of water vapor without the formation of a new solid species

results in the system being bivariant. This indicates that a solid solution is produced above 55.4°C.

The equilibrium vapor pressure versus temperature data was found to follow equation (5), page 25, for each hydrate species as shown by the linearity of the plots. The experimental enthalpies of dehydration found from these plots for the tetrahydrate and trihydrate were 10.81 kcal $mole^{-1}$ and 12.64 kcal $mole^{-1}$, respectively. These values are close to the enthalpy change required to convert one mole of ice to one mole of water vapor at 25°C. The approximate value for this conversion is found from the expression (21)

$$\Delta H_{sub} = \Delta H_{fus} + C_p(T_2-T_1) + \Delta H_{vap} = 12.4 \text{ kcal mole}^{-1} \qquad (9)$$

where ΔH_{fus} is 1.44 kcal $mole^{-1}$, T_2 is 25°C, T_1 is 0°C, and ΔH_{vap} is 9.172 kcal $mole^{-1}$ and C_p is one cal $g^{-1}deg^{-1}$.

The enthalpy change for the dehydration of the dihydrate is 7.47 kcal $mole^{-1}$ the lowest value obtained for any step. The removal of the last mole of water appears to be much higher due to unusual bond strength and similar results have been obtained in other studies. (2)

The entropy change required to change one mole of ice to vapor at 25°C is approximately 35.2 e.u. as determined from the expression (21)

$$\Delta S^{o}_{sub} = \Delta H^{o}_{fus}/T_1 + 2.303 \log T_2/T_1 + \Delta H^{o}_{vap}/T_2 = 35.2 \text{ e.u.} \qquad (10)$$

If the entropy values obtained for the dehydration steps are compared with the entropy for changing one mole of ice to vapor the values for the tetrahydrate, trihydrate, and monohydrate steps compare favorably. The entropy value of 15.2 e.u. $mole^{-1}$, obtained for the dihydrate is considerably lower than the other steps indicating a solid

phase formation with considerably more ordering.

The data from Table 13 indicates there is little change in the new complex formed with the loss of the first, second, and fourth moles of water. The loss of the third mole of water from the dihydrate gives values (ΔH^{o} and ΔS^{o}) that show an appreciable change in the new complex being formed. It is also noted that the color of the hydrate changes from a reddish violet for the dihydrate to a blue for the monohydrate also signaling a change in the solid phase being formed.

CHAPTER 4

SPECTRA

Background Discussion

The absorption spectra of potassium trichlorocobaltate (II) and its hydrates are characterized by a series of bands appearing in the visible and near IR regions. The absorptions occur through the process involving the excitation of an electron from one energy level to a higher level. These electronic transitions occur within the (3d) energy level of the cobalt (II) ion as a result of perturbations produced on it by the electric field of the ligands. The spectrum determined is dependent upon the energy of the "d" orbitals, their degeneracy, and the distribution of electrons in these orbitals: these features are in turn controlled by the oxidation number, number and type of ligand, and the geometry of the complex. A correct analysis of the nature of these perturbations can lead to a significant amount of information about the symmetry of the complex.

In the free ion the five "d" orbitals are degenerate, however, under the influence of the electric field produced by the ligands this degeneracy is removed. This loss of degeneracy in the "d" orbitals was first proposed by Bethe. (22) He considered the ligands as point charges and the interactions between the metal ion and ligands as purely

electrostatic. This approach is referred to as the crystal field theory.

The basic difficulty of the crystal field theory is that no account is taken for the metal-ligand overlap (covalency). This difficulty is partly overcome by the ligand field theory which adds parameters to account for the covalent bonding occurring between the metal and its ligands. It is this latter theory which will be used to explain the experimental spectra. An attempt will be made to explain the differences amoung the spectra of the identified complexes using ligand field theory along with the thermodynamic values and magnetic moments.

Two possible symmetries exist for the Co (II) ion with chloride and water as ligands. These are octahedral and tetrahedral with a ground state configuration of $^4T_{1g}(t_{2g}^5 e_g^2)$ and $^4A_2(e_g^4 t_2^3)$, respectively. These are weak field configurations, as would be expected with chloride ion and/or water as ligands. (23)

Theory

The quantitative approach is accomplished using the perturbation theory. The total Hamiltonian consist of the various perturbations required to explain the splitting of the "d" orbitals. The first perturbation is the octahedral potential provided by the ligands splitting the five degenerate "d" orbitals into two sets (e_g, t_{2g}) separated by the parameter, 10 Dq, (Figure 10). The second perturbation is the distortion of the octahedral or tetrahedral field by a tetragonal or trigonal disturbance. These perturbations further remove the degeneracy of the "d" orbitals. The two spectal parameters from this perturbation are referred

to as Ds and Dt for tetragonal distortion and Dσ and Dτ for trigonal distortion. The final perturbation is the spin-orbit coupling caused by the coupling of the spin angular momentum (S) and the orbital angular momentum (L). The crystal field splitting for the $(3d)^n$ systems is large compared to the LS splitting, therefore, this perturbation does not constitute a large error and can be neglected in first order calculations.

FIGURE 10

EFFECTS OF VARIOUS PERTURBATIONS ON "d" ORBITALS

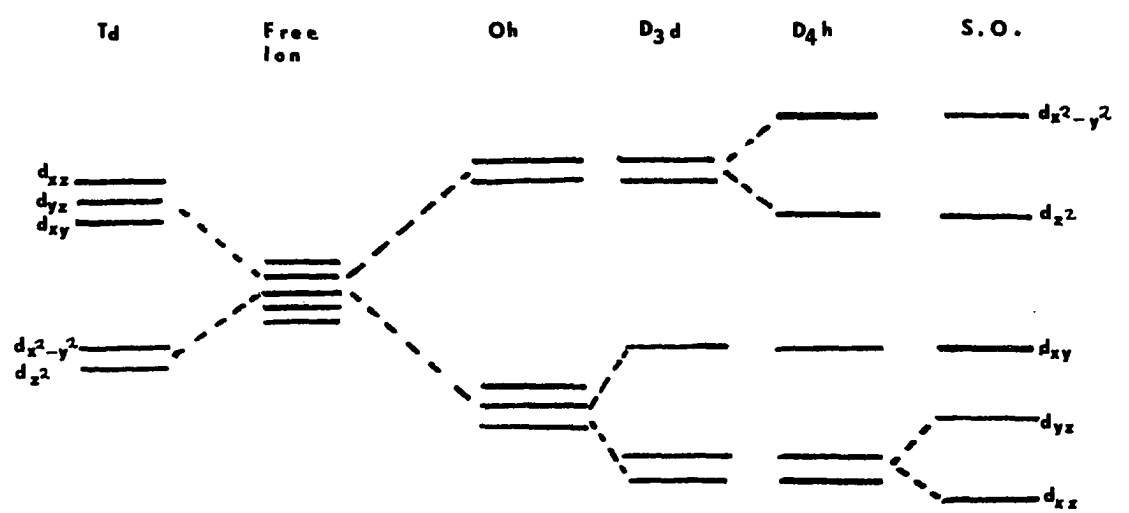

The energy of any electronic state can be theoretically determined from the integral in the form

$$E = \int \psi \hat{H} \psi \, dt$$

where ψ is the normalized wave function and $\hat{H}$ is the Hamiltonian operator.

The quantitative treatment for the model proposed will be to add

perturbation to the free ion Hamiltonian, $\hat{H}_f$, (23) taking the form

$$\hat{H}_f = h^2/2m\Sigma_i\nabla_i^2 - \Sigma_i\ ze^2/r_i + \frac{1}{2}\Sigma_{i\neq i} e^2/r_{ij} + \xi_i(r)l_i \cdot s_i$$

where the terms describe the kinetic energy, the electron core potential, the electron-electron repulsions and spin-orbit coupling, respectively. The Hamiltonian showing the previously discussed perturbations on the electrons of the metal ion in an octahedral system are

$$\hat{H}_o = \hat{H}_f' + \hat{V}_o + \hat{V}_t$$

or

$$\hat{H}_o = \hat{H}_f' + \hat{V}_o + \hat{V}_\tau$$

where $\hat{H}_f'$ is the Hamiltonian for the free ion under the influence of the ligands, $\hat{V}_o$ is the crystal field potential on the metal ion in an octahedral field and is represented by Dq. $\hat{V}_t$ and $\hat{V}_\tau$ are the distortion perturbations upon the octahedral field potential caused by the lower symmetry of the ligand field. $\hat{V}_t$ or tetragonal distortion results from a symmetry of D_4h or C_2v. V_τ or trigonal distortion results from a symmetry of D_3d.

Before investigating the application of these perturbations on the complex it is necessary to develop the energy levels and wave functions of the free ion in absence of the ligand field. The third term of the Hamiltonian, $\hat{H}_f$, is considered as a perturbation upon the electrons in the unfilled shell. Using LS coupling, the terms (energy levels of a system) of the free ion for a given $(3d)^n$ configuration can be derived. The configuration is characterized by two quantum numbers, L and S, where L is the total angular quantum number and S is the total spin quantum number. The states for a given configuration are designated by the term symbol, ^{2S+1}L, where 2S+1 is the multiplicity of the term. The states

arising out of a d^7 electron configuration are given in Table 14.

TABLE 14

THE TERM ENERGIES FOR A d^7 CONFIGURATION

Configuration	Term	Energy in "F" Parameters	Racah Parameters
d^3- d^7	^2P	$3F_o - 6F_2 - 12F_4$	$3A - 6B + 3C$
	a^2D- b^2D	$dF_o + 5F_2 + 3F_4 \pm \sqrt{193F_2^2 - 1650F_2F_4 + 8325F_4^2}$	$3A + 5B + 5C \pm \sqrt{193B^2 + 8BC + 4C^2}$
	^2F	$3F_o + 9F_2 - 87F_4$	$3A - 9B - 3C$
	^2G	$3F_o - 11F_2 + 13F_4$	$3A - 11B + 3C$
	^2H	$3F_o = 6F_2 + 12F_4$	$3A - 6B + 3C$
	^4P	$3F_o - 147F_4$	$3A$
	^4F	$3F_o - 15F_2 - 72F_4$	$3A - 15B$

Using the energies listed in Table 14 it is clear that the ^4F term lies lowest. The ^4F term is referred to as the ground term for a d^7 electron configuration.

The energies of the states arising out of the LS coupling scheme can be found by determining the wave functions by the use of lowering or raising operators. (23) Using the coulomb integral, $J=(ab|\ 1/r_{12}|\ ab)$ and the exchange integral, $K=(ab|1/r_{12}|\ ba)$, the energy of the free ion terms as a function of F_o, F_2, and F_4 can be determined. F_o is the radial parameter accounting for the symmetrical part of the electron repulsions of the free ion. These latter two parameters govern the

difference in energies of the terms for a given configuration. By expressing the energies using the Racah (24) parameters, B and C, where $B = F_2 - 5F_4$, and $C = 35F_4$, energy differences involving states of the same multiplicity will vary only in B while those energy differences between states of different multiplicity vary in both B and C. This is illustrated in Table 15.

TABLE 15

ENERGY DIFFERENCE BETWEEN d^7 TERMS

Configuration	Terms Involved	Energy Difference	
		Slater Parameters	Racah Parameters
$d^3 - d^7$	$^4F - {}^4P$	$15F_2 - 75F_4$	15B
	$^4F - {}^2H$	$9F_2 + 60F_4$	9B + 3C
	$^4F - {}^2G$	$4F_2 + 85F_4$	4B + 3C
	$^4F - {}^2F$	$24F_2 - 15F_4$	24B + 3C
	$^4F - {}^2_aD, {}^2_bD$	$20F_2 + 75F_4 \pm \sqrt{1952F_2^2 - 1650F_2F_4 + 8325F_4^2}$	$20B + 5C \pm \sqrt{193B^2 + 8BC + 4C^2}$
	$^4F - {}^2P$	$9F_2 + 60F_4$	9B + 3C

The absolute energies of the terms arising from a given configuration requires a knowledge of the wave functions of the electrons which depend upon the principal quantum number. In most treatments only the relative energies are needed which require only the approximate values of B and C. These are determined from the experimental spectra as in the case

of the parameter Dq.

The octahedral operator $\hat{V}_o$ is obtained by expanding a series of normalized spherical harmonics:

$$V_o = \sum_i \sum_l \sum_m Y_l^m(O_i,\phi_i)R_{nl}(r_i)$$

It can be shown that this expression takes the form (23)

$$V_o = \sum_1 \sqrt{1/\ 4\pi}R_o(r_i) + Y_4^o + \sqrt{4/14}\ (Y_4^o + Y_4^{-4})$$

where the first term is responsible for a uniform shift of the energy levels and will be ignored in discussing the electronic properties of the system.

The application of the $\hat{V}_o$ to the set of "d" orbitals result in the values obtained in Table 16

TABLE 16

EFFECT OF $\hat{V}_o$ ON THE "d" ORBITALS

$(d\pm2\|\hat{V}_o\|d\pm2) = Dq$
$(d\pm2\|\hat{V}_o\|d\mp2) = 5DQ$
$(d\pm1\|\hat{V}_o\|d\pm1) = -4Dq$
$(d_o\ \|\hat{V}_o\|d_o) = 6Dq$

The values of the "d" orbitals under tetrahedral symmetry are the same as those in Table 16 with (25)

$$Dq_{tet} = -4/9\ Dq_{oct}$$

Most complexes show deviations from octahedral or tetrahedral

symmetry. These deviations are treated as perturbations upon the higher symmetry by the tetragonal operator, $\hat{V}_t$ or trigonal operator, V_T. The $\hat{V}_t$ operator takes the form (23)

$$\hat{V}_t = AR_z(r)\ Y_2^o + BR_4'(r)Y_4^0$$

Tetragonal distortion is taken as a perturbation along the z axis changing the energies while not distorting the orbitals. The tetragonal operator, $\hat{V}_t$, may be put in different form to show where the distortion parameters Ds and Dt arise. Using operator technique (27) where 1_z is substituted for z in the spherical harmonics

$$Y_2^0 = \sqrt{5/4\pi}\ \sqrt{1/4}\ \frac{3z^2-r^2}{r^2}$$

and

$$Y_4^0 = \sqrt{9/4\pi}\ \sqrt{1/64}\ \frac{35z^4-30z^2r^2+3r^4}{r^4}$$

the expression below is obtained for the tetragonal operator

$$\hat{V}_t = Ds(\hat{1}_z^2 - 2) - Dt(35/12\ \hat{1}_z^4 - 155/12\ \hat{1}_z^2 + 6)$$

where Ds and Dt are splitting parameters composed of the radial part of the spherical harmonics

Table 17 shows the results of the application of V_t upon the set of "3d" orbitals.

TABLE 17

EFFECT OF $\hat{V}_t$ ON THE "d" ORBITALS

$(d_{\pm 2}\|V_t\|d_{\pm 2}) = 2Ds - Dt$
$(d_{\pm 1}\|V_t\|d_{\pm 1}) = -Ds + 4Dt$
$(d_o\ \|V_t\|d_o\ ) = -2Ds - 6\ Dt$

The sign and magnitude of the tetragonal splitting parameters Ds and Dt depend upon the nature of the tetragonal distortion.(27) These value are determined from experimental spectra as in the case of Dq, B, and C, however, the signs of Ds and Dt determine the ground state as seen from Table 18. Using the label $(d\pm m)$ where m=0, d_z2, m=±1, d_{xz} and d_{yz}, m=±2, d_{xy} and $d_{x^2-y^2}$, a positive Ds and Dt would result in the d_z2 being lowest.

If the octahedron is distorted along the trigonal axis, the splitting of the octahedral energy levels are close to those in tetragonal distortion. (Figure 10) The symmetry of the complex changes from O_h to D_{3d}. The correlation scheme from Oh symmetry to lower symmetries is given in Table 19. (28) The trigonal operator, $V\tau$, is identical in form to the tetrgonal operator, V_t, but operating on a different set of "d" orbitals. (23)

TABLE 18

GROUND STATE DEPENDENCE ON THE SIGN OF DS and DT

Sign Ds	Sign Dt	Distortion	$(d\pm2\|V_t\|d\pm2)$	$(d\pm1\|V_t\|d\pm1)$	$(d_o\|V_t\|d_o)$	Ground State
+	+	elongation	2Ds + Dt	-(Ds + 4Dt)	-(2Ds - 6Dt)	$^4A_{2g}$
-	+	compression	-(2Ds - Dt)	Ds - 4Dt	2Ds + 6Dt	^4E_g
-	-	compression	-(2Ds + Dt)	Ds + 4Dt	2Ds - 6Dt	^4E_g
+	-	elongation	2Ds - Dt	-(Ds - 4Dt)	-(2Ds + 6 Dt)	$^4A_{2g}$

TABLE 19

CORRELATION OF Oh TO LOWER SYMMETRIES

O_h	D_{4h}	D_{2d}	D_{3d}	C_{2v}
T_{1g}	$A_{2g} + E_g$	$A_2 + E$	$A_{2g} + E_g$	$A_2 + B_1 + B_2$
T_{2g}	$B_{2g} + E_g$	$B_2 + E$	$A_{1g} + E_g$	$A_1 + B_1 + B_2$
A_{2g}	B_{1g}	B_1	A_{2g}	A_2
A_{1g}	A_{1g}	A_1	A_{1g}	A_1
E_g	$A_{1g} + B_{1g}$	$A_1 + B_1$	E_g	$A_1 + A_2$

The last perturbation to be considered is spin-orbit coupling. The spin-orbit coupling in $(3d)^n$ complexes is small compared to the crystal field splitting and is neglected in most weak field treatments. Although it is small it can, however, be important in the magnetic properties (Chapter Five) of $(3d)^n$ complexes. Spin-orbit splitting of the absorption bands for first row transition metals is seldom observed (29) in the optical spectra because of poor resolution. The presence of spin-orbit coupling is responsible for the occurance of the "spin forbidden" absorption bands due to mixing of states of different multiplicity through relaxation of the spin selection rule.

The spin orbit operator, $\hat{H}_{s.o.}$ has the form

$$\hat{H}_{s.o.} = \xi \hat{l}.\hat{s}$$

where ξ is the one-electron spin-orbit coupling parameter, and $\hat{l}$ and $\hat{s}$ are the orbital and angular momentum operators. ξ is related to λ by the

expression

$$\xi = \pm \lambda/2S$$

where the positive sign holds for less than half-filled shell and a negative sign for an over half-filled shell. The d^7 electron configuration has a negative λ value.

The spin-orbit coupling operator takes the form

$$\hat{l}\cdot\hat{s} = (\hat{l}_z\cdot\hat{s}_z + \frac{1}{2}\hat{l}_+\cdot\hat{s}_- + \frac{1}{2}\hat{l}_-\cdot\hat{s}_+)$$

Through the application of the operator to the proper wave functions, the perturbation to the Hamiltonian by spin-orbit coupling is obtained.

By qualitative application of group theory it can be shown that only T_1 and T_2 states are split by spin-orbit coupling under octahedral symmetry. (25) The operator $L(=L_x + L_y + L_z)$ possesses the symmetry property of rotation about the three Cartesian axes. These belong to the irreducible representation of T_{1g} under Oh. The direct product

$$A_{1g} \times T_{1g} \times A_{1g},\ A_{2g} \times T_{1g} \times A_{2g},\ E_g \times T_{1g} \times E_g$$

do not contain an A_{1g} representation, therefore, all the matrix elements

$$(4_{A_{1g}}|L|4_{A_{1g}}),\ (4_{A_{2g}}|L|4_{A_{2g}}),\ (4_{E_g}|L|4_{E_g})$$

are zero. The direct products

$$T_{1g} \times T_{1g} \times T_{1g} \text{ and } T_{2g} \times T_{1g} \times T_{2g}$$

both contain an A_{1g}, therefore, the matrix elements

$$(4_{T_{1g}}|L|4_{T_{1g}}) \text{ and } (4_{T_{2g}}|L|4_{T_{2g}})$$

are not zero. The same arguments can be applied to tetrahedral symmetry and are shown to give identical results.

A simplified method proposed by Abragam and Pyrce (30,31) can be used for calculating the perturbation due to spin-orbit splitting. The roots obtained by the application of this procedure to the quartet state of Co(II) ion by Low (32) gives the three roots

$$E = 3/2\ \alpha\lambda \qquad (1)$$

$$= -\ \alpha\lambda \qquad (2)$$

$$= -\ 5/2\ \alpha\lambda \qquad (3)$$

For doublet states, the two roots are (23)

$$E = 1/2\ \alpha\lambda \qquad (4)$$

$$= -\ \alpha\lambda \qquad (5)$$

where λ is the spin-orbit coupling constant which is related to the spin-orbit coupling for the ground state. (23) Alpha (α) is a constant for each symmetry state and can be evaluated by application of the L_z, L_y, and L_x operators. (30,31,23) The (α) values have been calculated by Fogel (33) and are given in Table 20. The roots are calculated using octahedral symmetry and then assigned to the split states caused by the lower symmetry.

Under D_{4h} and D_{3d} symmetry, it can be show that roots (1), (2) and (3) belong to the doubly degenerate states (^4E and ^4E_g) while roots (1) and (2) belong to singly degenerate states ($^4A_1$, $^4A_2$, $^4B_{1g}$, $^4B_{2g}$, $^4A_{1g}$ and $^4A_{2g}$). For the doublet states, roots (4) and (5) are assigned to doubly degenerate states (^2E and ^2E_g) and root (4) to singlet states ($^2A_{1g}$, $^2A_{2g}$, $^2B_{1g}$, $^2B_{2g}$, $^2A_{1g}$, and $^2A_{2g}$).

Mention was made of configuration interaction in Chapter One. The effect is important in the d^7 electron configuration, since it is observed that, of the four quartet levels under Oh symmetry, two have

TABLE 20

VALUES OF THE PARAMETER ALPHA (α)

State	
$^4T_{1g}(F)$, $^2T_{1g}(F)$	-3/2
$^4T_{2g}(F)$, $^2T_{2g}(F)$, $^2T_{1g}(G)$	1/2
$^4T_{1g}(P)$, $^2T_{1g}(P)$	1.0
$^2T_{1g}(G)$	5/2
$^2T_{2g}(H)$	-5/2
$a^2T_{1g}(H)$	15/8
$b^2T_{1g}(H)$	-11/8
$^2T_{2g}(D)$	-1.0

exactly the same symmetry, $^4T_{1g}(^4F)$ and $^4T_{1g}(^4P)$. These levels will interact and is treated as a second order perturbation upon the Hamiltonian. The effect of this perturbation is to depress the energy of the lower level, $^4T_{1g}(^4F)$ and to raise the upper level, $^4T_{1g}(^4P)$ by an equivalent amount.

Under D_{4h} and D_{3d} symmetry the T_{1g} state splits into an A_{2g} and E_g state. Configuration interation can therefore arise between these states under the lower symmetry.

The energy change arising from configuration interaction mixing of the $^4T_{1g}(^4F)$ and $^4T_{1g}(^4P)$ is obtained from the integral ($<^4T_{1g}|V_o|^4T_{1g}>$) This interaction is the off-diagonal elements of the perturbation matrix. For first order calculations the off-diagonal elements are neglected.

The determination of the perturbation parameters, Dq, B, C, Ds Dt, or $D\sigma$ and $D\tau$ involves the evaluation of secular determinants using the wave functions for the different states. Table 21 gives the wave functions of the weak field terms arising from F and P states quantized along the four-fold and three-fold axis.

The secular determinants shown in Figures 11 and 12 are used in calculating the energies of the spin allowed states under D_{4h} and D_{3d} symmetry. The energies for these two determinants are given in Tables 22 and 23.

Selection Rules

The absorption of "visible" radiation (UV, visible, IR) by a transition metal complex arises from the ability of the oscillating electric vector to induce an electronic transition from one state with a wave function of ψ to a higher state with a wave function ψ' by the displacement of an electronic charge. This electric dipole mechanism is used to explain d-d transitions of the transition metals.

The explanation of this electric dipole mechanism using group theory is given in the general references by Cotton (28) and Figgis (25). The results are usually expressed in the form of the "selection rules" which predict whether an electronic transition will be "allowed" or "forbidden".

The first rule is the spin selection rule which states the number of unpaired electrons in the initial state must be identical with those in the final state.

The second rule is the Laporte selection rule which states that the elctronic transition is forbidden if it simply involves a redistribution of electrons in the same type of orbital in a given quantum shell. According to this rule, d-d type transitions in complexes having a center of symmetry are forbidden.

The transitions of interest in this study are all of the d-d type and must become partially allowed by some mechanism. In order for the absorption to be allowed by the electric dipole mechanism it is necessary that the transition moment, Q

$$Q = \langle \psi | r | \psi' \rangle$$

TABLE 21

WAVE FUNCTIONS OF WEAK FIELD TERMS ARISING FROM THE F AND P TERMS OF MAXIMUM MULTIPLICITY FOR d^7 ELECTRON CONFIGURATION

Free Ion Term	Ligand Field Term	Wave functions Quantized Four-fold Axis	Three-fold Axis
		Y_3^0	$2/3Y_3^0-1/3\ \ 5/2(Y_3^0-Y_3^{-3})$
^4F	$^4T_{1g}$	$\frac{1}{2}(\ 3/2Y_3^{-1}+\ 5/2Y_3^2)$	$5/8Y_3^2+\ 1/6Y_3^{-1}$
		$\frac{1}{2}(\ 3/2Y_3^1+\ 5/2Y_3^{-3})$	$5/6Y_3^{-2}-\ 1/6Y_3^1$
		$\frac{1}{2}(\ 5/2Y_3^{-1}-\ 3/2Y_3^3)$	$\frac{1}{2}(Y_3^3+Y_3^{-3})$
	$^4T_{2g}$	$\frac{1}{2}(\ 5/2Y_3^1-\ 3/2Y_3^{-3})$	$1/6Y_3^2-\ 5/6Y_3^{-1}$
		$\frac{1}{2}(Y_3^2+Y_3^{-2})$	$1/6Y_3^{-2}+\ 5/6Y_3^1$
	$^4A_{2g}$	$\frac{1}{2}(Y_3^2-Y_3^{-2})$	$1/3\ \ 2(Y_3^2-Y_3^{-3})-\ 5Y_3^0$
^4P	$^4T_{1g}$	Y_3^0	Y_3^0
		Y_3^1	Y_3^1
		Y_3^{-1}	Y_3^{-1}

FIGURE 11

SECULAR DETERMINANT FOR HIGH SPIN STATES

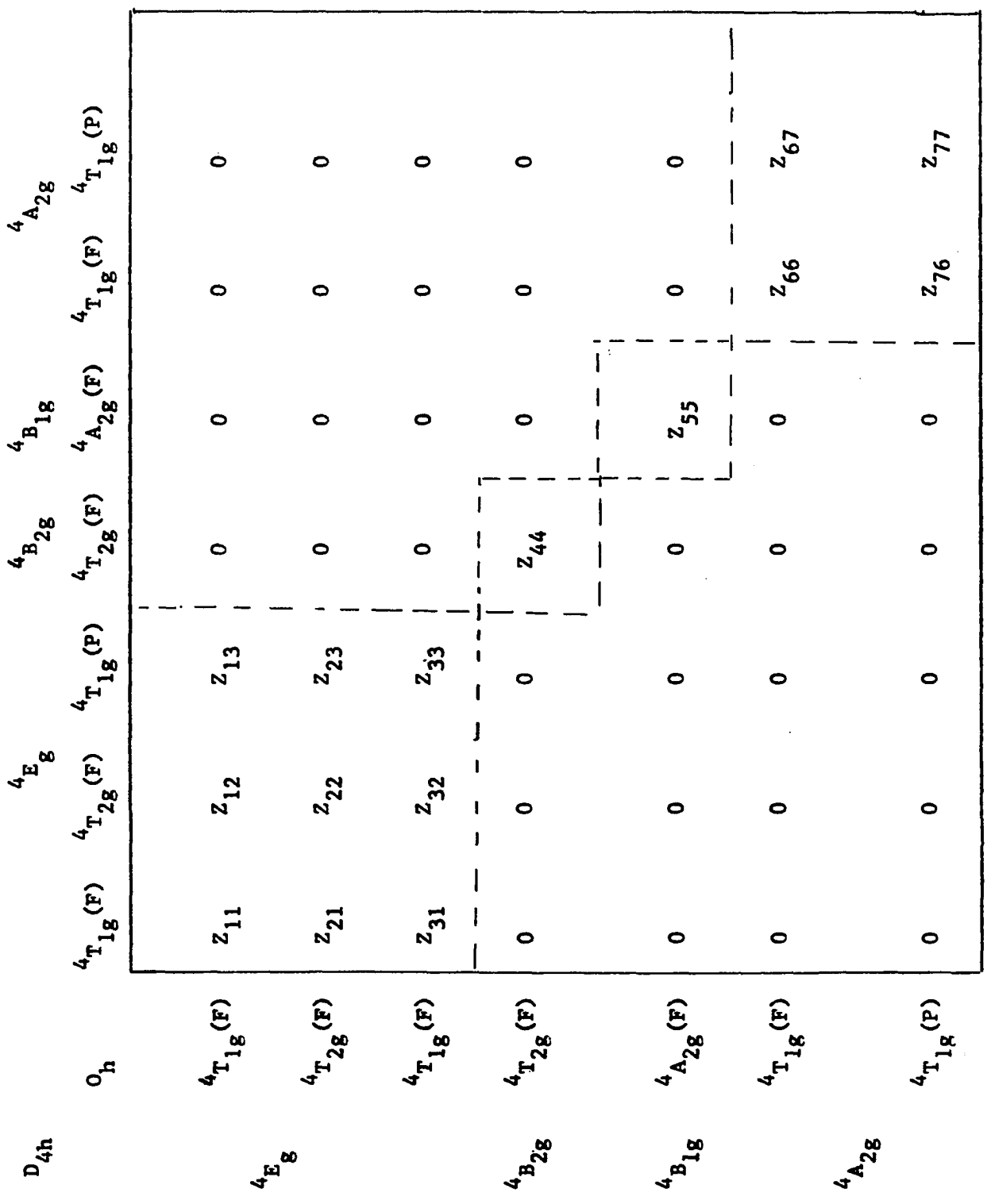

TABLE 22

NON ZERO ELEMENTS FOR THE SECULAR DETERMINANT IN FIGURE 11

Element		Energy
Z_{11}		-6Dq + 2/5Ds + 9/4Dt
$Z_{12} = Z_{21}$		15/5Ds - 15/4Dt
$Z_{31} = Z_{13}$		4Dq - 6/5Ds - 3/2Dt
Z_{22}		2Dq +7/4Dt
$Z_{23} = Z_{32}$		12/5Ds + 15/4Dt
Z_{33}	15B	-7/5Ds
Z_{44}		2Dq -7Dt
Z_{55}		12Dq -7Dt
Z_{66}		-6Dq -4/5Ds + 6Dt
$Z_{67} = Z_{76}$		4Dq + 12/5Ds - 4Dt
Z_{77}		+15/4Ds

FIGURE 12

SECULAR DETERMINANT FOR HIGH SPIN STATES

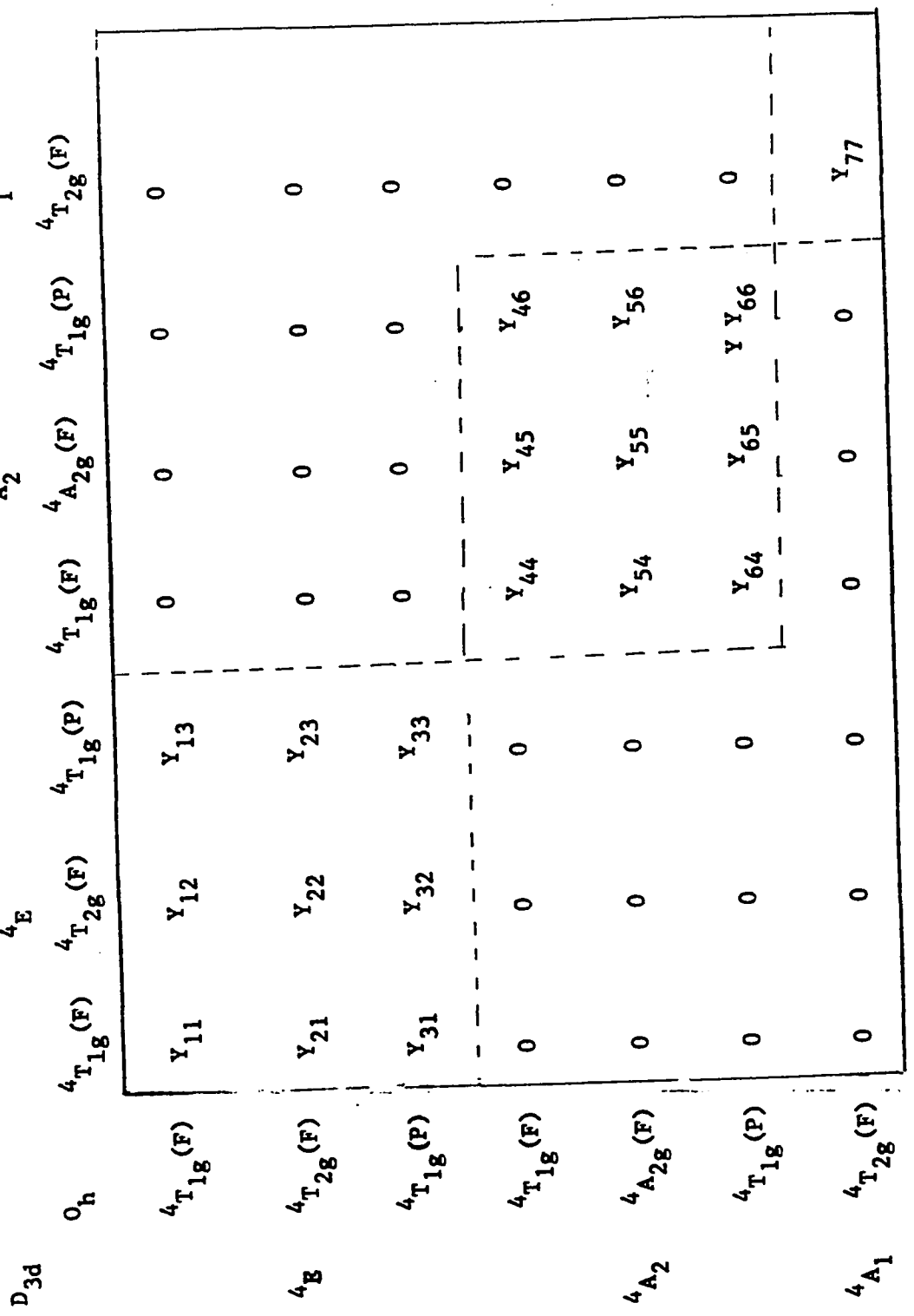

TABLE 23

NON ZERO ELEMENTS FOR THE SECULAR DETERMINANT IN FIGURE 12

Element	Energy
Y_{11}	$+6Dq + 1/10D\sigma + 17/3d\tau$
$Y_{12} = Y_{21}$	$- 5/10D\sigma + 4\ 5/3D\tau$
$Y_{13} = Y_{31}$	$+4Dq + 4/5D\sigma + D\tau$
Y_{22}	$-2Dq + 1/2D\sigma + 1/3D\tau$
$Y_{23} = Y_{32}$	$-8\ 5/10D\sigma + 5\ D\tau$
Y_{33} 15B	$+7/5D\tau$
Y_{44}	$+6Dq + 1/5D\sigma - 13/3D\tau$
$Y_{54} = Y_{45}$	$5(4/10D\sigma + 2/3D\tau$
Y_{55}	$-12Dq \qquad 14/3D\tau$
$Y_{64} = Y_{46}$	$+4Dq - 8/5D\sigma + 8/3D\tau$
$Y_{65} = Y_{56}$	$-8/10D\sigma - 4/3\ 5\ D\tau$
Y_{66}	$-14/5D\tau$
Y_{77}	$-2Dq - D\sigma - 3D\tau$

be non-zero, where r is the radial vector which has the symmetry of the electric dipole. The value of Q must be totally symmetric and contain the A_{1g} representation.

Complexes with O_h and D_{4h} symmetry contain a center of symmetry. In these complexes the "d" orbitals are symmetric to the center of inversion and transform to give only "g" representations. The x, y, and z components of the electric dipole vector transforms under these symmetries to give "u" representation, therefore, the direct product does not contain the A_{1g} component. By this argument the transition moment is zero and the transition is forbidden.

In O_h and D_{4h} complexes there exist a number of normal modes of vibration of which some are of the "u" type. If the complete wave function is taken as the product of the electronic wave function and the vibronic wave function, then the transition moment becomes non-zero during the vibration of the molecule when the inversion center no longer exist.

Applying group theory the vibronic modes are

$$A_{1g},\ E_g,\ 2T_{1u},\ T_{2g},\ \text{and}\ T_{2u}$$

in O_h symmetry, and

$$2A_{1g},\ B_{1g},\ B_{2g},\ E_g,\ 2A_{2u},\ \text{and}\ 3E_u$$

in D_{4h} symmetry.

The vibrational ground state is totally symmetric and belongs to the A_{1g} representation. Taking the direct product of the ground state, electric dipole vector, the excited state, and excited vibrational state decomposes to give an A_{1g} representation, therefore the transition is

allowed. All electronic transitions under O_h and D_{4h} are allowed due to one or more vibrational symmetry modes.

Tetrahedral complexes show two spin allowed transition as predicted from the selection rules. These are the $^4A_2 \rightarrow {}^4T_1(F)$ and the $^4A_2 \rightarrow {}^4T_1(P)$. The $^4A_2 \rightarrow {}^4T_2(F)$ transition is symmetry forbidden as well as not being in the region studied.

Under some conditions, it is not correct to assume that the wave function is completely factorized into an electronic wave function and a spin wave function. Where considerable spin-orbit coupling exist, it is possible for the spin to change as a result of the transition without the transition moment integral becoming zero. This results in a partial breakdown of the spin selection rule leading to the appearance of spin forbidden transitions in the absorption specta.

Experimental

The absorption spectra were obtained from powdered samples for $KCoCl_3 \cdot 4H_2O$, $KCoCl_3 \cdot 3H_2O$, $KCoCl_3 \cdot 2H_2O$, $KCoCl_3 \cdot H_2O$ and $KCoCl_3$. The spectrum for the tetrahydrate species was also obtained from the crystalline form.

The reflectance spectra were obtained using a Beckman DK-1 recording spectrophotometer equipped with a reflectance attachment, and a modified Brown potentiometric strip recorder. The diffusion sphere of the relectance attachment was coated with fresh magnesium oxide just prior to spectra determinations.

The samples were prepared by placing a small amount of each

species in a 15 mm microscope well slide. The well was covered with a thin glass cover slip, held in place with cellophane tape or glue. Since all samples were sensitive to moistrue, slide preparation was accomplished in minimal time followed by immediate specta determinations. After standing for a time (2-3 hrs.) exposed to the atmosphere, the samples changed composition and were discarded after each spectal determination.

The reference port of the reflectance sphere was covered with a slide containing freshly prepared MgO and covered in the same manner as the sample slide. Two such slides were prepared and the spectrophotometer was cycled through the region of interest to determine if the MgO absorbed in the region to be studied.

All spectra were determined using the same conditions. The recording conditions were: sensitivity 1.0; time constant 0.2; intensity range, 0-1; scan time, 3 minutes.

The PbS detector was used in the range of 2100 mu to 700 mu and the photomultiplier tube was employed in the region 700 mu to 400 mu. The energy source was a six (6) volt incadescent tungsten lamp for the IR and visible region.

The samples for each hydrate species were prepared by placing finely ground anhydrous $KCoCl_3$ over wet $Ca(NO_3)_2$ until the appropriate weight was gained. The slides were prepared and spectra determined. The spectrum was also taken for each hydrate species by forming them in the vapor pressure apparatus, Figure 1, page 12, from dry $KCoCl_3$. Both procedures produced identical spectra for each species.

A crystal of potassium trichlorocobaltate (II) tetrahydrate prepared by the method described in Chapter Two was planned to such a

thickness that light was transmitted through it. (In order to obtain the crystal spectra the Beckman DK-1 was modified with the apparatus shown in Figure 13). It was then mounted on an aluminum plate (A) over a small hole bored in the plate. The reference port was covered with an aluminum plate (B) with an appropriate sized hole so that the reference beam can be scaled to obtain both the maximum and minimum of the absorbance bands. The slide is inserted into slit (C) and the apparatus is inserted into the cell compartment of the DK-1. The cell compartment is flushed with dry nitrogen while the spectra is being recorded. This slows down the reaction of the crystal with atmospheric moistrue. For low temperature, liquid nitrogen is flushed through port (D) from a specially prepared Dewar. Using this procedure spectra for crystals can be otained at approximately liquid nitrogen temperature. (Note: Crystals of the tetrahydrate are very sensistive to atmospheric mosisture and were coated with mineral oil to prevent reaction during handling.) Attempts to grow crystals for the dihydrates and anhydrous species failed. Thus the calculations for the spectral fitting of the lower hydrates and the anhydrous salts are based upon reflectance spectra.

Spectra Fitting

The experimental spectra were fitted using a computer program written by H. Joy (1) which iterates the spectral parameters to obtain the best fit for the spectral assignments.

Inspection of the spectra for $KCoCl_3$, Figure 23, showed two absorption bands centered at 650 mu (15,385 cm^{-1}) and 1800 mu

FIGURE 13

ATTACHMENT USED TO OBTAIN LOW TEMPERATURE SPECTRA

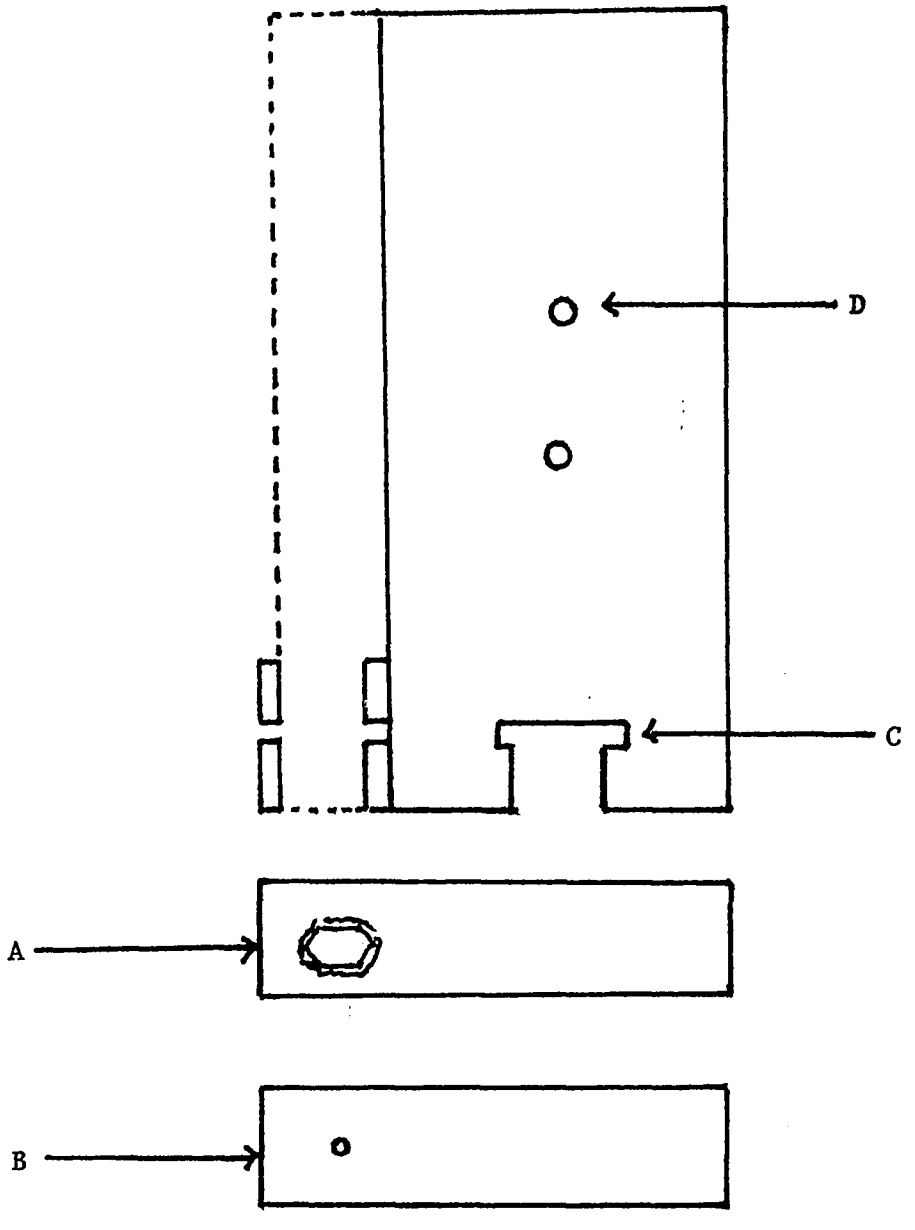

(5,500 cm^{-1}). These absorptions are characteristic of Co(II) tetrahedral complexes. (34) Assuming tetrahedral symmetry, the ground state for $KCoCl_3$ is $^4A_2$. (See Figure 15) The two observed transitions were tenatively assigned to the $^4T_1(P)$ and the $^4T_1(F)$ respectively. The spin allowed transition to the $^4T_2(F)$ is not observed since it is out of the spectral range studied. Dq was assigned 350 cm^{-1} based upon values obtained previously for tetrahedral chlorocobalt complexes. (25) B was assigned 775 cm^{-1}, 80% of the free ion value was predicted from the nephelauxetic series. (35) C/B was set at 4.4, Ds at 100 cm^{-1}, Dt at 50 cm^{-1} and S.O. at -170 cm^{-1} (free ion value). (25)

Spectral assignments were then made for the four spin allowed transitions under D_{4h} symmetry to the $^4E_g(F)$, $^4A_{2g}(F)$, $^4A_{2g}(P)$, and $^4E_g(P)$. The program was allowed to iterate until the best fit was obtained for the spin allowed transitions.

The spin forbidden transition were next assigned using the Tanabe-Sugano Diagram, Figure 14. Using the Dq and B obtained, the $^2T_{2g}$($^2B_{2g}$ and ^2E_g under D_{4h}) was predicted to appear on the high energy side of the $^4T_1(P)$ transition. From the observed spectra a shoulder is observed at 540 mu (18,500 cm^{-1}) which was assigned to the $^2T_{2g}$. All other parameters were fixed except C/B, and the program was allowed to iterate until the best fit for the spin forbidden transitions were obtained.

The next spectra to be fitted was the tetrahydrate, Figure 18. From the experimental spectra three absorption bands are observed. These are centered at 550 mu (18,300 cm^{-1}), 690 mu (14,500 cm^{-1}), and 1540 mu (6500 cm^{-1}). Assuming octahedral symmetry, the ground state was assigned

FIGURE 14

TANABE-SUGANO DIAGRAM FOR Cr(III) d^3

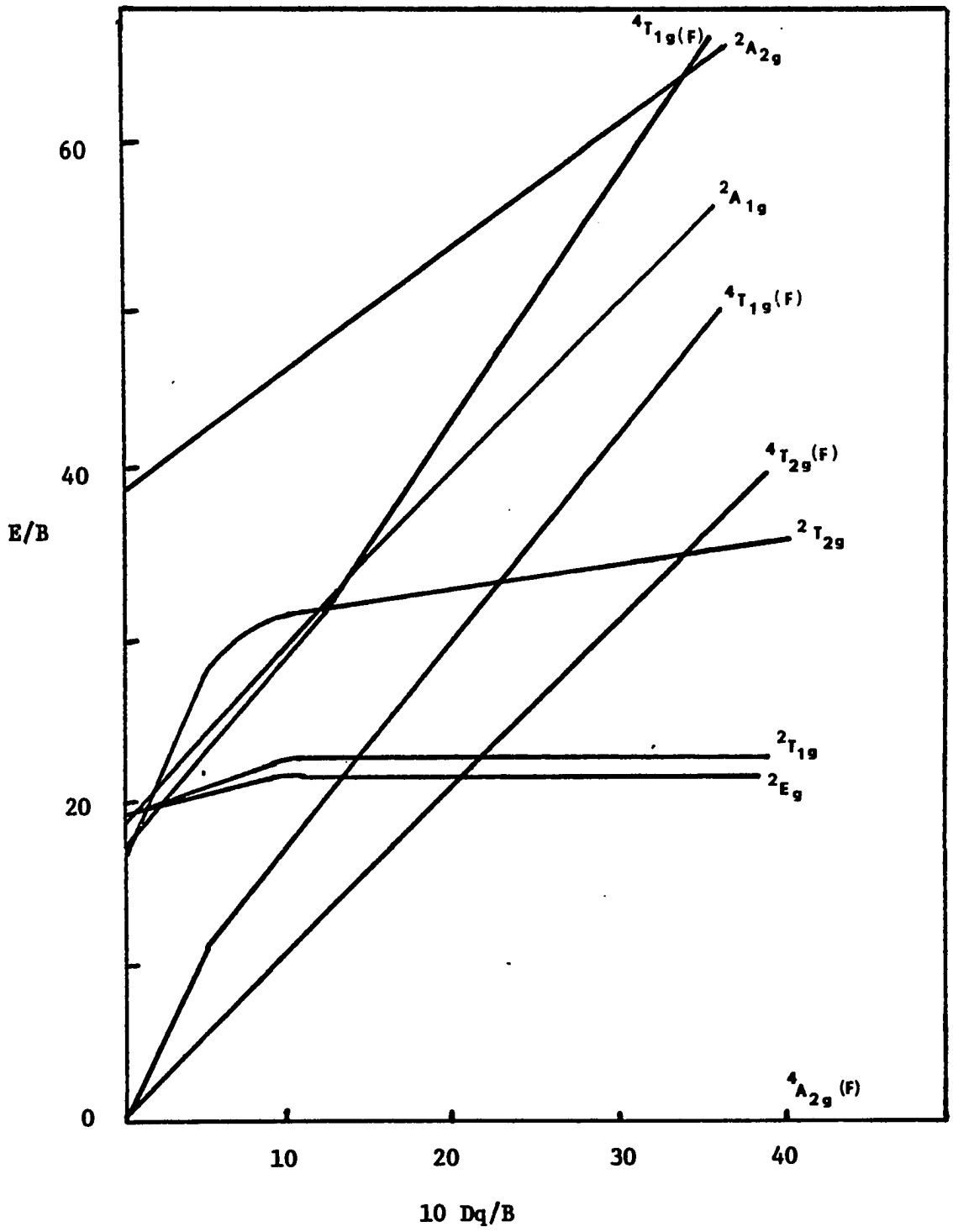

FIGURE 15

ENERGY LEVEL DIAGRAM FOR TETRAHEDRAL d^7 CONFIGURATION

SPIN ALLOWED

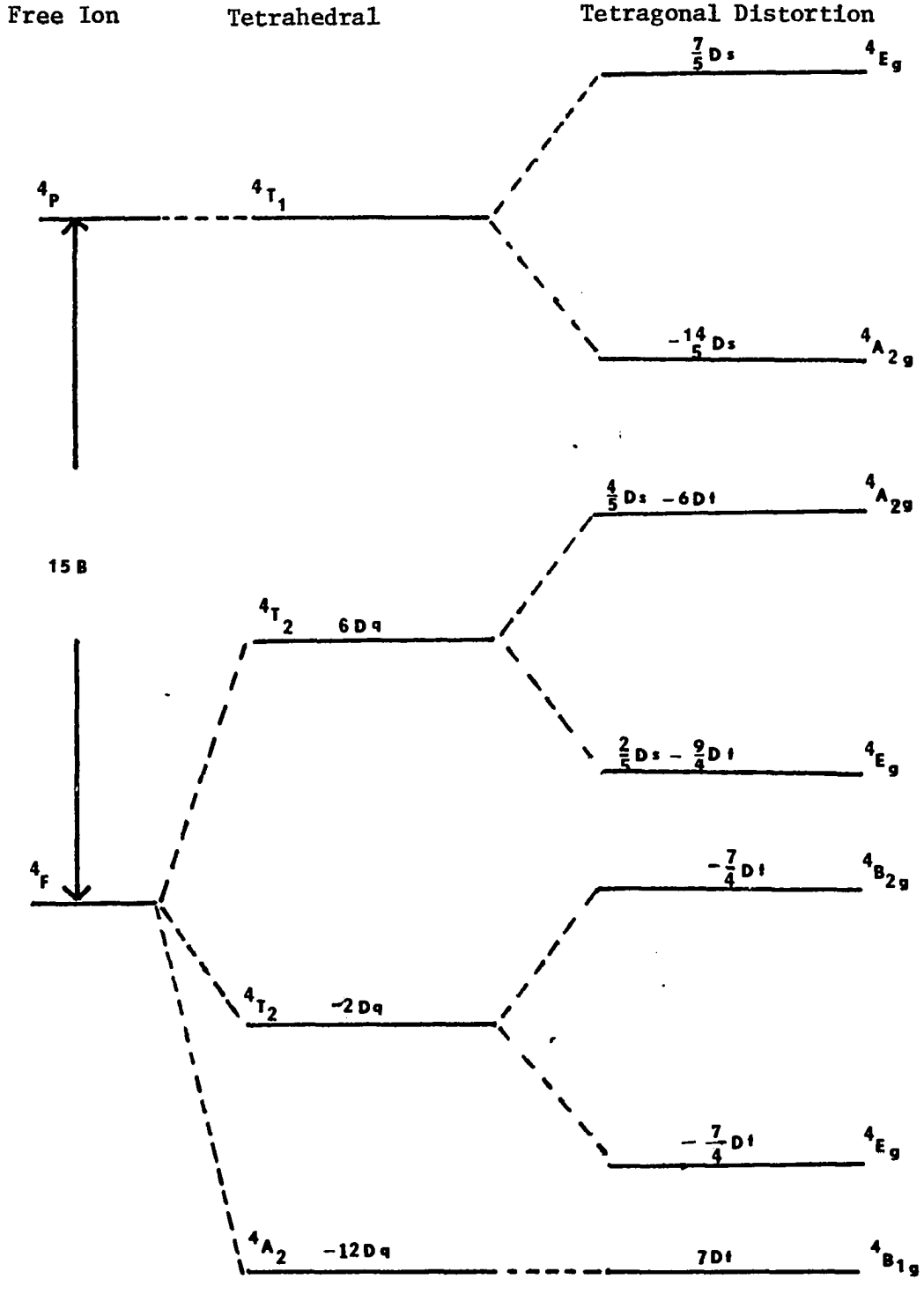

Reverse for Octahedral

to the $^4T_{1g}$ with transitions to the $^4T_{1g}(P)$, $^4A_{2g}(F)$, and $^4T_{2g}(F)$, Figure 15. The transition to the $^4A_{2g}(F)$ is a two electron transition and is very low in intensity (36). Dq was set at 840 cm^{-1} obtained from the $^4A_{2g}(F)$ transition, B was set at 860 cm^{-1} based on the position of H_2O and Cl^- ion in the nephelauxetic series, (35) C/B at 4.4, Ds at 100 cm^{-1}, Dt at 50 cm^{-1}, and S.O. at -170 cm^{-1}.

The program was permitted to iterate the spectral parameters until the best fit was obtained for the spin allowed transitions.

From the Tanabe-Sugano Diagram, Figure 13, using the determined values for Dq and B, the ^2E_g is predicted at a slightly lower energy than the $^4A_{2g}$ transition. Upon observing the experimental spectra, a weak transition was observed at 960 mu (10,400 cm^{-1}). This shoulder was assigned to the ^2E_g transition. Fixing all parameters except C/B, the program was again used to obtain the spin forbidden assignments.

Spectral parameters for the trihydrate and dihydrate were obtained using the same procedure assuming some type of tetragonal distortion.

A suitable fit for the monhydrate spectra could not be obtained assuming tetragonal distortion. The possibility that trigonal distortion could be present was investigated because of the failure to assign the observed transition at 520 mu (19,250 cm^{-1}), Figure 22. Assuming a tetrahedral symmetry, the two absorption bands in the visible region were assigned to the $^4T_1(P)$. The broad band in the near IR region was assigned to the $^4T_1(F)$. Using the energy diagram, Figure 16, the spectral parameters were obtained using first order calculations. A Dq of 300 cm^{-1}, B of 840 cm^{-1}, $D\sigma$ of 916 cm^{-1}, $D\tau$ of -170 cm^{-1} were obtained.

These values were then entered in the D_{3d} program for iteration. The D_{3d} program iterated the assigned parameters giving the best fit for the spin allowed transitions. No attempt was made to fit the spin forbidden transitions for the monohydrate. Attempts were made to fit the monohydrate spectra using other symmetries without success.

The collected spectra data is show in Table 24 giving the predicted transitions and the observed transitions. Table 25 gives a summary of the spectral parameters obtained for each of the four hydrated species and the anhydrate.

Summary

Attempts were made to fit the spectra of the upper hydrates using both $^4A_{2g}$ and ^4E_g ground states. The signs of Ds and Dt were varied to give all possible combinations. The anhydrous $KCoCl_3$ was fitted using tetrahedral symmetry with tetragonal distortion obtaining reasonable results. The monohydrate was the most difficult of all the species to obtain a reasonable fit, however, if tetrahedral symmetry was assumed with trigonal distortion a reasonable fit was obtained.

The Dq values varied from 819 cm^{-1} for the $KCoCl_3 \cdot 4H_2O$ to 260 cm^{-1} for the $KCoCl_3 \cdot H_2O$ with a value of 350 cm^{-1} for $KCoCl_3$. B values decreased as the water molecules were replaced from the Co(II) ion by chloride ions. Ds and Dt or $D\sigma$ and $D\tau$ values indicated the magnitude of distortion present and the shift in ground states. The spin-orbit coupling constant was held at -170 cm^{-1} throughout the spectral fitting. The ratio of C/B ranged between 4.18 for the $KCoCl_3 \cdot 2H_2O$ to 4.4 for $KCoCl_3 \cdot H_2O$ which lie in the range predicted for Co(II) complexes with water and chloride as ligands. (25)

FIGURE 16

ENERGY LEVEL DIAGRAM FOR TETRAHEDRAL d^7 CONFIGURATION

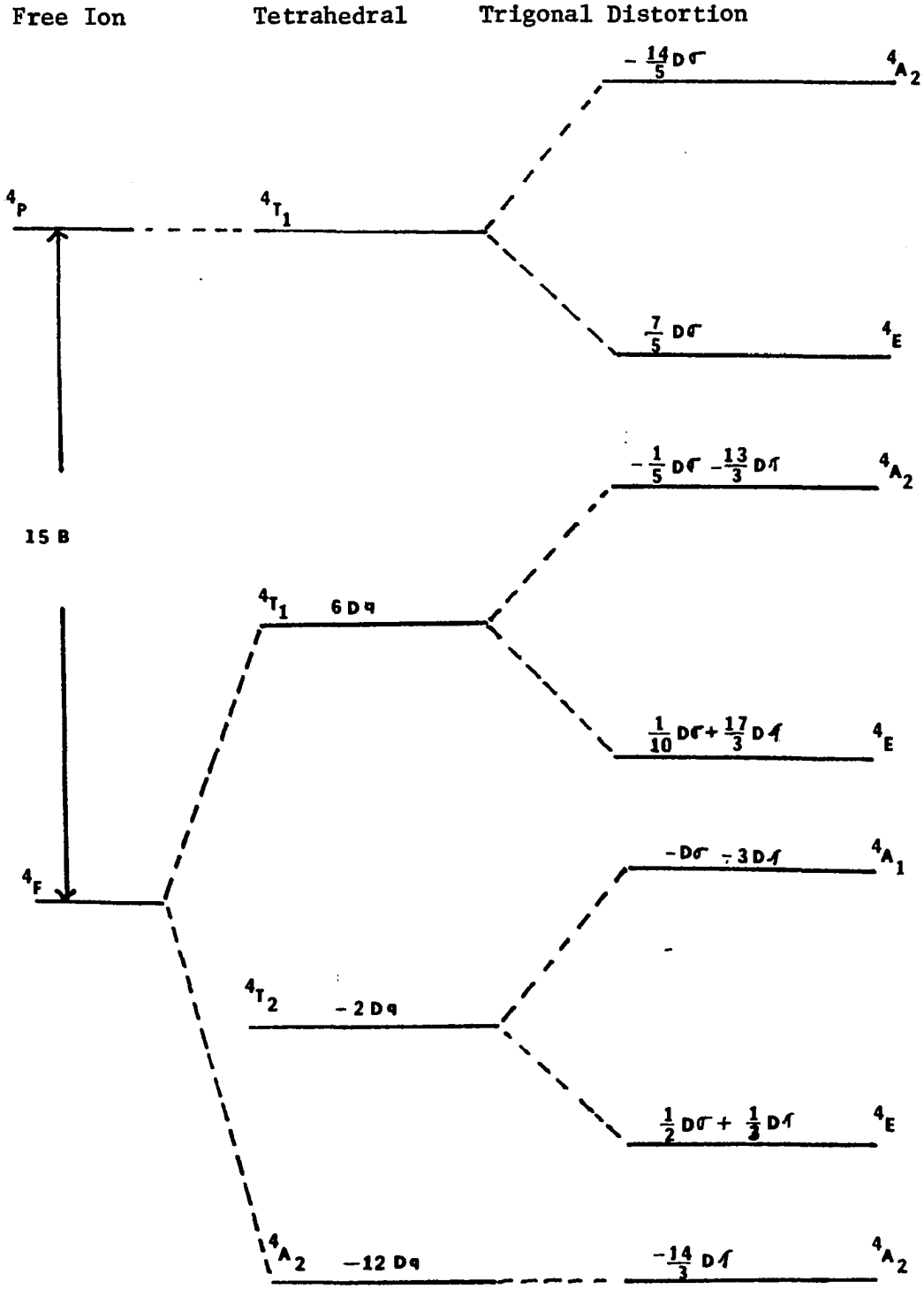

FIGURE 17

TANABE-SUGANO DIAGRAM FOR Co(II) d^7

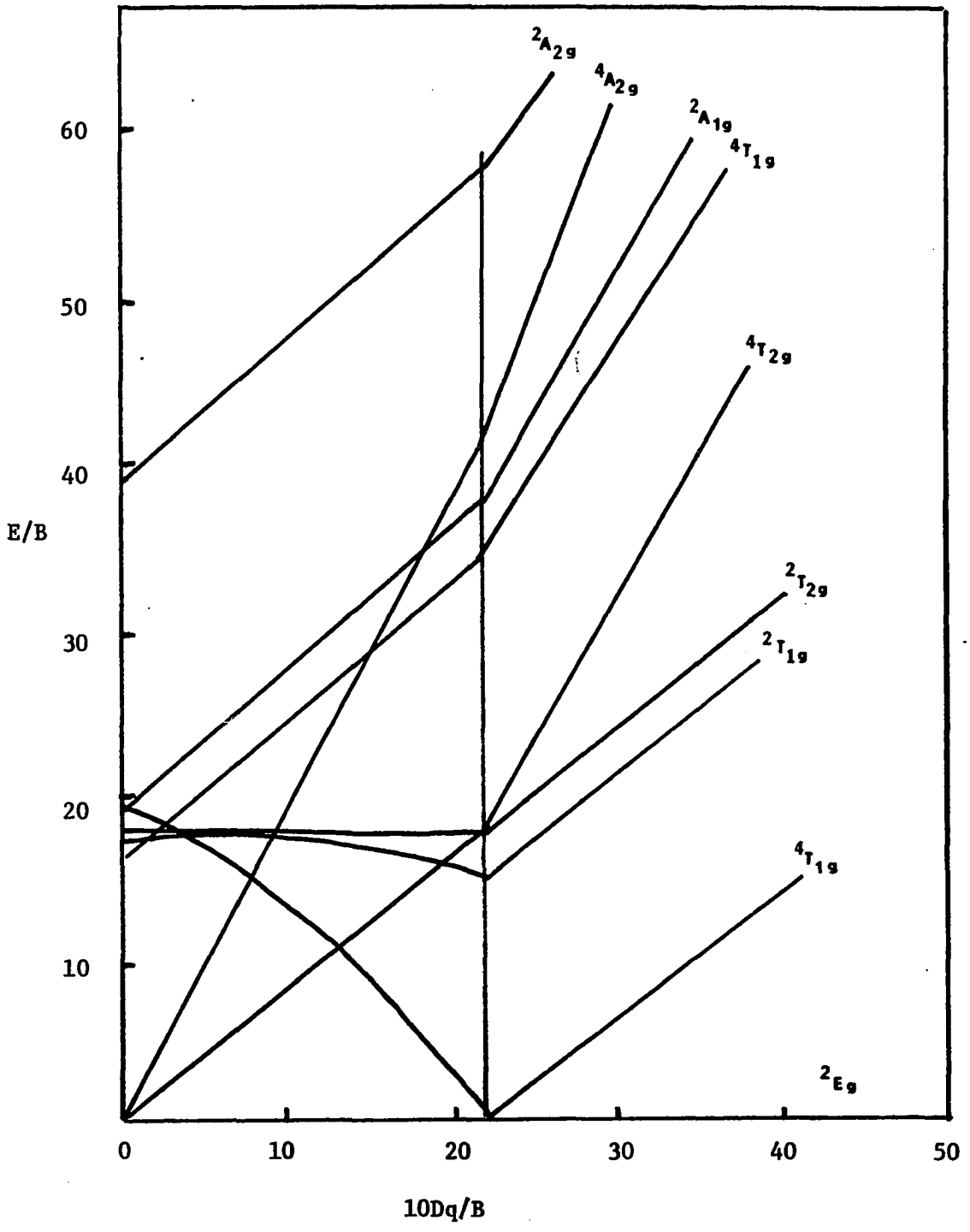

FIGURE 18

CRYSTAL SPECTRUM OF $KCoCl_3 \cdot 4H_2O$

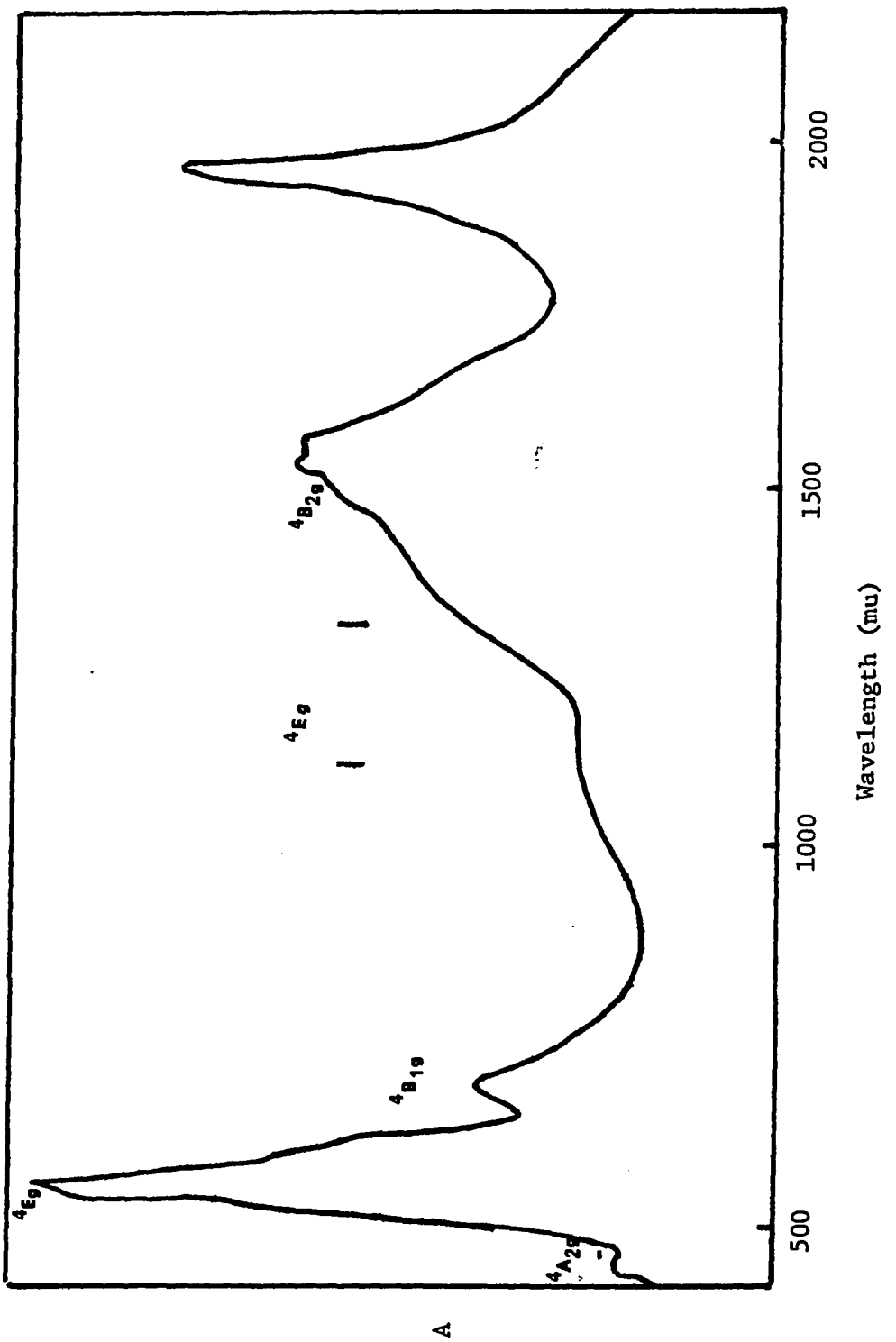

FIGURE 19

REFLECTANCE SPECTRUM OF $KCoCl_3 \cdot 4H_2O$

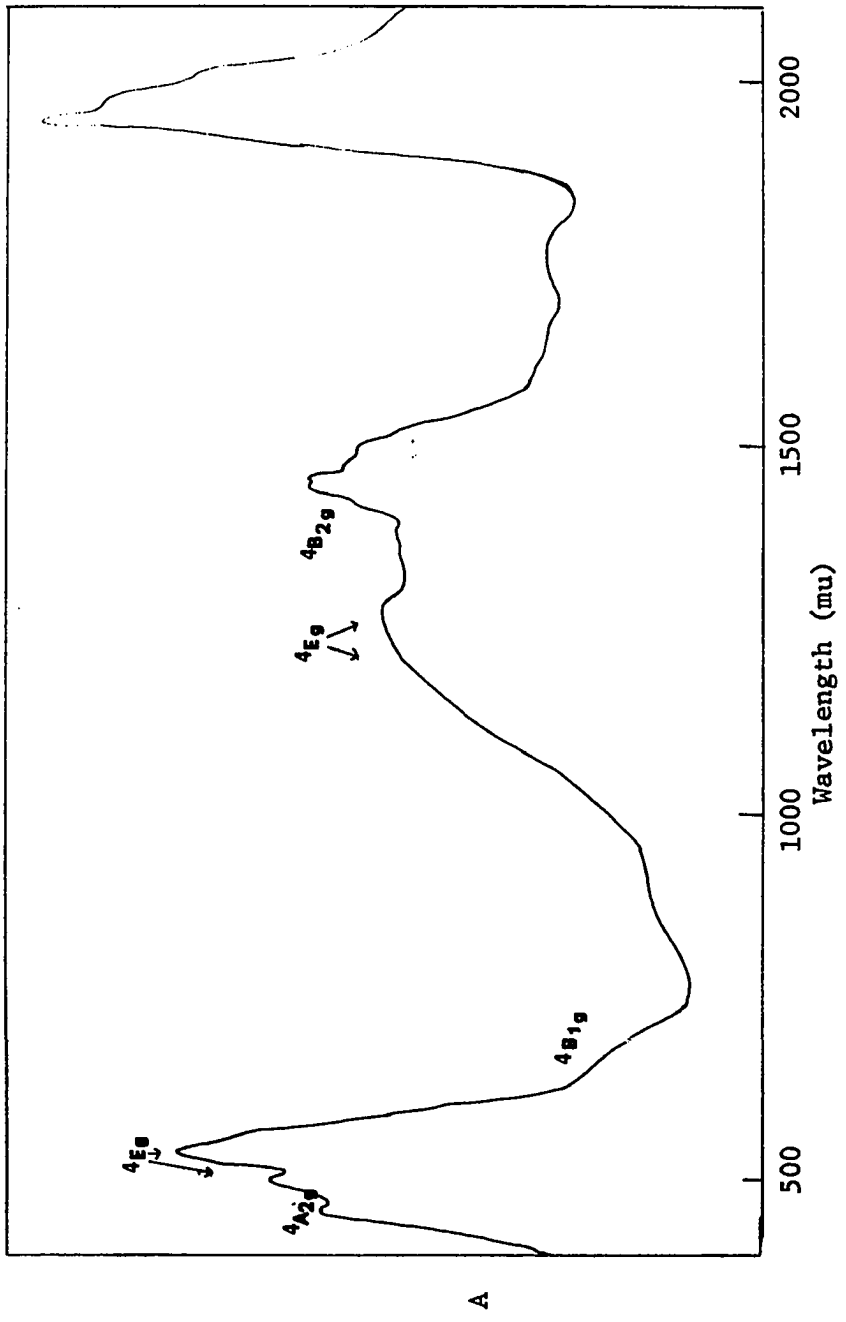

FIGURE 20

REFLECTANCE SPECTRUM OF $KCoCl_3 \cdot 3H_2O$

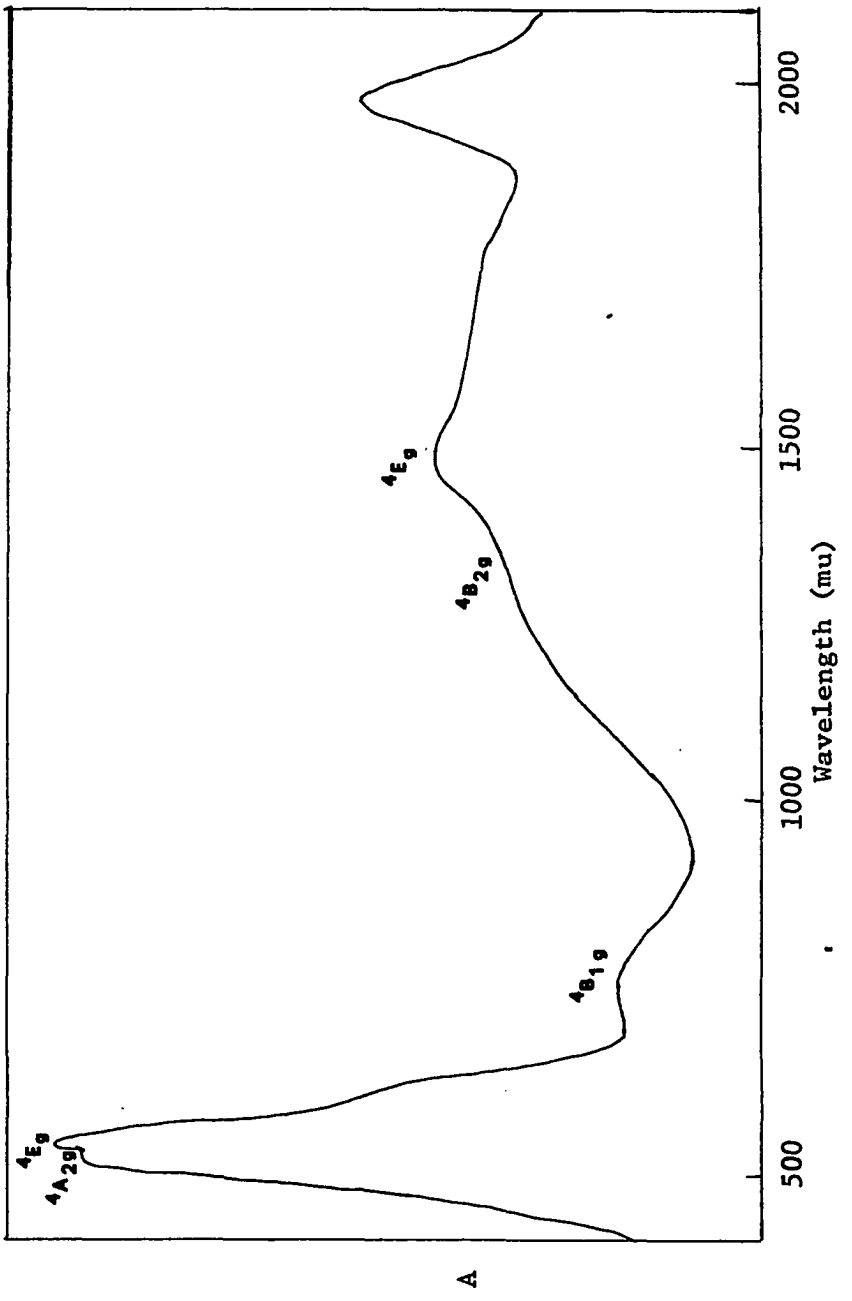

FIGURE 21

REFLECTANCE SPECTRUM OF $KCoCl_3 \cdot 2H_2O$

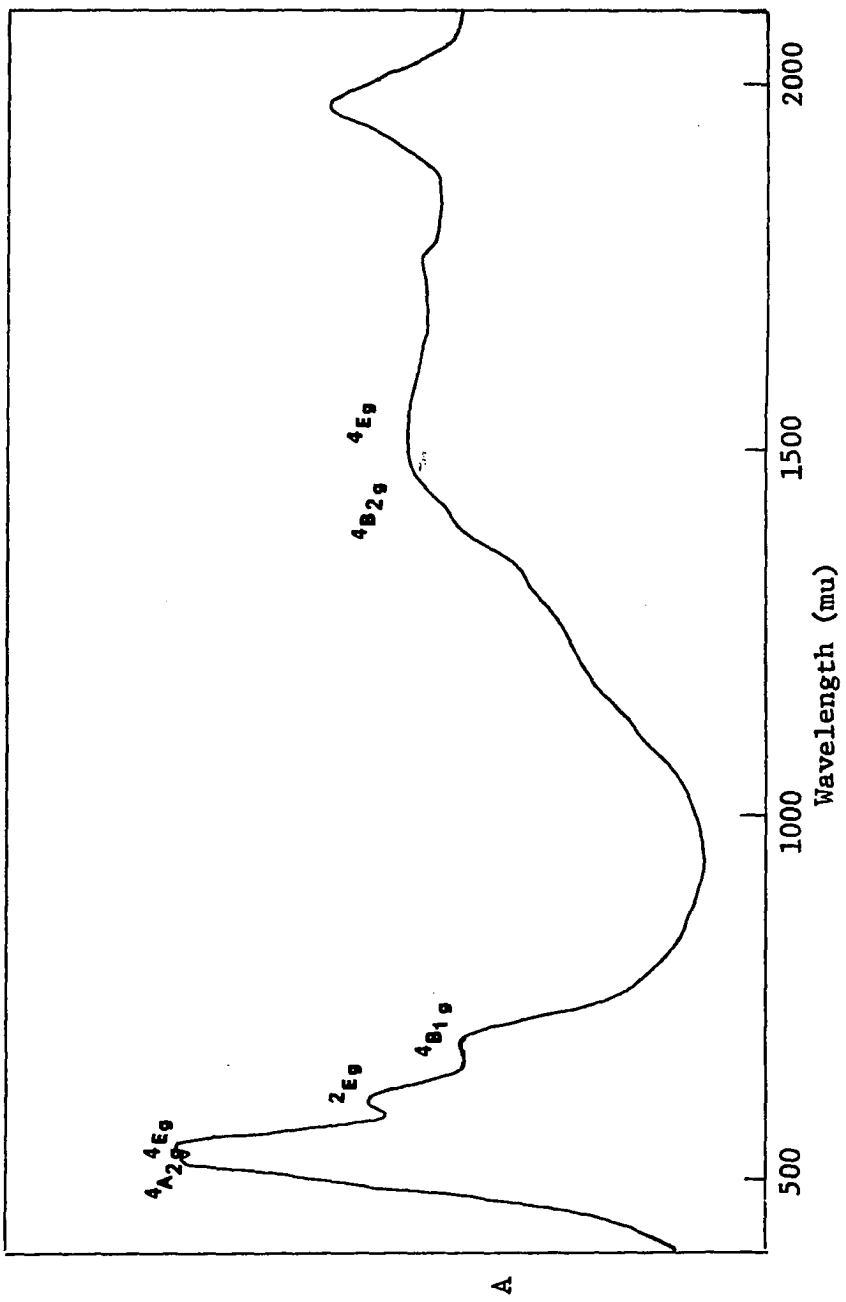

FIGURE 22

REFLECTANCE SPECTRUM $KCoCl_3 \cdot H_2O$

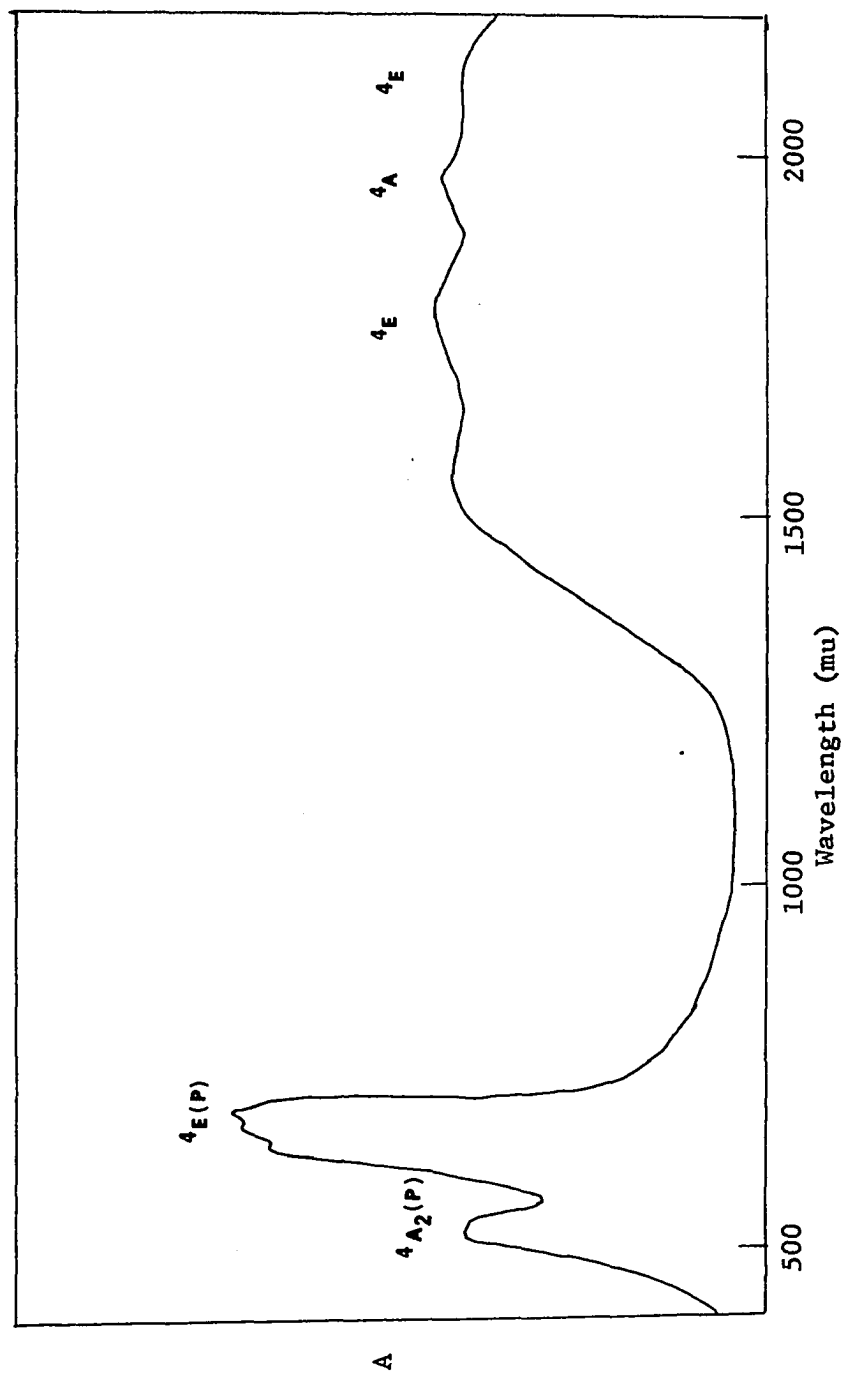

FIGURE 23

REFLECTANCE SPECTRUM OF $KCoCl_3$

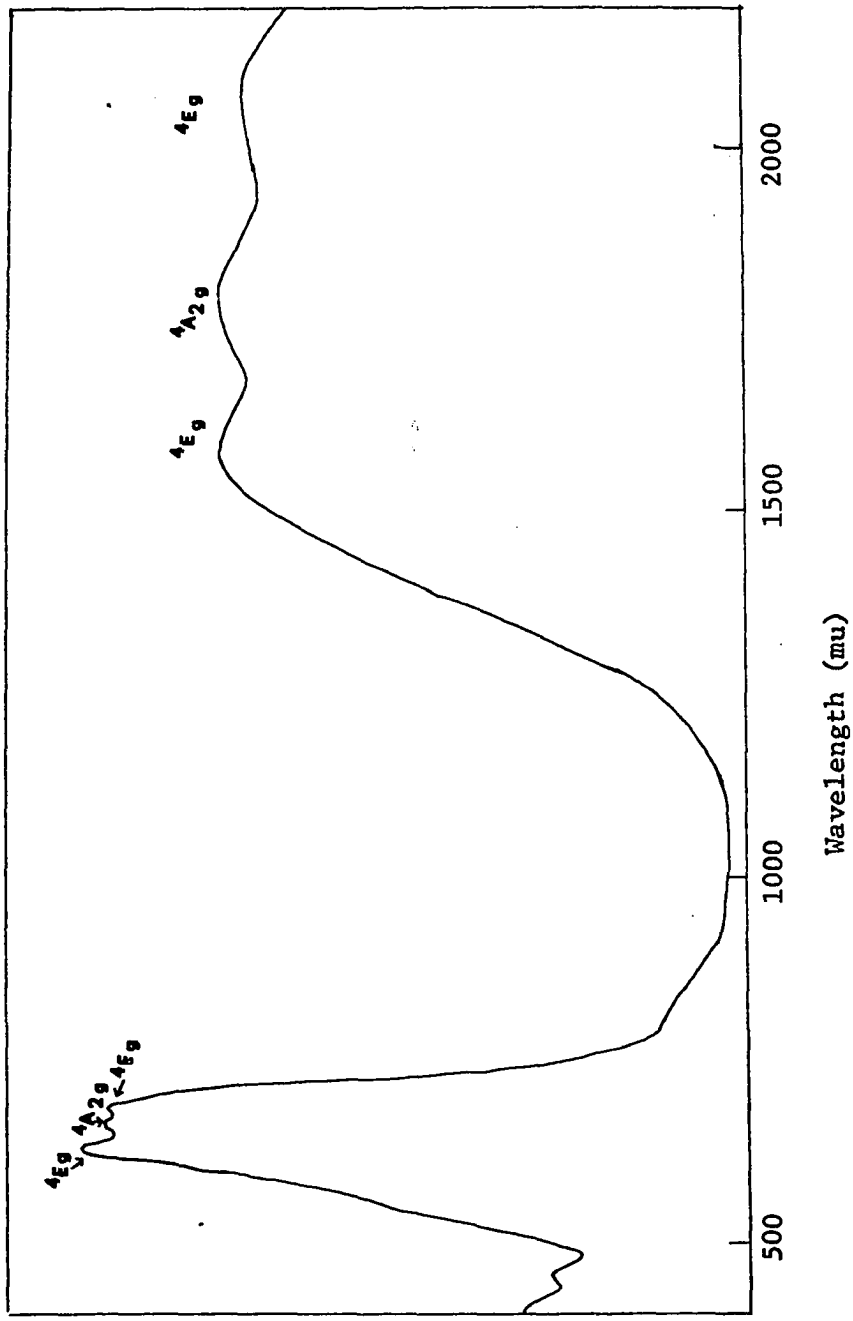

TABLE 24

COLLECTED SPECTRAL DATA

	Transition	Calculated cm^{-1}	Calculated mu	Observed mu	Peak Description
		$KCoCl_3 \cdot 4H_2O$			
1.	$^4A_{2g}$ $^4B_{2g}(T_{2g}F)$	6677	1498	1500	sharp peak
2.	$^4E_g(T_{2g}F)$	7446	1343	1340	broad peak
3.	$^4E_g(T_{2g}F)$	7788	1284	1260	broad peak
4.	$^4B_{1g}(A_{2g}F)$	14,788	676	660	shoulder on $T_{1g}(P)$
5.	$^4E_g(T_{1g}P)$	18,531	540	535	sharp peak
6.	$^4E_g(T_{1g}P)$	19,176	521	520	sharp peak
7.	$^4A_{2g}(T_{1g}P)$	22,192	451	455	medium sharp peak
8.	$^2A_{1g}(E_gG)$	10,073	993	960	broad peak
9.	$^2B_{1g}(E_gG)$	12,910	775		not observed
10.	$^2E_g(T_{2g}G)$	16,312	613	625	shoulder on $T_{1g}(P)$
11.	$^2E_g(T_{2g}G)$	17,837	561		not observed
12.	$^2B_{2g}(T_{1g}G)$	18,657	536		not observed
13.	$^2E_g(T_{1g}G)$	21,273	470	490	very sharp peak
14.	$^2E_g(T_{1g}G)$	25,221	396		not observed
15.	$^2A_{1g}(A_{1g}G)$	22,462	445		not observed
		$KClCl_3 \cdot 3H_2O$			
1.	$^4A_{2g}$ $^4B_{2g}(T_{2g}F)$	6857	1458		broad peak
2.	$^4E_g(T_{2g}F)$	6554	1526		broad peak
3.	$^4E_g(T_{2g}F)$	6894	1451		broad peak
4.	$^4B_{1g}(A_{2g}F)$	13,872	721	740	broad peak partially hidden

TABLE 24-Continued

	Transition	Calculated cm^{-1}	Calculated mu	Observed mu	Peak Description
		$KCoCl_3 \cdot 3H_2O$ continued			
5.	$^4A_{2g}$ ^4E_g ($T_{1g}P$)	18,075	553	545	very sharp
6.	^4E_g ($T_{1g}P$)	18,716	534	535	very sharp
7.	$^4A_{2g}$($T_{1g}P$)	19,353	517	520	very sharp
8.	$^2A_{2g}$(E_g G)	10,238	976		not observed
9.	$^2B_{1g}$(E_g G)	10,763	929		not observed
10.	$^2B_{2g}$(T_{2g}G)	16,652	601	607	shoulder on very sharp peak
11.	^2E_g (T_{2g}G)	16,258	615	610	shoulder on very sharp peak
12.	^2E_g (T_{2g}G)	16,068	622	617	shoulder on very sharp peak
13.	$^2B_{2g}$(T_{1g}G)	23,482	426		not observed
14.	^2E_g (T_{1g}G)	20,292	493		not observed
15.	^2E_g (T_{1g}G)	23,549	425		not observed
		$KCoCl_3 \cdot 2H_2O$			
1.	^4E_g $^4A_{2g}$(T_{1g}P)	19,322	517	519	sharp peak
2.	^4E_g (T_{1g}P)	19,297	518	520	sharp peak
3.	^4E_g (T_{1g}P)	18,666	536	540	sharp peak
4.	$^4B_{1g}$(A_{2g}F)	14,367	696	690	shoulder on sharp peak
5.	$^4B_{2g}$(T_{2g}F)	7,227	1383	1385	broad peak
6.	^4E_g (T_{2g}F)	7,069	1415	1420	broad peak
7.	^4E_g (T_{2g}F)	6,729	1486	1500	broad peak
8.	$^2B_{1g}$(E_g G)	10,263	974		not observed

TABLE 24-Continued

	Transition	Calculated cm^{-1}	Calculated mu	Observed mu	Peak Description
		$KCoCl_3 \cdot 2H_2O$ continued			
9.	^4E_g $^2A_{1g}(E_g\ G)$	10,255	975		not observed
10.	^2E_g $(T_{2g}G)$	16,137	620	615	shoulder on sharp peak
11.	^2E_g $(T_{2g}G)$	16,243	616	605	shoulder on sharp peak
12.	^2E_g $(T_{1g}G)$	20,366	491	495	shoulder on sharp peak
13.	^2E_g $(T_{1g}G)$	23,724	421		not observed
14.	$^2B_{2g}(T_{2g}G)$	16,423	608		shoulder on 10
15.	$^2A_{2g}(T_{1g}G)$	15,847	631		shoulder on 10
		$KCoCl_3 \cdot H_2O$			
1.	$^4A_2$ $^4A_1$ (T_2F)	3,841	2503		not in the region studied
2.	^4E (T_2F)	2,599	3847		not in the region studied
3.	^4E (T_2F)	2,286	4373		not in the region studied
4.	^4E (T_1F)	4,686	2133	2125	broad peak
5.	^4F (T_1F)	5,284	1892	1860	broad peak
6.	$^4A_2$ (T_1F)	4,852	2062	2075	broad peak
7.	^4E (T_1P)	15,630	639	630	sharp peak
8.	^4F (T_1P)	15,345	651	660	sharp peak
9.	$^4A_2$ (T_1P)	19,250	519	520	medium peak
		$KCoCl_3$			
1.	$^4B_{1g}$ $^4E_g(T_2F)$	3,303	3,027		not in region studied
2.	$^4E_g(T_2F)$	2,968	3,369		not in region studied
3.	$^4B_{2g}$	3,502	2,855		not in region studied

TABLE 24-continued

	Transition	Calculated cm^{-1}	Calculated mu	Observed mu	Peak Description
		$KCoCl_3$ continued			
4.	$^4B_{1g}$ ^4E_g (T_1 F)	5,098	1,961		broad peak
5.	^4E_g (T_1 F)	6,087	1,642		broad peak
6.	$^4A_{2g}$(T_1 F)	5,330	1,876	1,825	broad peak
7.	^4E_g (T_1 P)	15,878	630	630	sharp peak
8.	^4E_g (T_1 P)	15,225	657	670	sharp peak
9.	$^4A_{2g}$(T_1 P)	15,286	654	652	sharp peak
10.	$^2A_{1g}$(A_1 G)	14,387	695		not observed
11.	$^2A_{2g}$(T_1 G)	14,875	672		not observed
12.	^2E_g (T_1 G)	14,812	675		not observed
13.	^2E_g (T_1 G)	16,596	602	610	very sharp peak
14,	$^2B_{2g}$(T_2 G)	19,175	522	530	shoulder on very sharp peak
15.	^2E_g (T_2 G)	18,864	530	530	shoulder on very sharp peak
16.	^2E_g (T_2 G)	19,328	517		not observed
17.	$^2A_{1g}$(E_g G)	16,096	621		not observed
18.	$^2B_{1g}$(E_g G)	20,679	484		not observed

TABLE 25

SPECTRAL FITTING PARAMETERS

Compound	Dq	B'	C'/B	Ds or Dσ	Dt or Dτ	B'/B
$KCoCl_3 \cdot 4H_2O$	819	893	4.33	671	127	0.92
$KCoCl_3 \cdot 3H_2O$	709	856	4.26	168	-9	0.88
$KCoCl_3 \cdot 2H_2O$	722	868	4.18	-46	32	0.89
$KCoCl_3 \cdot H_2O$	260	860	4.40	821	-16	0.89
$KCoCl_3$	352	752	4.37	98	47	0.78

CHAPTER FIVE

MAGNETIC MOMENTS

Discussion

The magnitude of the magnetic moments are useful when used in conjunction with the electronic spectra to establish the symmetry and electronic ground state of cobalt (II) complex compounds. As previously mentioned in Chapter Four, there are two possibilities for the ground state in complexes with d^7 electron configuration considering only octahedral and tetrahedral symmetry. These are the $^4T_{1g}$ for octahedral complexes and the $^4A_2$ for the tetrahedral complexes.

Assuming perfect octahedral or tetrahedral symmetry, the ground electron distribution for Co (II) ion under the influence of weak field ligands such as Cl^- and/or H_2O is given in the diagram below. Both electron configurations result in three unpaired electrons.

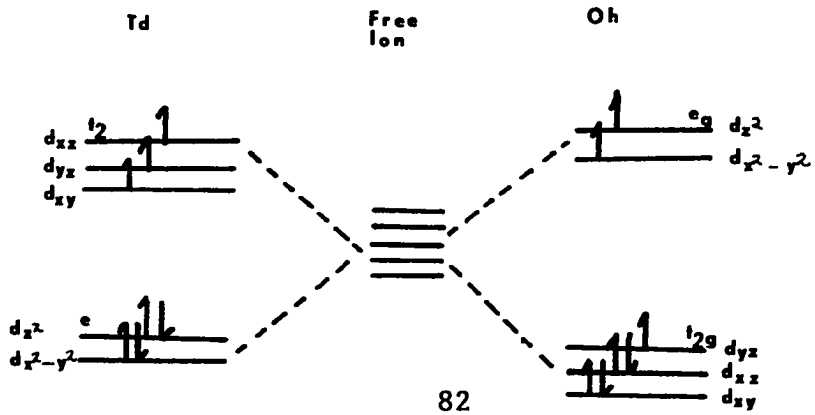

Since both octahedral and tetrahedral environments result in three unpaired electrons, the magnetic moment based upon the spin angular momentum only has the same value as that found from the expression

$$\mu_{eff} = [n(n + 2)]^{1/2} \qquad (1)$$

where n is the number of unpaired "d" electrons. This value for three unpaired electrons is 3.87 Bohr magnetons.

In addition to the spin angular contribution there is the orbital contribution to the total magnitude of the magnetic moment exhibited by a complex. If the electrons of the Co (II) ion could be free of the influence of the crystal field and spin-orbit coupling, such as would be found in the free ion, the effective magnetic moment would be given by the sum of the spin and orbital contributions as shown by

$$\mu_{eff} = [4S(S + 1) + L(L + 1)]^{1/2} \text{ B.M.} \qquad (2)$$

This would give an effective magnetic moment of 5.20 B. M. for an S (spin angular momentum) value of 3/2 and L(orbital angular momentum) value of 3. For cobalt (II), values close to 5.20 B. M. are observed experimentally for octahedral complexes with values less than this for tetrahedral complexes. This suppressing of the orbital contribution can be qualitatively explained by consideration of the crystal field effects upon the "d" orbitals.

For octahedral complexes the orbital contribution to the magnetic moment can be shown by the rotation property of the "d" orbitals.

In order for an electron to have an orbital angular moment and therefore an orbital moment with reference to an axis, it must be able to transform into an equivalent orbital by rotation about that axis. This requires the availability of an orbital with the same shape and degeneracy as the orbital containing the electron.

In the free ion, rotation of the $d_{x^2-y^2}$ orbital by 45° about the "z" axis brings it into the d_{xy} orbital. The d_{yz} rotated by 90° brings it into the fully equivalent d_{xz}. This leads to an orbital contribution to the total magnetic moment.

If the ion is placed in an octahedral environment, the degeneracy of the five "d" orbitals is removed into equivalent d_{xy}, d_{xz}, d_{yz} set and a $d_{x^2-y^2}$ and d_{z^2} set. The d_{xy} cannot be rotated into a fully equivalent $d_{x^2-y^2}$ by rotation about the "z" axis because of the energy difference caused by a crystal field, however, the d_{yz} and d_{xz} can still transform into equivalent orbitals. This gives a contribution to the total magnetic moment from the orbital moment for the $t_{2g}^5 e_g^2$ or $^4T_{1g}$ electronic ground state.

For tetrahedral symmetry, the splitting of the five "d" electron orbitals are identical with that of the octahedral symmetry but reversed. The electron configuration of $e^4t_2^3$ results in a filled "e" level and a half-filled "t_2" level. The d_{xz} and d_{yz} are no longer equivalent by rotation about the "z" axis because the d_{yz} and d_{xz} each already contain one electron. This configuration results in a quenching of the orbital contribution to the total magnetic moment. (37)

It can be shown by group theory arguments that only a "T" ground state will result in an orbital contribution. (25)

In general, the magnitude of the magnetic moment can be used to indicate the symmetry of cobalt (II) complexes. The largest values are found for octahedral coordination ($^4T_{1g}$ ground state) and lower values for tetrahedral coordination ($^4A_2$ ground state). (38)

Some information as to the amount of relative distortion in octahedral complexes can be obtained by noting that when the symmetry is low enough so that the d_{xz} and d_{yz} orbitals no longer transform into one another by having different energies, some of the orbital contribution is suppressed. This can occur in an octahedral complex by elongation or compression of the "z" axis.

Theory of Magnetic Susceptibilities

The magnetic susceptibility for singlet A_1 or A_2 ground states with excited states large compared to kT can be calculated using the following equations (23)

$$\chi = N\left[\sum_{nm} \frac{(E_{om}^{(1)})^2}{J_m kT} - 2 \sum_{nm} \frac{E_{om}^{(2)}}{J_m} \right] \tag{3}$$

where

$$E_{om}^{(1)} = \langle \psi_{om} | \mu_i | \psi_{om} \rangle \tag{4}$$

and

$$E_{om}^{(2)} = \Sigma | (\psi_{om} | \mu_i | \psi_{nm}) |^2 \tag{5}$$

with

$$\mu_i = \beta(\hat{L}_i + 2\hat{S}_i)$$

where j_m is the multiplicity of the ground state, β is the Bohr magneton, $\hat{L}_i$ is the operator for the orbital angular momentum and $\hat{S}_i$ is the operator for the spin angular momentum.

The first term in equation (3) gives the energy contribution of the first order Zeeman effect on the nth level due to the magnetic field acting on that level. The second term gives the energy contribution due to second order Zeeman effect arising from the change in energy due to "mixing-in," influenced by the magnetic field, of levels which originally were not degenerate with the nth level. The first and second terms in equation (3) are called respectively the low and high frequency terms.

Assuming $E_o - E_n >>$ [illegible] regarding the second term of (3), the temperature depende[illegible] magnetic susceptibility is given by

$$\chi_{1f}$$ [illegible] (6)

where "g" is the sp[illegible] the amount of orbital contribution possessed [illegible] for the free ion, the Lande splitting factor is obta[illegible]

$$g = 1 + \frac{S(S + 1) - L(L + 1) + J(J + 1)}{2J(J + 1)} \qquad (7)$$

If L is zero (no orbital contribution) then "g" is 2.00 which is the case when spin angular momentum only accounts for the magnetic moment.

$$\mu_i = \beta(\hat{L}_i + 2\hat{S}_i)$$

where j_m is the multiplicity of the ground state, β is the Bohr magneton, $\hat{L}_i$ is the operator for the orbital angular momentum and $\hat{S}_i$ is the operator for the spin angular momentum.

The first term in equation (3) gives the energy contribution of the first order Zeeman effect on the nth level due to the magnetic field acting on that level. The second term gives the energy contribution due to second order Zeeman effect arising from the change in energy due to "mixing-in," influenced by the magnetic field, of levels which originally were not degenerate with the nth level. The first and second terms in equation (3) are called respectively the low and high frequency terms.

Assuming $E_o - E_n >> kT$ and disregarding the second term of (3), the temperature dependent contribution to the magnetic susceptibility is given by

$$\chi_{1f} = \frac{N\beta^2 g^2}{3kT} S(S+1) \qquad (6)$$

where "g" is the splitting factor, a measure of the amount of orbital contribution possessed by the ground state. For the free ion, the Lande splitting factor is obtained from

$$g = 1 + \frac{S(S+1) - L(L+1) + J(J+1)}{2J(J+1)} \qquad (7)$$

If L is zero (no orbital contribution) then "g" is 2.00 which is the case when spin angular momentum only accounts for the magnetic moment.

The problem when $L \neq 0$ is to calculate the amount of contribution the orbital momentum contributes to the value of the "g" factor.

Ions with a ligand field symmetry lower than cubic (Oh or Td) show magnetic properties which are anisotopic. (39) The general relationship for "g" in ions showing anisotopic behavior is (23)

$$g = 2(\delta_{ij} - \lambda \Lambda_{ij})$$

where δ_{ij} is known as the Kroneker delta with values of unity when i=j or zero when i≠j, and Λ is given by the expression below (23)

$$\Lambda_{ij} = \sum_{n \neq o} \frac{(\psi_o|\hat{L}_i|\psi_n)(\psi_n|\hat{L}_j|\psi_o)}{E_n - E_o} \qquad (8)$$

In the first order approximation the orbital contribution to the "g" factor is obtained by considering the energy of the interaction between the ground state wave function and the first excited state. This gives a parallel contribution in the "z" direction and a perpendicular contribution in the "x" and "y" direction. The calculated "g" factor for a Co (II) ion in a trigonal field can be shown to give (23)

$$g = 2(1 - \frac{4\lambda}{\Delta_1}) \text{ and } g = 2(1 - \frac{4\lambda}{\Delta_2})$$

where λ is the spin-orbit coupling constant, Δ_1 and Δ_2 being the energy differences between the ground state and the split first upper excited state. A better understanding of Δ_1 and Δ_2 can be obtained from the diagram below. (40)

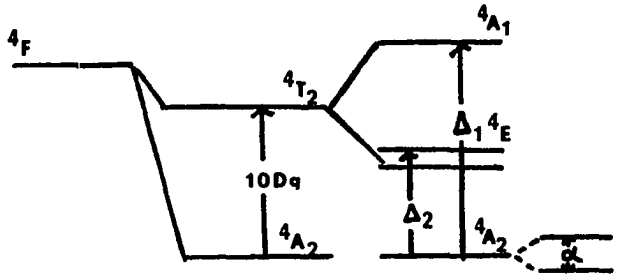

The high frequency term in equation (3) arises from the "mixing-in" of the upper excited state with the ground state by spin-orbit coupling. This is the temperature independent contribution to the magnetic susceptibility. This contribution is determined by summing over the M_s values to give

$$\chi_{hf} = \frac{8N\beta^2}{\Delta_1} \quad \text{and} \quad \chi_{hf} = \frac{8N\beta^2}{\Delta_2}$$

By combining the high frequency and low frequency contributions, the expressions for the total magnetic susceptibility are obtained as shown by

$$\chi_{||} = \frac{15N\beta^2}{3kT}\left(1 - \frac{4\lambda}{\Delta_1}\right)^2 + \frac{8N\beta^2}{\Delta_1} \tag{9}$$

and

$$\chi_{\perp} = \frac{15N\beta^2}{3kT}\left(1 - \frac{4\lambda}{\Delta_2}\right)^2 + \frac{8N\beta^2}{\Delta_2} \tag{10}$$

Using the equation for X_i, a contribution parallel (X_{11}) and a contribution perpendicular ($X_\perp$) to the "z" axis can be calculated.

Under D_4h and D_3d symmetry the "x" and "y" contributions are taken to be equal and the average magnetic susceptibility is given by

$$\bar{\chi} = \frac{(\chi_{11}) + 2(\chi_{\perp})}{3} \tag{11}$$

This average susceptibility should correspond to the susceptibility obtained for a finely ground powdered sample.

The magnetic moment is calculated from the expressions

$$\mu_{11} = \mu_{s.o}(1 - \frac{4\lambda}{\Delta_1}) \tag{12}$$

and

$$\mu_{\perp} = \mu_{s.o}(1 - \frac{4\lambda}{\Delta_2}) \tag{13}$$

Expressions developed here are for the magnetic susceptibility and magnetic moments for the ion in a trigonal field, however, the same result is obtained with the ion in a tetragonal field.

Experimental

The magnetic susceptibility of the complex compounds, $KCoCl_3$, $KCoCl_3 \cdot H_2O$, $KCoCl_3 \cdot 2H_2O$, $KCoCl_3 \cdot 3H_2O$ and $KCoCl_3 \cdot 4H_2O$ were measured using a Faraday type balance, Figure 24. A temperature range of 77° A to 296° A was studied using various coolants.

The coolants used were liquid nitrogen, n-propanol slush, dry-ice-acetone, ice-water, and a circulated cold bath.

A small powered sample of anhydrous compound (0.005 to 0.015

grams) was suspended in a fused quartz bucket (A) attached to a quartz spring (B) by a long rigid fiber (C). The sample mass was determined by measuring the extension of the quartz spring which was previously calibrated. [The force constant for the spring used was found to be 0.19649 cm/mg by adding standard weights to the empty bucket and measuring the distance traveled with cathetometer (D) (± 0.005 cm)]. The quartz spring is attached to the top of the cylindrical vacuum chamber (E) by means of a glass hook. The lower end of the chamber is fitted with a reduced size glass joint to be encased by a Dewar flask (F) specially designed to control the temperature. The entire chamber housing the quartz fiber can be evacuated through a Teflon stopcock (G).

A manometer (H), attached to the housing chamber allows a measurement of the pressure inside the chamber.

A dry inert gas (nitrogen or carbon dioxide) is used to insure thermal contact between the coolant and the sample.

Magnetic susceptibility measurements are made by passing a two pole magnet (I) upward past the sample until the field is entered as noted by the deflection through the cathetometer (J). The magnet is then reversed until maximum deflection is noted just before the sample leaves the magnetic field. The deflection noted through the cathetometer (± 0.0005 cm) is read and recorded. The procedure is repeated for ten (10) readings and then the same procedure is repeated as the sample leaves the magnetic field by moving the magnet upward. This results in a maximum deflection in both directions giving more uniform readings. The total deflection for the sample is one-half the

FIGURE 24

DIAGRAM OF FARADAY TYPE MAGNETIC BALANCE

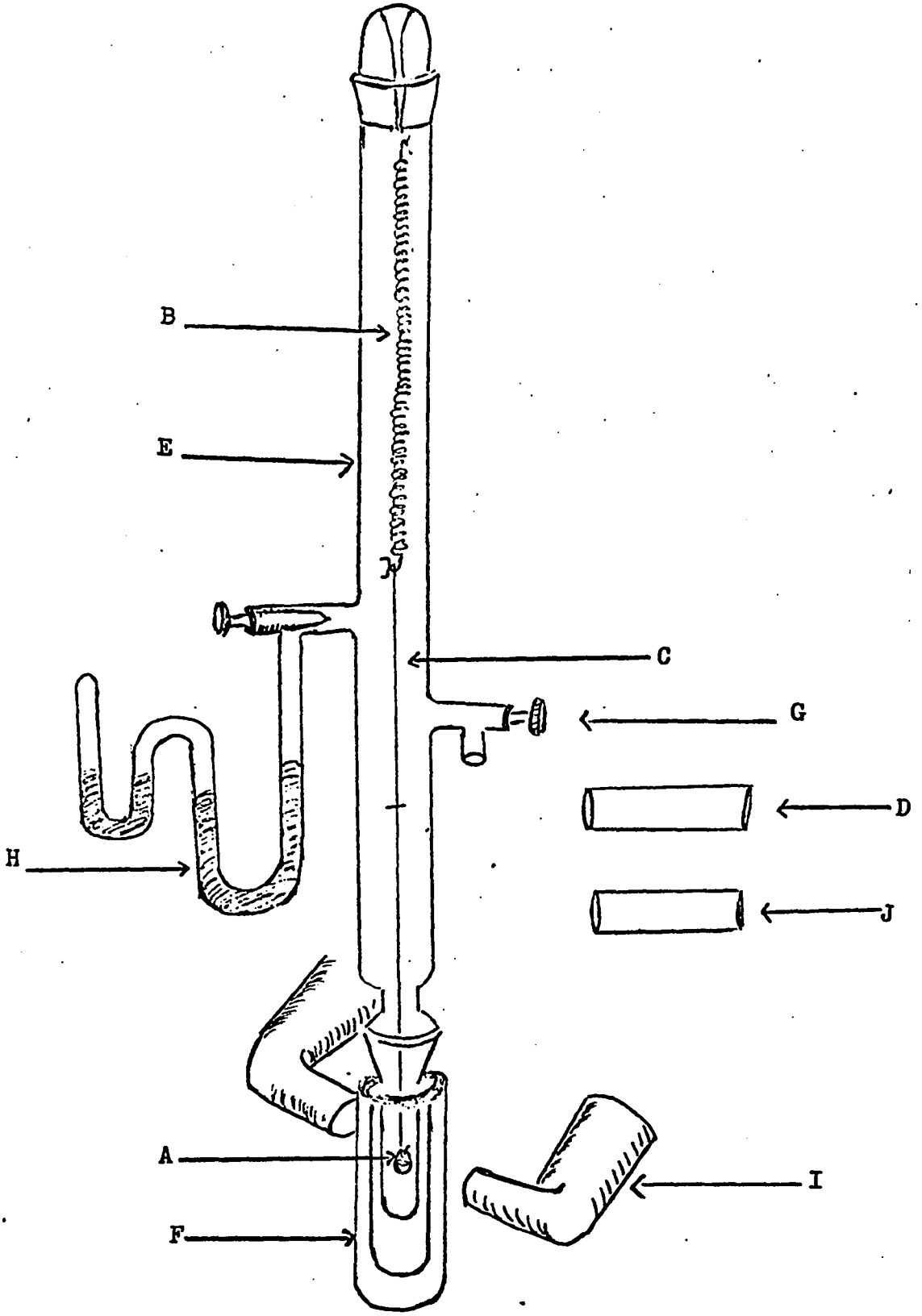

difference of the average upward and downward deflections.

Magnetic susceptibility measurements were made twice for each of the five temperatures or until a variation of not more than 5% is noted. For liquid nitrogen, dry-ice-acetone, n-propanol slush and ice bath, this procedure was used to indicate that an equilibrium with the coolant had been reached. Once the five measurements were determined for $KCoCl_3$, water vapor was permitted to enter through (G) until the $KCoCl_3 \cdot H_2O$ species had been formed as noted by the mass increase. The chamber (E) was evacuated slowly while maintaining a low temperature around the sample to prevent the loss of water vapor by dehydration. After the chamber was evacuated, dry nitrogen was allowed to enter to give thermal conductivity between the coolant and sample.

The same procedure was followed for each of the remaining species ($KCoCl_3 \cdot 2H_2O$, $KCoCl_3 \cdot 3H_2O$ and $KCoCl_3 \cdot 4H_2O$) until five temperatures were studied for each complex hydrate.

Calculations

The total deflection and mass of the sample gave the gram susceptibility, χ_g, at a given temperature from the equation

$$\chi_g = \frac{K(\Delta + \Delta_{dia})}{M} \tag{14}$$

where K is the calibration constant for the Faraday balance, Δ is the total deflection, Δ_{dia} is the diamagnetism for the bucket, and M is the mass of the sample. [The diamagnetism for the bucket used in this study was found to be 0.00190 cm.] The calibration constant for the

balance was found by using a crystalline sample of $HgCo(SCN)_4$ having a known gram susceptibility of ($\chi_g = 16.44 \times 10^{-4}$ cgs at 20°C). (41) The calibration constant (K) was found to be 9.000×10^{-3} c.g.s. for the balance.

The molar susceptibility was found from the equation

$$\chi_m = \chi_g \cdot F.W. \tag{15}$$

where F.W. is the formula weight of the compound.

A correction for the diamagnetism of the cobalt (II) ion and other ligands is added to the experimentally determined, χ_m. The Pascal constants (42) of interest are: cobalt (II), 12×10^{-6}; chloride, 26×10^{-6}; potassium, 13×10^{-6}; water, 13×10^{-6} c.g.s. units. The corrected molar susceptibility is designated by χ_m^c found from the equation

$$\chi_m^c = \chi_m - \Sigma\chi_{dia} \tag{16}$$

The diamagnetic contribution, χ_{dia}, is always negative, therefore, the corrected molar susceptibility is greater than the uncorrected value.

The compounds studies were found to obey the Curie-Weiss Law

$$\chi_m^c = \frac{C_M}{(T + \theta)} \tag{17}$$

where C_M is the Curie constant, θ is the Weiss Constant, and T is the absolute temperature.

The equation can be rearranged to give

$$T = \frac{C_M}{\chi_m^c} - \theta \tag{18}$$

A plot of T versus $(\chi_m^c)^{-1}$, Figures 25-29, gives a straight line with a slope of C_M and an intercept of θ on the T axis.

A more precise statement of the Curie-Weiss Law is

$$\chi_m^c = \frac{C_M}{(T+\theta)} + TIP \tag{19}$$

where TIP is the temperature independent paramagnetism. A plot of χ_m^c versus $(T+\theta)^{-1}$, Figures 29-33, gives a straight line with a slope of C_M and an intercept of TIP.

The Curie constant, C_M, has the value

$$C_M = \frac{N(\mu_{eff})^2\beta^2}{3k} \tag{20}$$

where N is Avogadro's number, k is Boltzmann's constant, μ_{eff} is "the effective magnetic moment," and β is the Bohr magneton, 0.927×10^{-20} erg/gauss. The effective magnetic moment, μ_{eff}, which after the values of the constants are substituted and solved for μ_{eff} gives the equation

$$\mu_{eff} = 2.83(C_M)^{1/2} \tag{21}$$

where C_M is the slope determined from the least square analysis of plots in Figures 30-34. (43) The data analyzed using the above equations gave values of μ_{eff}, θ, and TIP as shown in the summary Table 27.

FIGURE 25

T^{o} A versus $1/X_m^c$ for $KCoCl_3 \cdot 4H_2O$

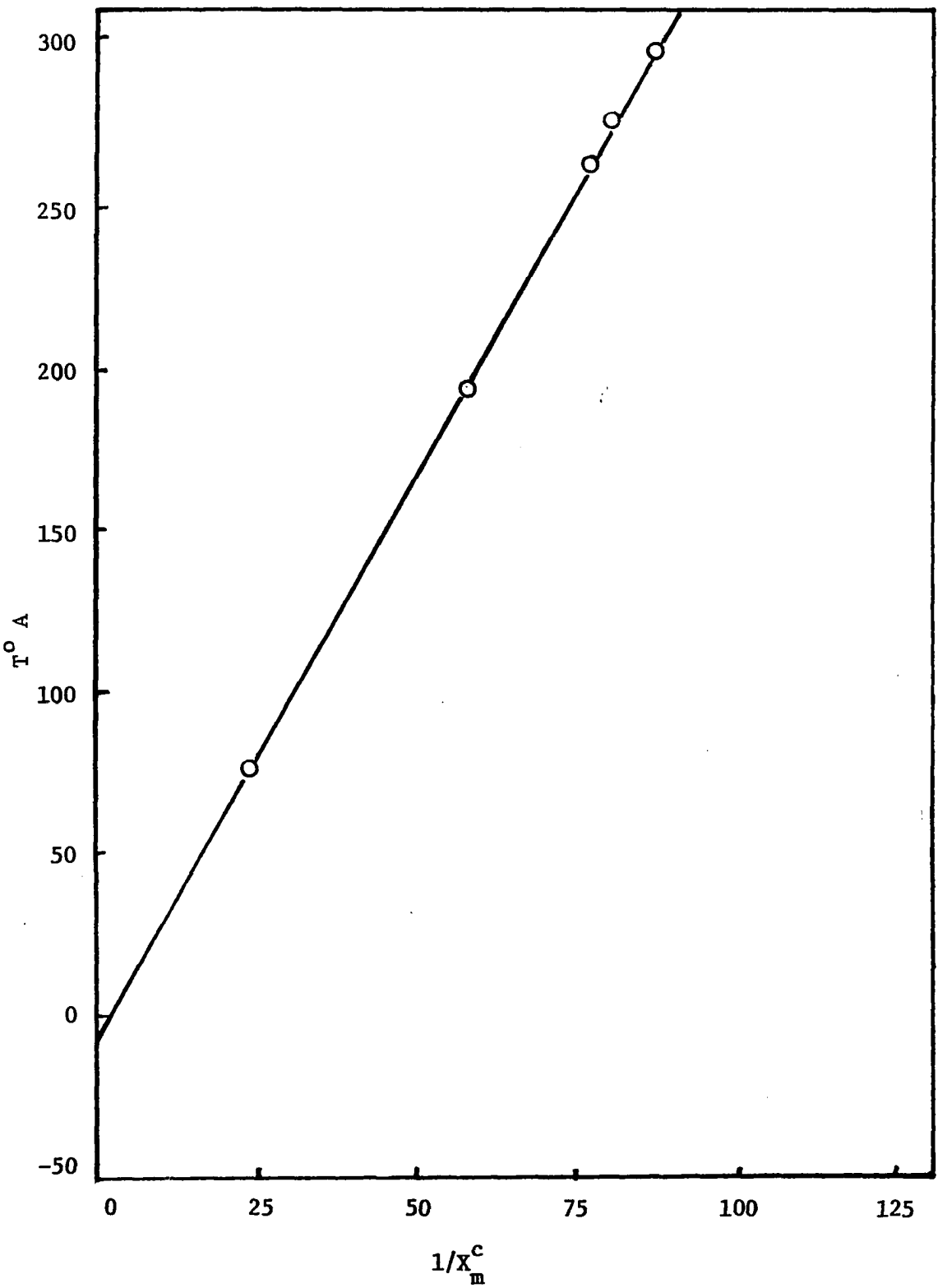

FIGURE 26

T^{o} A versus $1/X_m^c$ for $KCoCl_3 \cdot 3H_2O$

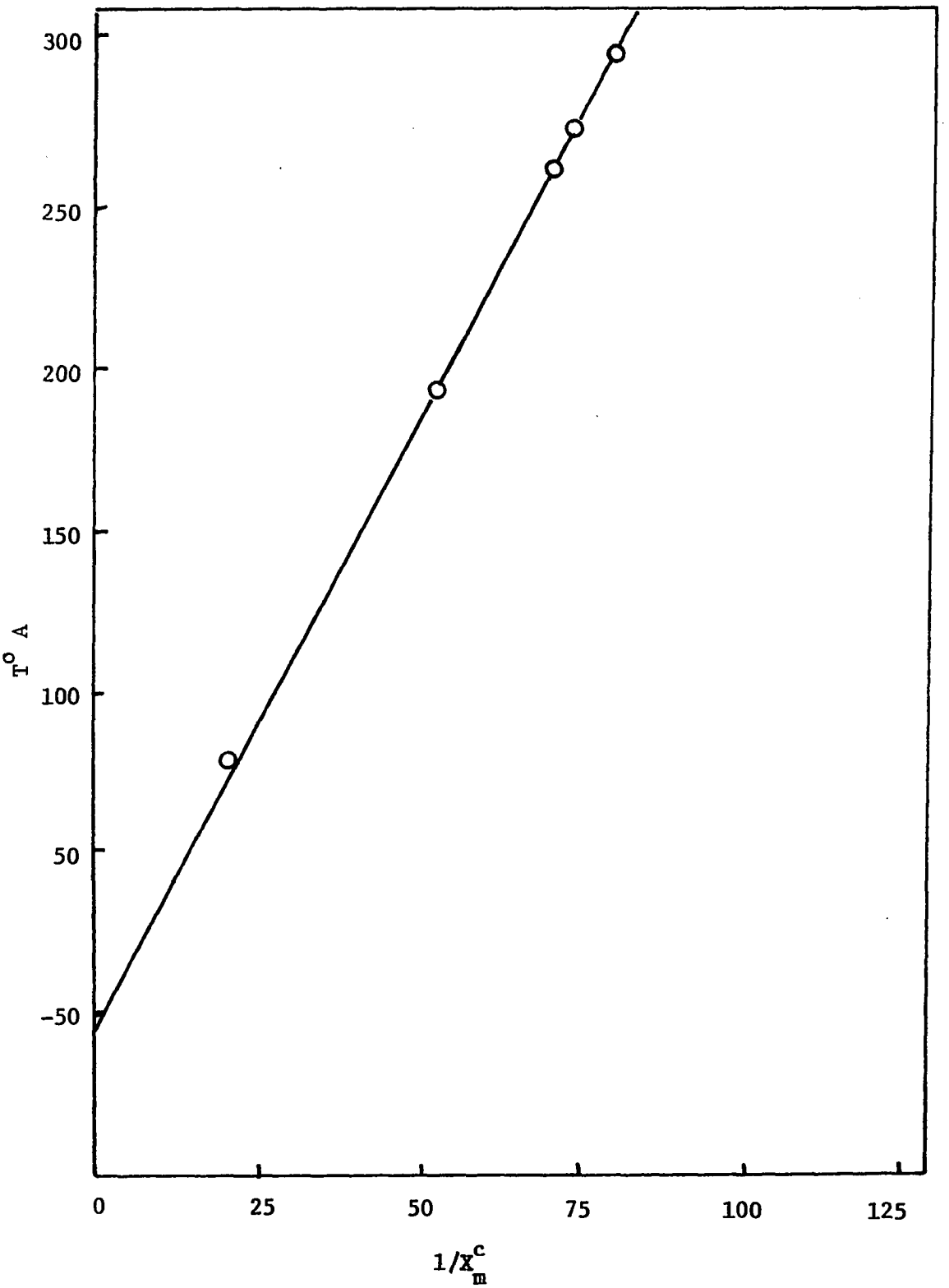

FIGURE 27

T^{o} A versus $1/X_m^c$ for $KCoCl_3 \cdot 2H_2O$

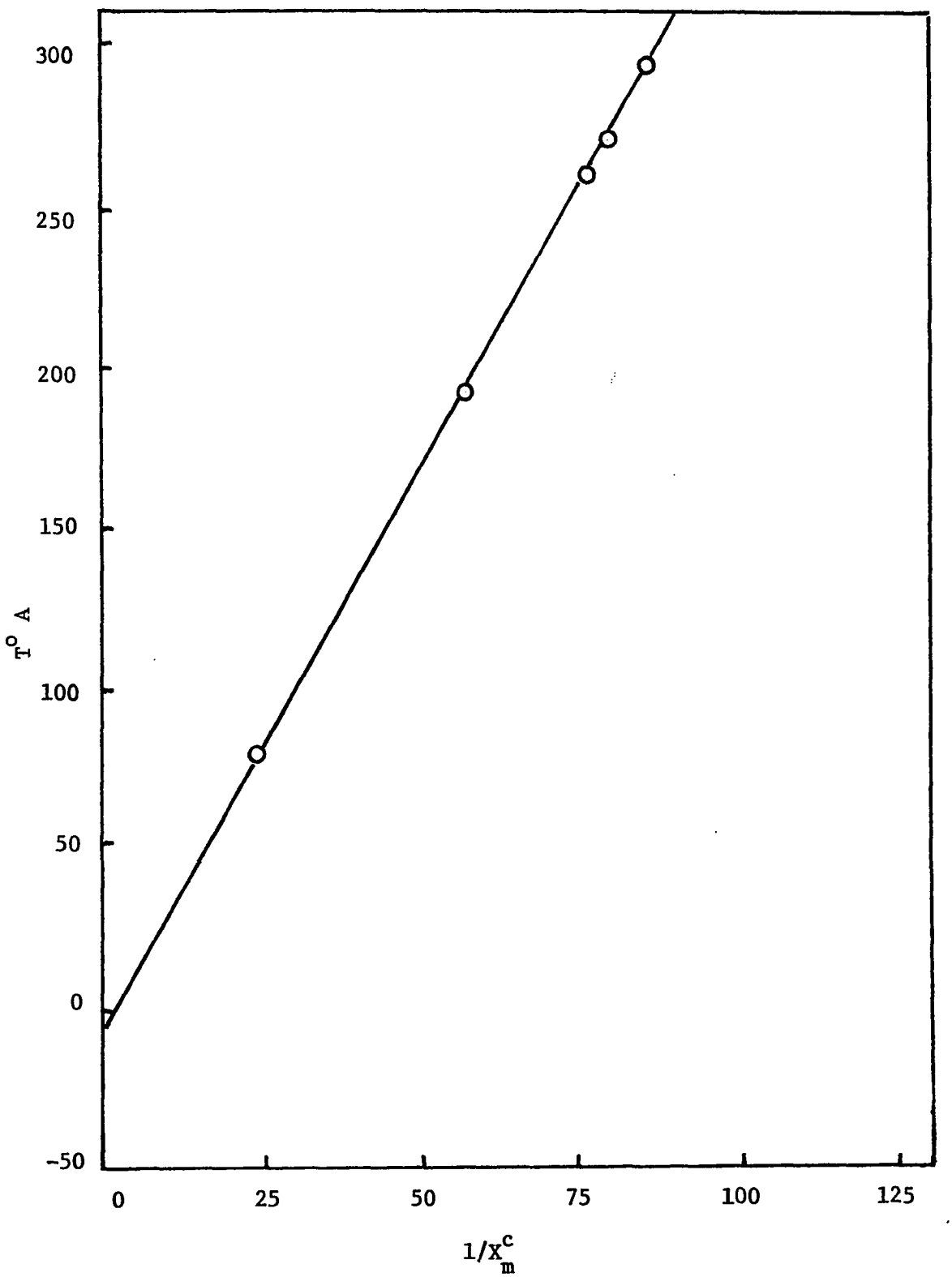

FIGURE 28

T^{o} A versus $1/X_m^c$ for $KCoCl_3 \cdot H_2O$

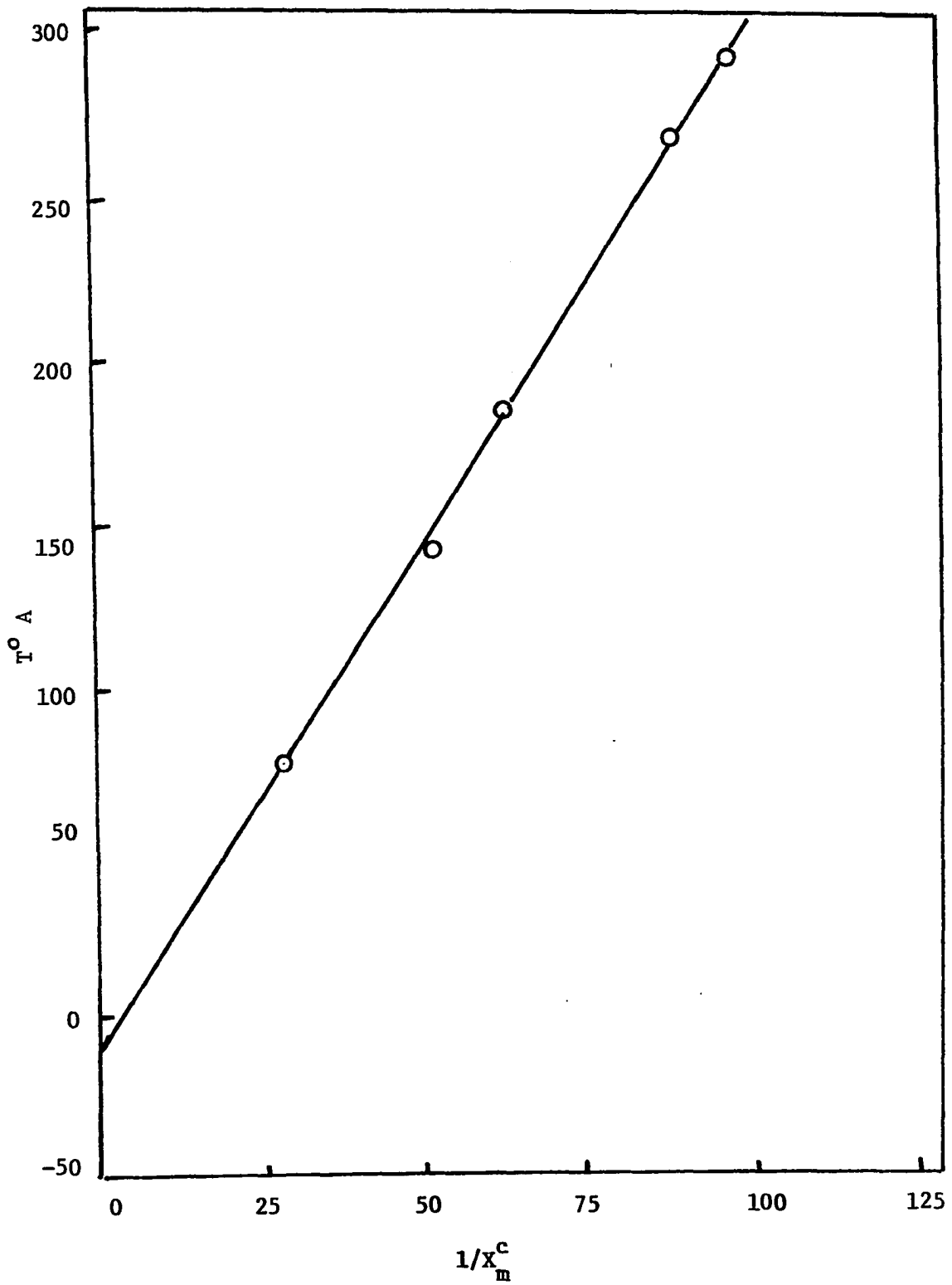

FIGURE 29

T^{o} A VERSUS $1/X_m^c$ FOR $KCoCl_3$

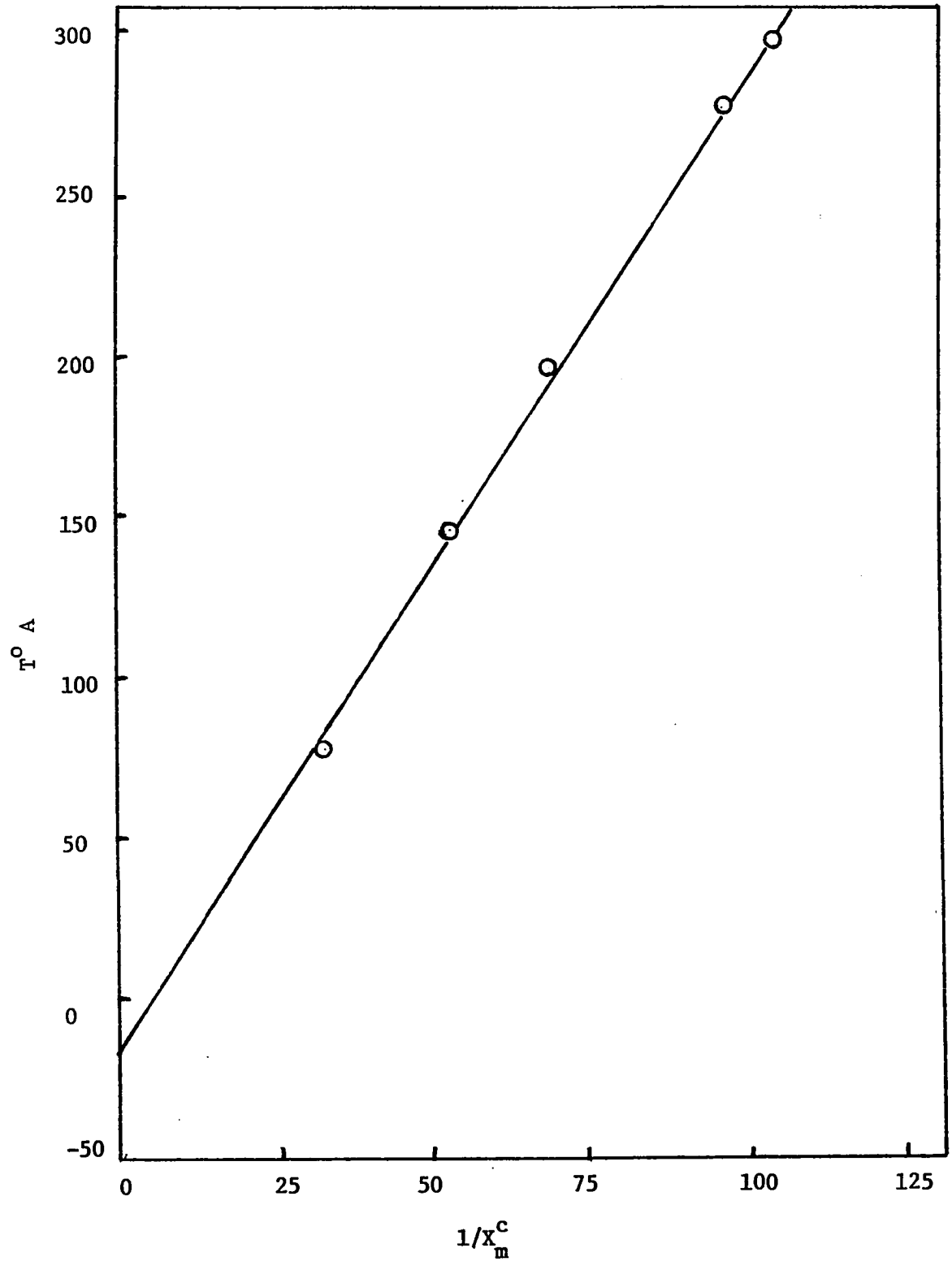

FIGURE 30

X_m^c versus $1/T+\theta$ for $KCoCl_3 \cdot 4H_2O$

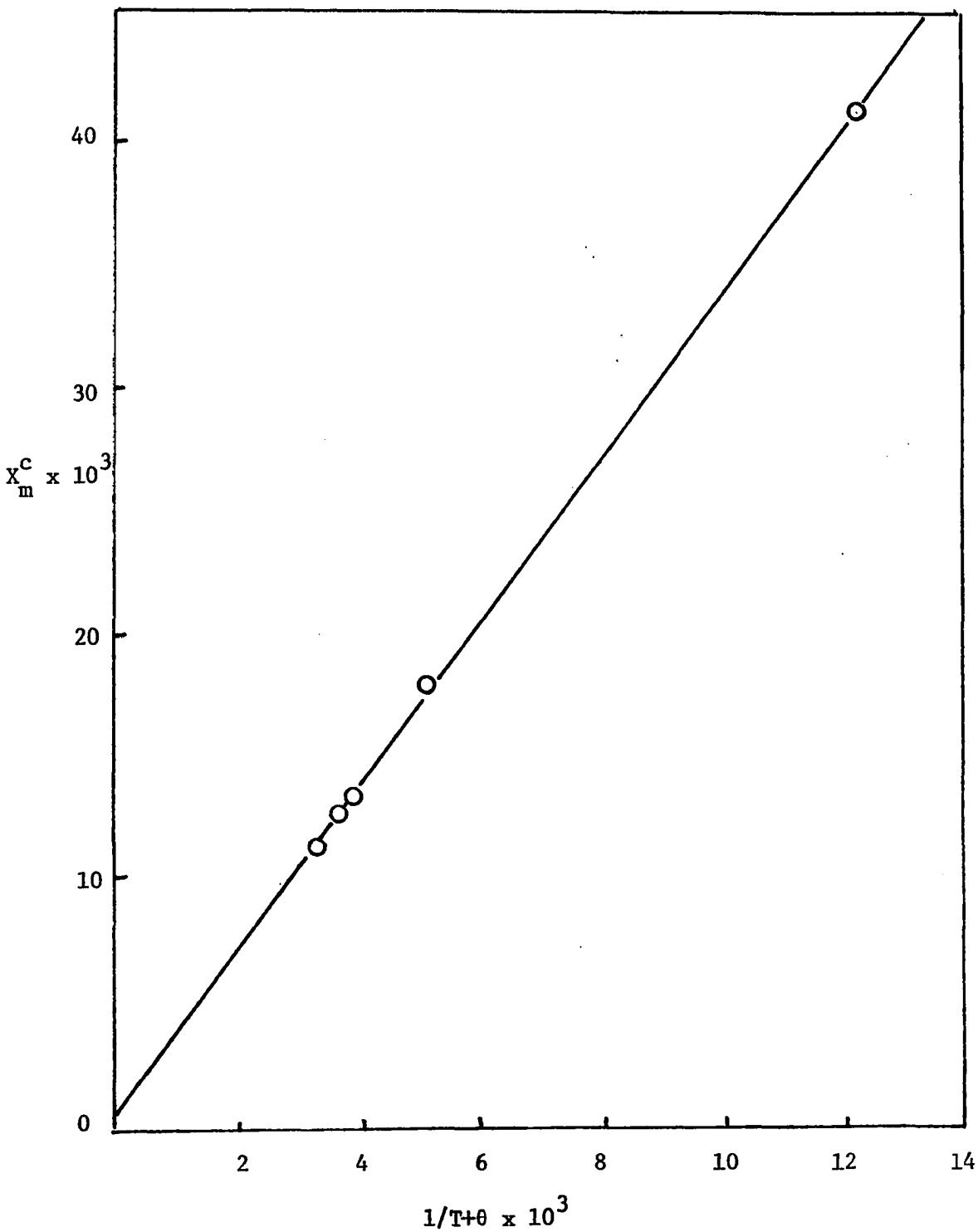

FIGURE 31

X_m^c versus $1/T+\theta$ for $KCoCl_3 \cdot 3H_2O$

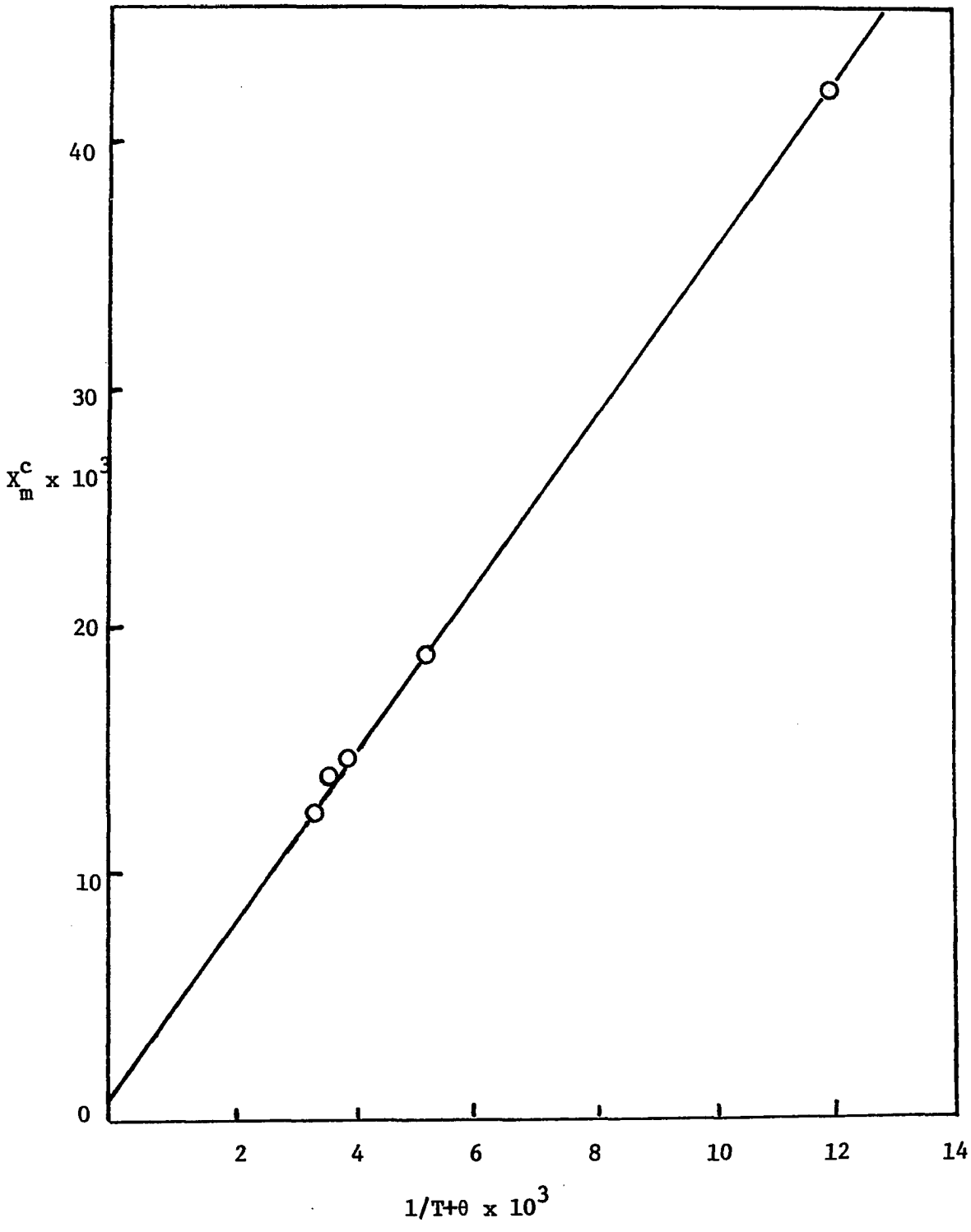

FIGURE 32

X_m^c versus $1/T+\theta$ for $KCoCl_3 \cdot 2H_2O$

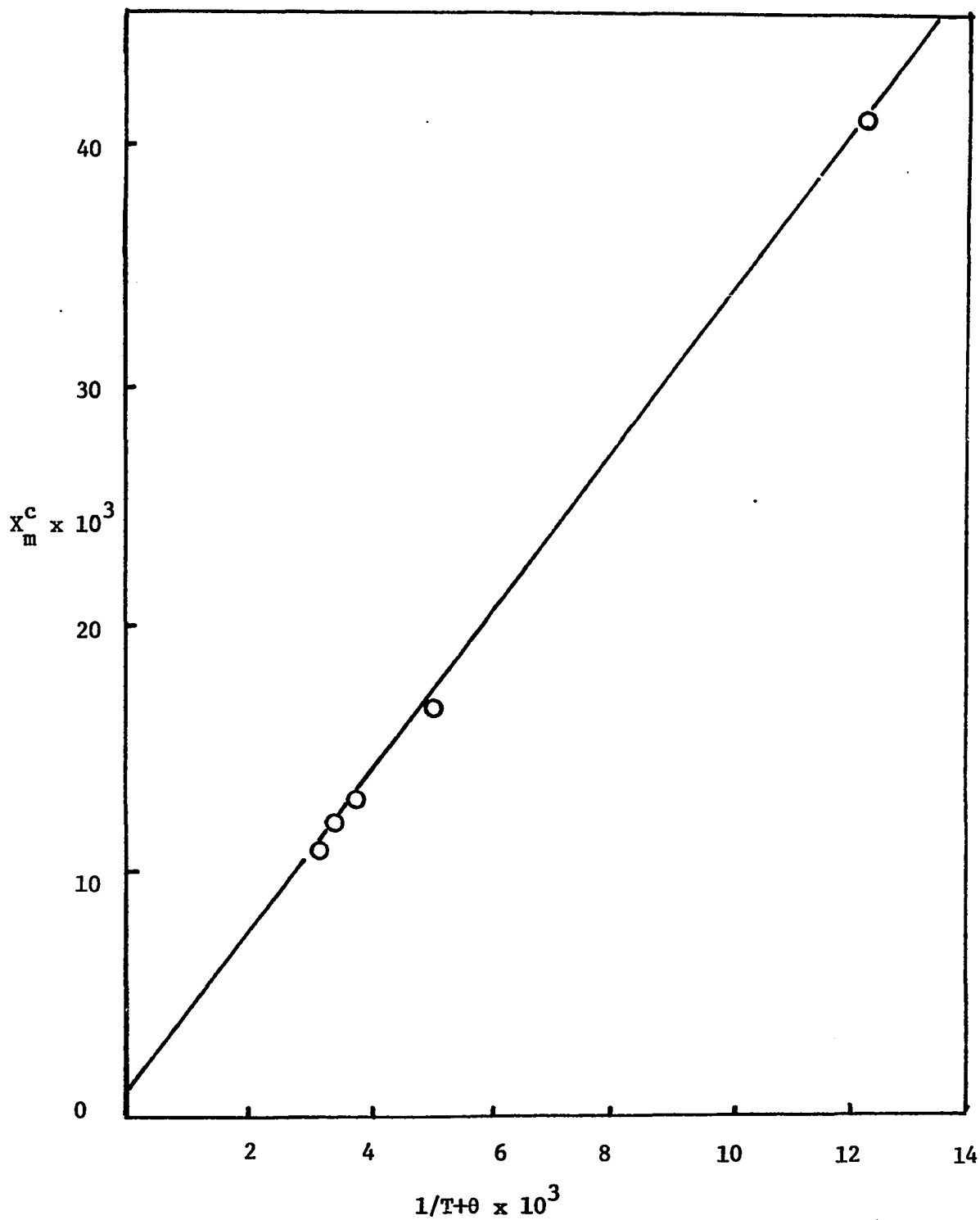

FIGURE 33

X_m^c versus $1/T+\theta$ for $KCoCl_3 \cdot H_2O$

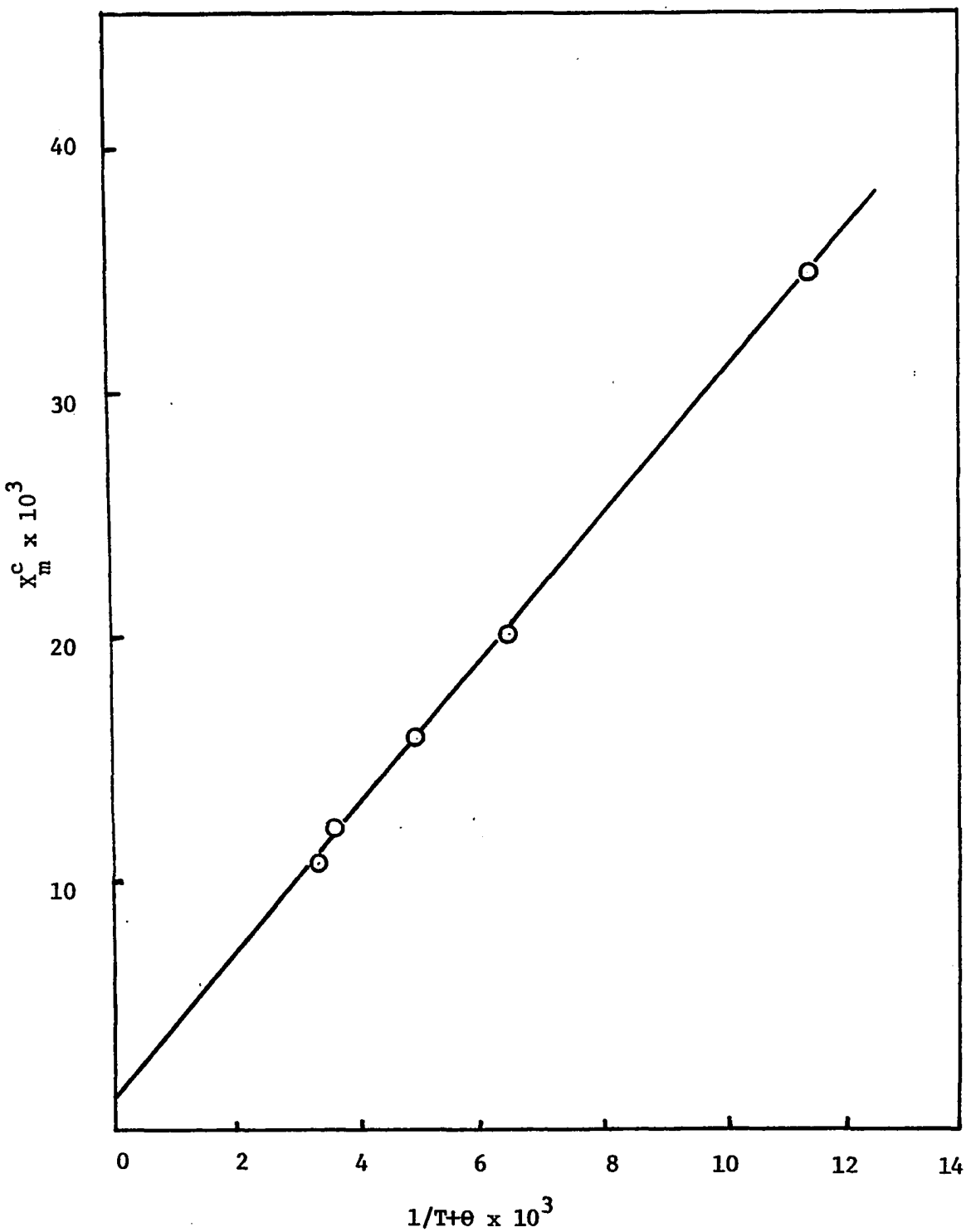

FIGURE 34

X_m^c versus $1/T+\theta$ for $KCoCl_3$

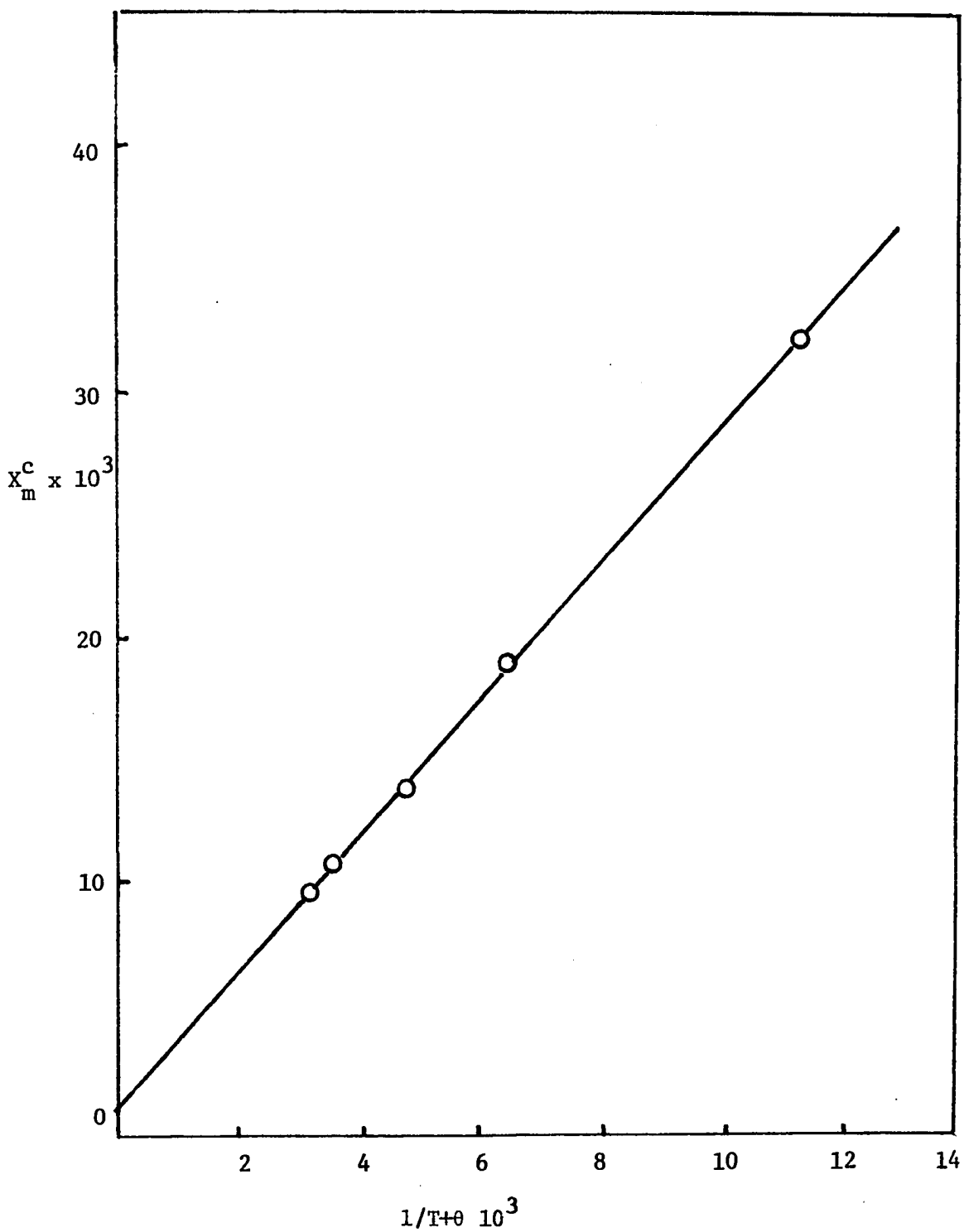

TABLE 26

MAGNETIC SUSCEPTIBILITY DATA

T° A	$X_m^c \times 10^6$ (c.g.s.)	$(X_m^c)^{-1}$	θ	$(1/T+\theta) \times 10^3$
		$KCoCl_3 \cdot 4H_2O$		
298	10,946	91.31	2.0	3.33
273	12,120	82.26	2.0	3.64
265	12,330	81.10	2.0	3.75
195	16,525	60.51	2.0	5.08
77	40,771	24.52	2.0	12.66
		$KCoCl_3 \cdot 3H_2O$		
296	12,598	79.37	3.0	3.34
273	13,525	73.94	3.0	3.62
264	13,855	72.17	3.0	3.73
195	18,371	54.43	3.0	5.05
77	43,796	22.83	3.0	12.50
		$KCoCl_3 \cdot 2H_2O$		
296	11,569	86.44	4.0	3.33
273	12,520	79.86	4.0	3.61
264	13,272	75.34	4.0	3.73
195	17,079	58.54	4.0	5.03
77	42,485	23.54	4.0	12.35

TABLE 26-continued

$T^{o}A$	$X_m^c \times 10^6$	$(X_m^c)^{-1}$	θ	$(1/T+\theta) \times 10^3$
296	10,535	94.90	12.0	3.25
273.4	11,491	87.02	12.0	3.50
195	15,870	63.01	12.0	4.83
146	19.108	52.30	12.0	6.33
77	35,031	28.55	12.0	11.24
		$KCoCl_3$		
296	9,473	105.56	13.0	3.24
273	10,332	96.79	13.0	3.50
196	14,222	70.31	13.0	4.79
146	19,273	51.89	13.0	6.30
77	31,838	31.31	13.0	11.15

TABLE 27

MAGNETIC DATA SUMMARY

Compound	Exp.(μB.M.)	Cal.(μB.M.)	$\theta(^{o}A)$	TIP $\times 10^6$ (c.g.s.)
$KCoCl_3 \cdot 4H_2O$	5.07		2.0	370
$KCoCl_3 \cdot 3H_2O$	5.25		3.0	700
$KCoCl_3 \cdot 2H_2O$	5.27		4.0	200
$KCoCl_3 \cdot H_2O$	4.92	4.82	12.0	760
$KCoCl_3$	4.76	4.69	13.0	600

Summary and Conclusions

The magnetic moments for the tetrahydrate, trihydrate and dihydrate are in the range for those reported for Co (II) octahedral complexes with a $^4T_{1g}$ ground state. The value of 5.07 B. M. is close to that of 5.13 B. M. reported for $Co(H_2O)_4Cl_2$ by Grindstaff (2) suggesting similar structure for this species. The values of 5.25 and 5.27 B. M. for the trihydrate and dihydrate compounds indicate only small changes in structure occur in these during the dehydration from the next higher hydrate species. The magnetic moment of 4.92 B. M. for the monohydrate together with the spectral data indicates a change to a $^4A_2$ ground state caused by a shift in the symmetry from octahedral to tetrahedral. A further decrease in the magnetic moment to 4.76 B. M. indicates the anhydrous complex goes to a more symmetrical tetrahedral configuration. The magnetic moments of the monohydrate and anhydrous compounds are in the range expected for cobalt (II) surrounded by four chloride ions and is close to reported values for K_2CoCl_4 (44) and $(NH_4)_2CoCl_4$ (45). These values are high for symmetrical complexes and are indicative of distortion.

The magnetic susceptibilities for the monohydrate can be calculated by using equations (9), (10) and (11) at the experimental temperatures reported by using the spectral assignments given in Table 24 for the Δ_1 ($^4A_2 \rightarrow {}^4A_1$) and Δ_2 ($^4A_2 \rightarrow {}^4E$) transitions. Upon substituting the appropriate values for the constants in equations (9) and (10) the following equations are used for the final calculations.

$$\chi_{11} = 2.597/T + 543 \times 10^{-6} \qquad (22)$$

and

$$\chi_{\perp} = 3.0641/T + 853.8 \times 10^{-6} \qquad (23)$$

The calculated values are compared with the experimental values in Table 28. The agreement is quite good and adds support to the presence of trigonal distortion in the monohydrate.

In most cases the value of $\bar{X}_m$(exp) is lower than the corresponding $\bar{X}_m$(cal) with this trend becoming larger at lower temperatures. This can be explained on the basis that in the development of equations (9) and (10) no consideration was made for the removal of the spin degeneracy of the $^4A_2$ state resulting from second-order spin-orbit coupling with the $^4A_1$ and ^4E upper excited states. When this new perturbation is included, equations (9) and (10) become (40)

$$\chi_{11} = \frac{15N\beta^2}{3kT}\left[\left(1 - \frac{4\lambda}{\Delta_1}\right)^2\left(1 + \frac{2\alpha}{5kT}\right)\right] + \frac{8N\beta^2}{\Delta_1} \qquad (24)$$

and

$$\chi_{\perp} = \frac{15N^2}{3kT}\left[\left(1 - \frac{4\lambda}{\Delta_2}\right)^2\left(1 - \frac{\alpha}{5kT}\right)\right] + \frac{8N\beta^2}{\Delta_2} \qquad (25)$$

where α is the splitting of the spin degeneracy of the $^4A_2$ state obtained from the expression (40)

$$\alpha = 8\lambda^2(1/\Delta_1 - 1/\Delta_2)$$

This new term becomes significant only at low temperatures. The splitting value α of the spin degeneracy for the monohydrate using the above expression is 35 cm^{-1}.

TABLE 28

CALCULATED MAGNETIC SUSCEPTIBILITIES FOR $KCoCl_3 \cdot H_2O$

Temp ^oA	$\overline{X}_m$(cal)	$\overline{X}_m$(cal)[a]	X_m(exp)
296	$10,577 \times 10^{-6}$	$10,540 \times 10^{-6}$	$10,540 \times 10^{-6}$
273	$11,404 \times 10^{-6}$	$11,362 \times 10^{-6}$	$11,490 \times 10^{-6}$
195	$15,666 \times 10^{-6}$	$15,593 \times 10^{-6}$	$15,870 \times 10^{-6}$
146	$20,672 \times 10^{-6}$	$20,524 \times 10^{-6}$	$19,100 \times 10^{-6}$
77	$38,524 \times 10^{-6}$	$37,993 \times 10^{-6}$	$35,031 \times 10^{-6}$

$\overline{X}_m$(cal)[a] values are obtained using equations (24) and (25)

CHAPTER 6

RESULTS AND CONCLUSIONS

From the experimental evidence obtained in the dehydration study of potassium trichlorocobaltate (II) tetrahydrate, the stereochemistry of the five species formed can be deduced as well as the probable structural changes which occur during dehydration. A correlation of the spectral, magnetic, and thermodynamic properties of potassium trichlorocobaltate (II) hydrates during dehydration can be made with those of $CoCl_2 \cdot 6H_2O$, $CoCl_2 \cdot 4H_2O$ and $K_2CoCl_4 \cdot 2H_2O$.

The diffused reflectance spectrum of the tetrahydrate is very close in appearance to that of $CoCl_2 \cdot 6H_2O$ and $CoCl_2 \cdot 4H_2O$ reported by Grindstaff (2). These compounds have been shown by X-ray analysis to be composed of $Co(H_2O)_4Cl_2$ octahedra units. (46) The Co(II) ion is surrounded by four waters adjacent to each other forming a plane with the chloride ions perpendicular to the plane. This gives a tetragonally distorted octahedron with the Cl^- at a longer distance than the in-plane waters. The experimental spectrum of $KCoCl_3 \cdot 4H_2O$ fits a tetragonally distorted octahedron with a $^4A_{2g}$ ground state under D_{4h} symmetry caused by the elongation of the "z" axis. If the Cl^- ions are in the axial position, a structure similar to that of $CoCl_2 \cdot 4H_2O$ would be indicated. The magnetic moment of 5.07 B. M. is also quite close

to the value reported for $CoCl_2 \cdot 4H_2O$ of 5.13 B. M. (2) The experimental results found in this study supports an octahedral coordination with a probable formula of $KCl \cdot Co(H_2O)_4Cl_2$.

The first dehydration step involves the loss of one mole of water from the tetrahydrate. The enthalpy change of 10.81 kcal $mole^{-1}$ is only slightly less than the energy change for the conversion of one mole of ice to vapor at 25° (12.4 kcal $mole^{-1}$). This indicates some additional energy is released through possible rearrangement of Cl^- and H_2O during the dehydration. In a constant environment, bonding would remain approximately the same and only energy changes associated with the ice-vapor reaction would be noted. The entropy change of 27.48 e.u. $mole^{-1}$ is less than that for the ice-vapor reaction (35.2 e.u. $mole^{-1}$) indicating the trihydrate is in a more ordered state. The spectra of the trihydrate shows less band splitting indicating a more symmetrical configuration. This is further supported by the ease with which the spectra was fitted to a symmetrical octahedral ligand field. The magnetic moment of the trihydrate is 5.27 B. M. indicating a large orbital contribution also confirming an octahedral structure. The results of this study supports an octahedral structure with the Co (II) ion surrounded by three Cl^- and three H_2O trans to each other. In this configuration the ligands would give an average symmetrical field around the Co (II) ion which is necessary for the spectra found.

The diagram below illustrates the proposed structure for the trihydrate.

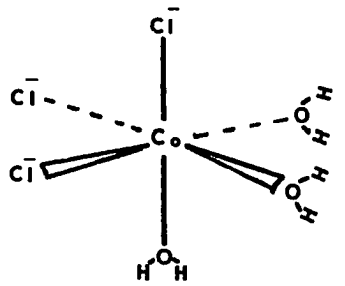

The second dissociation step involves the loss of one mole of water forming the dihydrate species. The enthalpy change of 12.64 kcal $mole^{-1}$ is very close to the ice-vapor reaction at 25°C (12.4 kcal $mole^{-1}$). The entropy change of 33.11 e.u. $mole^{-1}$ is close to the entropy change for the ice-vapor reaction (35.2 e.u. $mole^{-1}$) also confirming very little change in the bonding. The spectrum indicated a marked change in the shape of the absorption band corresponding to the $^4T_{1g}(F) \rightarrow {}^4T_{1g}(P)$ transition (octahedral symmetry). This transition splits under tetragonal distortion (D_4h symmetry) to a ^4E_g and $^4A_{2g}$. The $^4A_{2g}$ was fitted at a lower energy in the dihydrate indicating the distortion is a compression or shortening of the "z" axis. The structure of $CsCoCl_3 \cdot 2H_2O$ (14) has been determined by X-ray analysis to be an octahedron with four chloride ions and two waters in the cis position. The two cis waters are hydrogen-bonded to chloride ions in adjoining octahedra units. The octahedra units form chains linking through Cl^-. The thermochemistry and spectra fitting indicates potassium trichlorocobaltate (II) dihydrate shows a similar structure linking octahedra units through trans chloride ions. This can occur during the dehydration of the trihydrate by adjacent octahedra units linking up through the Cl^- ions on one unit to the Co(II) ion in an adjacent unit. The possible

structure of the dihydrate is shown below.

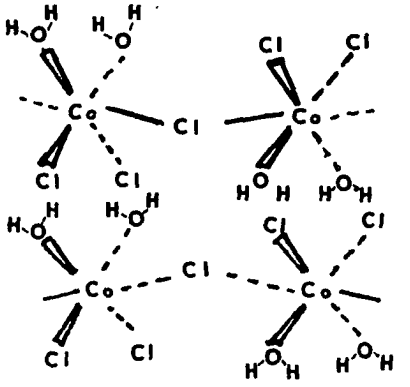

The experimental magnetic moment of 5.25 B. M. for the dihydrate indicates octahedral coordination around the Co(II) ion and also indicates only a small change in configuration has occurred in the transition from the trihydrate.

The removal of the third mole of water resulted in the smallest energy change for any of the dehydration steps. The enthalpy change of 7.47 kcal $mole^{-1}$ for the step signals that a change in configuration is occurring. The difference in the enthalpy change for the dehydration reaction and that of the ice-vapor reaction at 25°C (12.4 kcal $mole^{-1}$) comes from different heats of formations of the dihydrate and monohydrate species, equation (7), page 36. This energy change can arise from the structural change from the octahedral dihydrate to the tetrahedrally distorted monohydrate. The entropy change is also low (15.2 e.u. $mole^{-1}$) indicating a major structural change.

The dehydration of the dihydrate was attempted above 55.4°C and resulted in the system being bivariant. (See Figure 4, Chapter 3). The formation of two phases is thought to result from the structures

of the dihydrate and monohydrate being similar at this temperature forming one phase.

The spectra of the monohydrate fits a badly distorted tetrahedron. The distortion is angle distortion and not bond distortion as encountered with the tetrahydrate and dihydrate. A Dq value of 260 cm^{-1} is also low indicating a distorted configuration. A magnetic moment of 4.92 B. M. indicates a change in ground state to a $^4A_2$.

From the spectral, thermochemical, and magnetic moment studies it appears that both water molecules are removed from the inner coordination sphere during the dehydration of the dihydrate. One water molecule is completely expelled while one is held in the outer coordination sphere. The chloride ions link up to Co(II) ions in adjacent chains forming $Co_2Cl_6^=$ units distorted by the water so as to have a pseudo tetrahedral symmetry. This would give a structure similar to that of $KCuCl_3$ (47) which has $Cu_2Cl_6^=$ units in layered packing with Cu(II) to Cl^- interactions between layers. In the case of $KCoCl_3 \cdot H_2O$, the water is the interacting species forcing the linking chlorides out of plane and into a tetrahedral-like geometry.

A second possibility exists during the dehydration of the dihydrate. This would involve the linking of the Cl^- ions with Co(II) ions in adjacent octahedra to form a chain sharing opposite faces of the octahedra. This type of structure has been found in the $CsCoCl_3$ species. (13) This structure was ruled out for $KCoCl_3 \cdot H_2O$ and $KCoCl_3$ because the spectra obtained for these species definitely fit a tetrahedral ligand field, a definite monohydrate species was formed, and the magnetic moment indicated a change in ground state.

The removal of the final mole of water requires slightly more energy than the ice-vapor reaction at 25°C (14.68 kcal $mole^{-1}$ versus 12.4 kcal $mole^{-1}$). This extra energy could occur if the water molecule is being shared by other Cl^- ions through hydrogen-bonding. The entropy change is quite close to the entropy change for the ice-vapor reaction at 25°C supporting the formation of a more symmetrical structure for the anhydrous compound. The spectrum was easily fitted to a tetrahedral symmetry with a Dq value of 352 cm^{-1}. This value is close to the value reported by Figgis (48) for Co(II) tetrahedrally surrounded by chloride ions. The magnetic moment of 4.76 B. M. also indicates the coordination of $KCoCl_3$ as being tetrahedral. A value of 4.77 B. M. has been reported for tetrahedral $(NH_4)_2CoCl_4$ by Fogel, et. al. (45)

The thermochemical, magnetic moments and spectral results support a structure for the anhydrous compound similar to the monohydrate without the influence of the water molecule. The $Co_2Cl_6^=$ units in the $KCoCl_3$ can go to a more symmetrical geometry similar to that found in triphenylphosphinium trichlorocuprate (II). (49) The proposed structure for $KCoCl_3$ is shown below.



From this study it appears that the most logical way in which potassium trichlorocobaltate (II) tetrahydrate undergoes rearrangement is the one described. The upper hydrates show octahedral coordination

going to tetrahedral coordination for the monohydrate and anhydrous compound. This change in structure occurs during the dehydration of the dihydrate as was found in the study of $K_2CoCl_4 \cdot 2H_2O$ by Grindstaff (2). The tetrahedral form of the complex was found to be indefinitely stable in a dry atmosphere at room temperature. This is supported by identical spectral and magnetic data obtained over a period of two years. The formation of the trichlorocobaltates by fusion methods have been shown by Gilmore (11) to have distorted octahedral configurations by spectral studies. In that study the samples were formed under conditions which could lead to a metastable condition with the complex formed not in a true equilibrium. More investigation in this area is needed to prove conclusively that this phenomenon is occurring.

It was again indicated in this study that the preferred structure of Co(II) ion with a mixture of Cl^- and H_2O as ligands is a distorted octahedron. The change in structure from a distorted octahedron to a tetrahedral geometry by dehydration can be indicated by the thermochemical values as proposed in a previous study. (2) The enthalpy change and entropy change for the dehydration of the lower hydrates in this study and that by Grindstaff (2) are contrasted in Table 29. The change in enthalpy appears to be in the range of 6-7.5 kcal $mole^{-1}$ for the dehydration step involving the change in structure. The entropy change appears in all steps to be a more sensitive indicator of small structural changes than the enthalpy.

TABLE 29

ENTHALPY AND ENTROPY VALUES FOR THE REACTIONS

(1) $KCoCl_3 \cdot nH_2O_{(s)} = KCoCl_3 \cdot mH_2O_{(s)} + (n-m)H_2O_{(g)}$

(2) $K_2CoCl_4 \cdot nH_2O_{(s)} = K_2CoCl_4 \cdot mH_2O_{(s)} + (n-m)H_2O_{(g)}$

Reaction	n	m	ΔH^o kcal mole^{-1}	ΔS^o e.u. mole^{-1}
1	2	1	7.47	15.2
2	2	1	6.96	14.2
1	1	1	14.68	34.65
2	1	1	12.71	32.0

Further work in this area could consist of the dehydration studies of other complex halides with the formula, AMX_3, such as $CsCoCl_3 \cdot 2H_2O$, $RbCoCl_3 \cdot 2H_2O$, $KNiCl_3 \cdot 2H_2O$, and $KCuCl_3 \cdot 2H_2O$. (50)

Other anions beside chloride needs to be investigated to see if thermochemical data is a universal indicator of structural change or occurs only for the chloride-water exchange.

PART II

THE DEHYDRATION OF $[Cr(H_2O)_6Cl_3$ WITH LIGAND FIELD TREATMENT OF $[Cr(H_2O_2]Cl_3$ AND TRANS $[Cr(H_2O)_4Cl_2]Cl$

CHAPTER 1

THE DEHYDRATION OF $[Cr(H_2O)_6]Cl_3$ WITH LIGAND FIELD TREATMENT OF $[Cr(H_2O)_6]Cl_3$ and trans $[Cr(H_2O)_4Cl_2]Cl$

Introduction

The hexahydrate of chromium (III) chloride forms three hydrate isomers which are the green $[Cr(H_2O)_5Cl]Cl_2 \cdot H_2O$, $[Cr(H_2O)_4Cl_2]Cl \cdot 2H_2O$, and the violet $[Cr(H_2O)_6]Cl_3$. Only a few examples of such compounds exist and most belong to the "inert" d^3 or d^6 electron configuration. This "inert" behavior makes studies involving the configurational changes occurring during dehydration extremely time consuming. The time required for re-establishing equilibrium between species being in some cases weeks.

As a second part of this study, the dehydration of $[Cr(H_2O)_6]Cl_3$ was studied at room temperatures. The dissociation pressure versus compositon and temperature was measured with the apparatus in Figure 1, Chapter 3. Only the first step of the dehydration was accomplished due to the time involved. The study showed by mass loss and chloride analysis that the species formed was $[Cr(H_2O)_4Cl_2]Cl$.

The absorption spectra of both $[Cr(H_2O)_6]Cl_3$ and $[Cr(H_2O)_4Cl_2]Cl$ were measured and fitted to the crystal field model using the computer program by H. Joy. (1)

Previous Studies

The dehydration of $[Cr(H_2O)_6]Cl_3$ has been investigated by Cathers and Wendlandt (51) by differential thermal analysis. The results of this study indicates $CrCl_3 \cdot 3/2H_2O$ is formed in the temperature range of 100°-250°C. The reaction given was

$$2[Cr(H_2O)_6]Cl_3 = (CrCl_3)_2 \cdot 3H_2O + 8H_2O_{(g)} + H_2O_{(1)}$$

No HCl gas was released by the violet $[Cr(H_2O)_6]Cl_3$ or green $[Cr(H_2O)\ Cl]\ Cl_2 \cdot H_2O$ below 250°C.

The X-ray structure of $[Cr(H_2O)_4Cl_2]Cl \cdot 2H_2O$ has been shown by Dance and Freeman (52) to be trans $Cr(H_2O)_4Cl_2^+$ octahedra units. The octahedra units are linked together by hydrogen bonds between the water molecule bonded to the metal and the Cl^- ion in the outer sphere. The X-ray structure of $[Cr(H_2O)_6]Cl_3$ has been reported by Andress and Carpenter (53) to be composed of $Cr(H_2O)_6^{+3}$ octahedra.

The electronic spectra of $Cr(H_2O)_6^{+3}$ in solution was shown by Schläfer(37) to have two spin allowed and one spin forbidden transitions at 17,400, 24,630, and 14,970 cm^{-1} respectively. These absorptions correspond to the transitions from the $^4A_{2g}$ ground state to the $^4T_{2g}$, $^4T_{1g}$, and ^2E_g. The spectrum of chrome alum, $KCr(SO_4)_2 \cdot 12H_2O$ measured by Spedding and Nutting (54,55) showed these same bands at 18,000, 24,600, and 14,900 cm^{-1}, respectively. The absorption spectra for D_{4h} symmetry involving CrX_4Y_2 complexes where X is water and Y is chloride have been investigated in acid solution (56,57) showing two absorptions in the visible region at 15,750 and 22,200 cm^{-1}. No spectra has been reported for the solid $[Cr(H_2O)_6]Cl_3$ or $[Cr(H_2O)_4Cl_2]Cl$ compound.

Compound Formation and Analysis

The formation of the violet $[Cr(H_2O)_6]Cl_3$ isomer was prepared by placing 100 grams of $Cr(III)(NO_3)_3 \cdot 6H_2O$ (reagent grade) in 100 mls of H_2O and 100 mls of concentrated HCl. The mixture was cooled in an ice bath while dry HCl gas was bubbled into the mixture until crystallization was complete. The crystalline product was re-crystallized from a water and HCl mixture removing the last traces of HCl by washing with acetone.

The sample was dried in a vacuum desiccator and chloride analysis determined gravimetrically. (16) The chromium concentration was obtained gravimetrically by oxidizing the chromium(III) with hydrogen peroxide in a basic solution to chromate and precipitating as barium chromate. The water concentration was obtained by difference. The analysis showed: Cl 39.78% exp.; 39.90% calcd.; Cr 20.36% exp.; 19.52% calcd.; H_2O 39.86% exp.; 40.58% calcd.

The formation of the green $[Cr(H_2O)_4Cl_2]Cl$ was prepared by placing reagent grade $[Cr(H_2O)_4Cl_2]Cl \cdot 2H_2O$ over concentrated H_2SO_4 in a desicaator. The chloride concentration was obtained gravimetrically by boiling a sample for several hours to remove the Cl^- ion from the inner sphere and precipitating from acid solution. The concentration of chromium was found gravimetrically as barium chromate. The concentration of water was determined by difference. The analysis showd: Cl 45.95% exp.; 46.17% calcd.; Cr 38.74% exp.; 38.20% calcd.; H_2O 15.34% exp.; 15.63% calcd.

Experimental

A sample of $[Cr(H_2O)_6]Cl_3$ was placed in the vapor pressure apparatus, Figure 1, Chapter 3. The apparatus was placed in an oil bath thermostated at 55.4°C and evacuated with a vacuum pump. The system was permitted to reach equilibrium as noted by a constant manometer pressure. The accumulated vapor was removed by a vacuum pump and again allowed to re-equilibrate as indicated by the dissociation pressure reaching the same constant value. This procedure was repeated until a composition equal to that of the $[Cr(H_2O)_4Cl_2]Cl$ was obtained when the pressure dropped. The sample was removed from the system and titrated for Cl^- ion indicating two Cl^- ions in the inner sphere and one Cl^- in the outer sphere. This supports the formation of $[Cr(H_2O)_4Cl_2]Cl$ species.

A new sample of $[Cr(H_2O)_6]Cl_3$ was placed in the vacuum system and pumped until a composition with equal amounts of the $[Cr(H_2O)_6]Cl_3$ and $[Cr(H_2O)_4Cl_2]Cl$ was reached. The pressure was studied as a function of temperature over a range of 35° degrees. As a test for equilibrium, the temperature was varied several degrees above and below the original temperature. The system was given time to re-equilibrate (usually several days) and then returned to the original temperature. The return to the same pressure was used as evidence that equilibrium had been reached. The vapor pressure versus temperature is shown in Figure 35. The vapor pressure versus temperature data is shown in Table 31.

The dissociation pressure displayed as a function of composition in Figure 36 indicated that $[Cr(H_2O)_6]Cl_3$ dissociated according to the reaction:

$$[Cr(H_2O)_6]Cl_{3(s)} = [Cr(H_2O)_4Cl_2]Cl_{(s)} + 2H_2O_{(g)}$$

The dissociation pressure was found to follow the expression:

$$\text{Log } P = -\Delta H^{o}/\Delta n\ 2.303RT + \Delta S^{o}/\Delta n\ 2.303R$$

where R is 1.987 cal.mole^{-1} deg^{-1} and Δn is the moles of water removed. The standard enthalpy and entropy of reaction obtained from this expression was found to be: ΔH^{o} = 7.92 kcal mole^{-1} and ΔS^{o} = 15.33 e.u. mole^{-1}.

The diffused reflectance spectra for $[Cr(H_2O)_6]Cl_3$ and $[Cr(H_2O)_4Cl_2]$ Cl were obtained by placing a small amount of the finely ground sample in a microscope well slide prepared in the same manner as in Chapter 4. The sample was placed in the DK-1 spectrophotometer and the absorption spectra obtained in the range of 2000 mu to 700 mu with the Pb detector and tungsten lamp. The 250-700 mu range was determined by using the photo-multiplier detector and H_2 lamp. All d-d transitions occur in the 300 mu to 1000 mu region and are displayed in Figure 37.

Spectra Fitting

The spectrum of $[Cr(H_2O)_4Cl_2]Cl$, Figure 37 shows three bands located at 16,400 cm^{-1}, 22,500 cm^{-1} and 32,200 cm^{-1}. Assuming a D_{4h} symmetry with a ground state of $^4B_{1g}$, the first transition was assigned to the $^4B_{1g} \rightarrow {}^4B_{2g}$ and $^4B_{1g} \rightarrow {}^4E_g$, and the second transition to the $^4B_{1g} \rightarrow {}^4A_{2g}$ and $^4B_{1g} \rightarrow {}^4E_g$. Dq was set at 1640 cm^{-1} obtained from the first transition, B was set at 700 cm^{-1}, C/B at 4.0, Ds and Dt at 100 cm^{-1} and S.O. at 60 cm^{-1}. All parameters were iterated by the program until the best fit for the spin allowed transitions were obtained. The transition at 18,800 cm^{-1} was next tentatively assigned to the $^2T_{1g}(G)$ in O_h symmetry from the Tanabe-Sugano diagram, Figure 15. All parameters were fixed except C/B and from the computed program the best fit for the

Log P versus $1/T \times 10^3$ (A^o)

$[Cr(H_2O)_6]Cl_{3(s)} = [Cr(H_2O)_4Cl_2]Cl_{(s)} + 2H_2O_{(g)}$

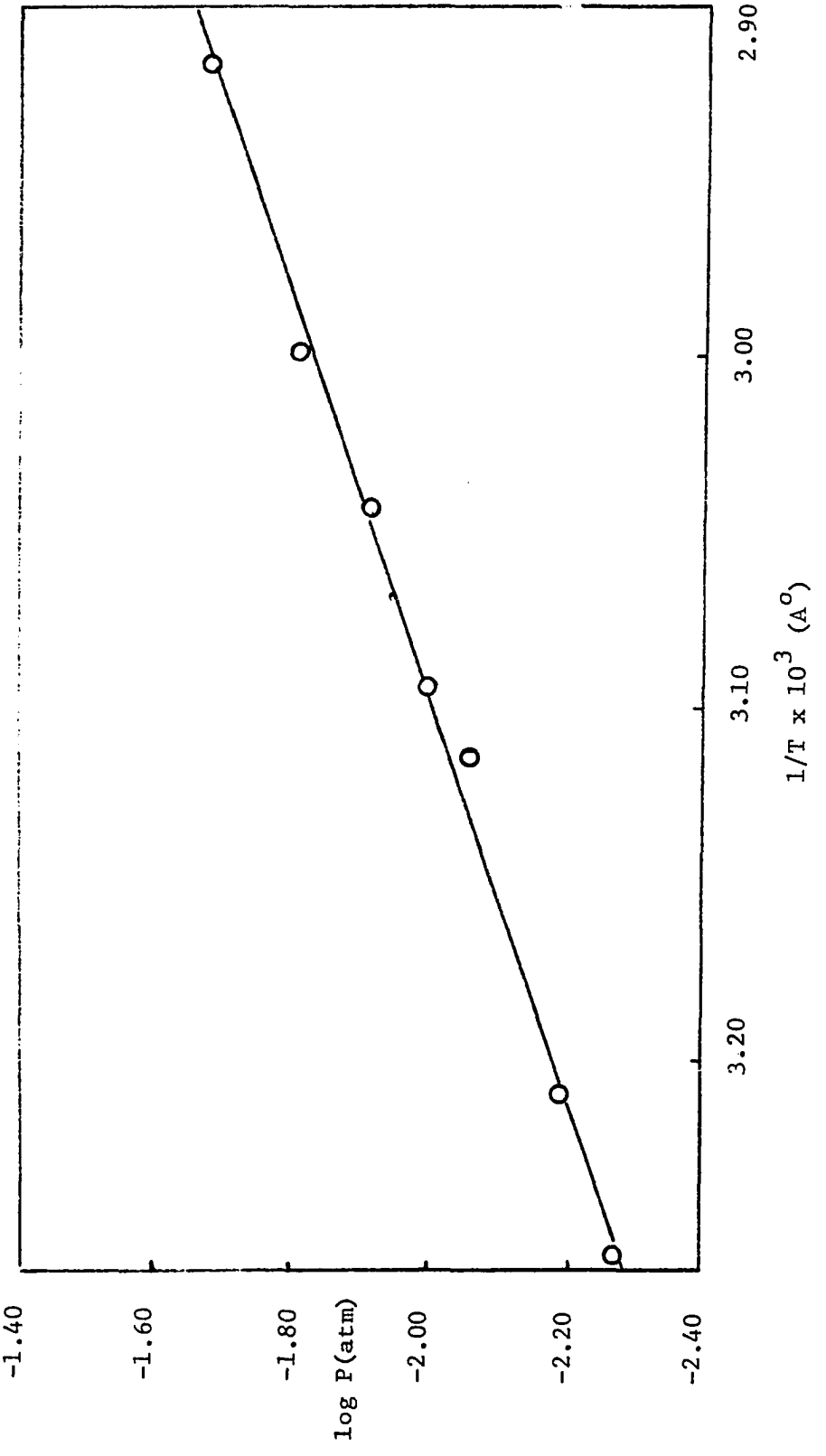

TABLE 30

VAPOR PRESSURE DATA

$$Cr(H_2O)_6\ Cl_{3(s)} = [Cr(H_2O)_4Cl_2]Cl_{(s)} + 2H_2O_{(g)}$$

T°C	P(mm)	f	T°C	P(mm)	f
55.4	10.55	1.682	55.4	8.65	1.487
	9.40	1.670		7.40	1.468
	8.60	1.654		5.30	1.458
	8.85	1.618		1.80	1.450
	8.80	1.608			
	8.85	1.558			
	8.95	1.519			

TABLE 31

Log P(atm) vs $1/T \times 10^3$ (A^o) Data

$$[Cr(H_2O)_6]Cl_{3(s)} = [Cr(H_2O)_4Cl_2]Cl_{(s)} + 2H_2O_{(g)}$$

P(mm)	$P \times 10^3$(atm)	Log P(atm)	T(A^o)	$1/T \times 10^3$(A^o)
4.05	5.329	-2.273	307	3.257
4.85	6.382	-2.195	311.2	3.213
6.50	8.553	-2.068	320.0	3.125
7.60	10.000	-2.000	323.0	3.096
8.85	11.644	-1.934	328.4	3.045
11.45	15.065	-1.822	334.0	2.994
15.70	20.657	-1.685	343.0	2.915

FIGURE 36

VAPOR PRESSURE OF $[Cr(H_2O)_6]Cl_3$ AS A FUNCTION OF COMPOSITION

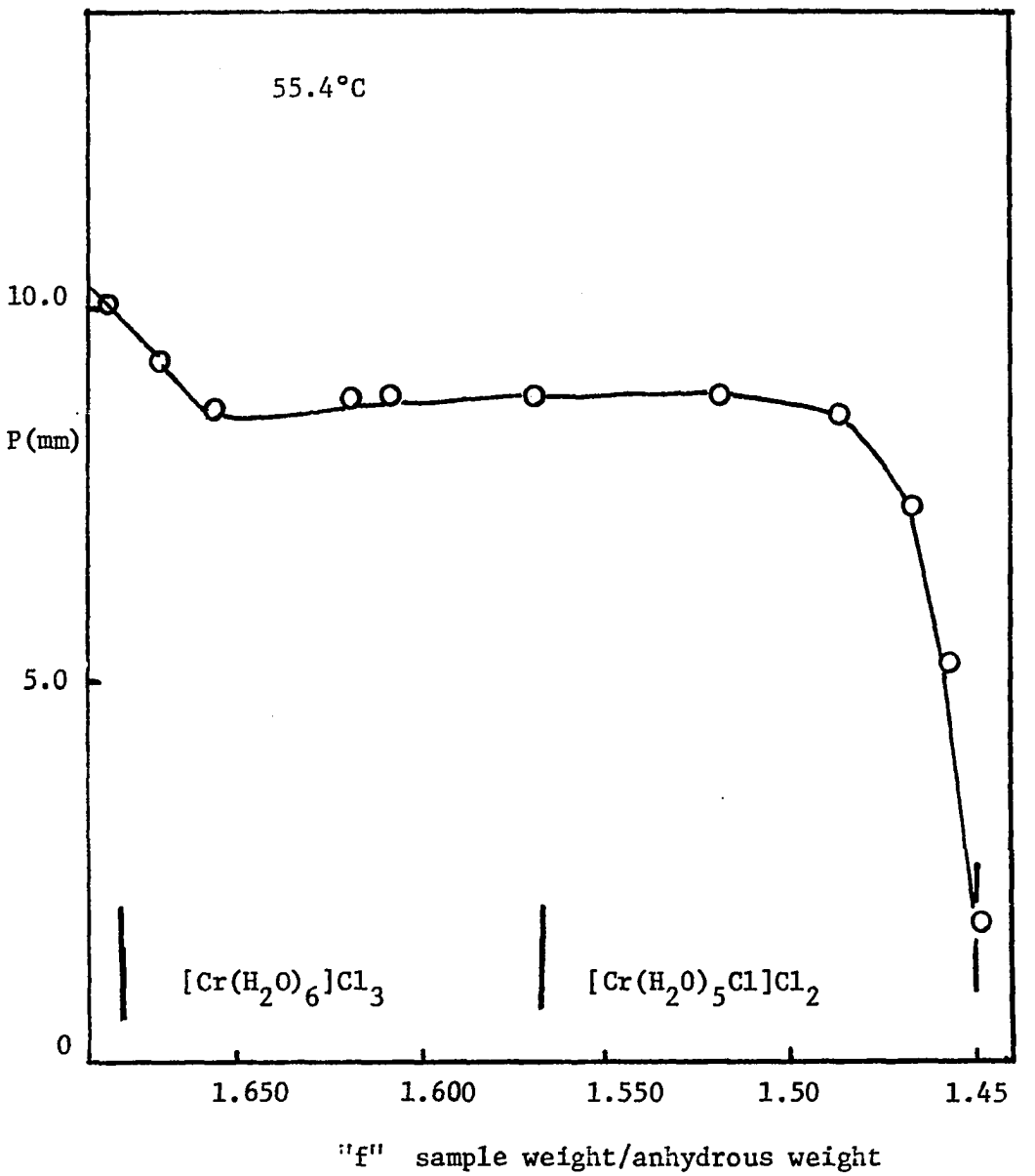

FIGURE 3

REFLECTANCE SPECTRA

_____ $[Cr(H_2O)_6]Cl_3$

- - - - - $[Cr(H_2O)_4Cl_2]Cl$

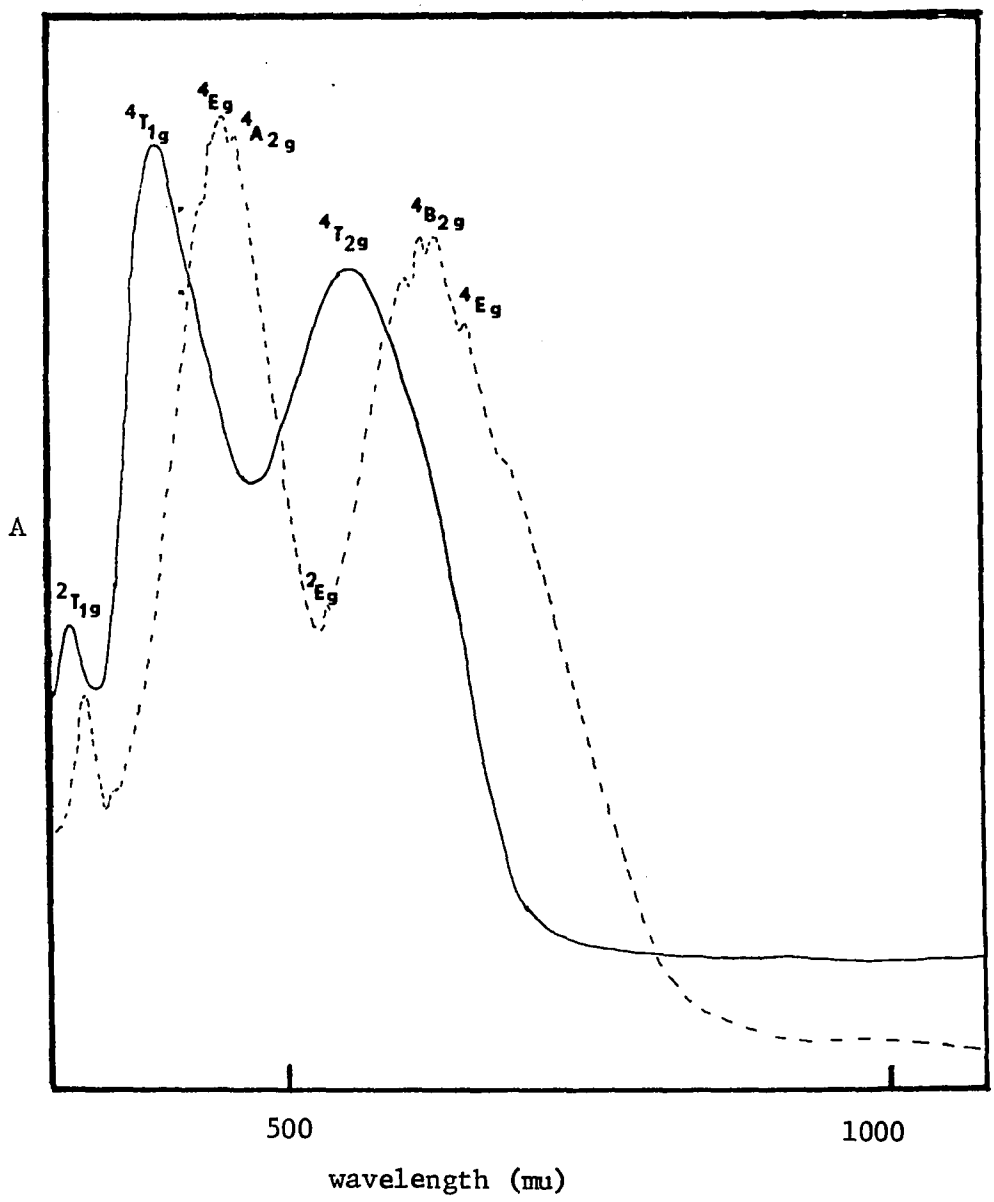

TABLE 32

COLLECTED SPECTRA DATA

	Transition		Calculated cm^{-1}	Calculated mu	Observed mu	Peak Description
			$[Cr(H_2O)_4Cl_2]Cl$			
1.	$^4B_{1g}$	$^4E_g(^4T_{2g}F)$	15,610	640.6	642	shoulder on intense peak
2.		$^4E_g(^4T_{2g}F)$	15,491	645.5	645	shoulder on intense peak
3.		$^4B_{2g}(^4T_{2g}F)$	16,478	606.8	610	intense peak
4.		$^4E_g(^4T_{1g}F)$	22,382	446.8	445	narrow intense peak
5.		$^4E_g(^4T_{1g}F)$	22.442	445.6	445	narrow intense peak
6.		$^4A_{2g}(^4T_{1g}F)$	21,910	456	455	shoulder on narrow intense peak
7.		$^4E_g(^4T_{1g}P)$	35,034	285.4		not observed
8.		$^4E_g(^4T_{1g}P)$	34,975	285.9		not observed
9.		$^4A_{2g}(^4T_{1g}P)$	34,780	287.5		not observed
10.		$^4A_{1g}(^2E_gG)$	12,316	811.9		not observed
11.		$^2B_{1g}(^2E_gG)$	12,329	811.1		not observed
12.		$^2B_{2g}(^2T_{2g}G)$	18,685	535.2	532	small peak in valley
13.		$^2E_g(^2T_{2g}G)$	18,696	534.8	535	small peak in valley
14.		$^2E_g(^2T_{2g}G)$	18,704	534.6	535	small peak in valley
15.		$^2E_g(^2T_{1g}G)$	27,735	360.6		part of narrow peak
16.		$^2E_g(^2T_{1g}G)$	27,667	361.4		part of narrow peak
17.		$^2A_{2g}(^2T_{1g}G)$	28,885	346.3		part of narrow peak
18.		$^2A_{1g}(^2A_{1g}G)$	25,970	385.06		part of narrow peak
19.		$^2E_g(^2A_{1g}H)$	29,815	335.4	333	small peak

TABLE 32-continued

	Transition	Calculated cm^{-1}	Calculated mu	Observed mu	Peak Description
20.	$^4B_{1g}$ $^2E_g(^2B_{1g}H)$	30.013	333.2	330	small peak
21.	$^2E_g(^2T_{1g}H)$	33,052	302	309	small peak
22.	$^2E_g(^2T_{1g}H)$	32,939	303	310	small peak
23.	$^2A_{2g}(^2T_{1g}H)$	32,763	305	312	small peak
		$Cr(H_2O)_6Cl_3$			
1.	$^4A_{2g}$ $^4T_{2g}(F)$	17,807	561	557	medium symmetrical band
2.	$^4T_{1g}(F)$	25,278	395.6	390	tall symmetrical band
3.	$^4T_{1g}(P)$	39,526	253		not observed
4.	$^2E_g(G)$	13,707	729.5		not observed
5.	$^2T_{2g}(G)$	14,444	692.3		hidden under band 1 on lower energy side
6.	$^2T_{1g}(G)$	20,806	480.6	485	shoulder on 1
7.	$^2T_{1g}(H)$	31,900	313.5	314	low peak
8.	$^2T_{2g}(H)$	31,424	318.2	318	shoulder on 7
9.	$^2E_g(H)$	33,442	299.03		not observed

TABLE 33

SUMMARY OF FITTING PARAMETERS

Complex	Dq	B'	C/B	D_s	Dt	B'/B
$[Cr(H_2O)_4Cl_2]Cl$	1643	637	4.0	103	96	.69
$[Cr(H_2O)_6]Cl_3$	1780	760	3.58	0	0	.83

spin-forbidden transitions were obtained.

The spectrum for $[Cr(H_2O)_6]Cl_3$, Figure 37, showed three bands at 17,800 cm^{-1}, 25,300 cm^{-1} and 31,900 cm^{-1}. Assuming Oh symmetry with a $^4A_{2g}$ ground state, the first transition was assigned to the $^4A_{2g} \rightarrow {}^4T_{1g}(F)$, and the second transition to the $^4A_{2g} \rightarrow {}^4T_{2g}$. Dq was set at 1780 cm^{-1}, B was set at 740 cm^{-1}, C/B at 4.0, Ds and Dt at zero, and S.O. at 60 cm^{-1}. The program was allowed to determine the best fit for the spin allowed transitions. The spin forbidden transition at 31,900 cm^{-1} was assigned to the $^2T_{1g}(G)$. Again all parameters were fixed except C/B and the program iterated this assignment giving the best value for C/B and the spin forbidden transitions.

The collected spectral data is given in Table 32 and the fitting parameters obtained are given in Table 33.

Results and Conclusions

The dehydration of $[Cr(H_2O)_6]Cl_3$ indicated that $[Cr(H_2O)_4Cl_2]Cl$ was formed at the temperatures studied. The enthalpy of 7.92 kcal $mole^{-1}$ for the dehydration is definitely in agreement with that of $CoCl_2 \cdot 6H_2O$, $K_2CoCl_4 \cdot 2H_2O$ (20) and $KCoCl_3 \cdot 4H_2O$ where a change in structure occurs. The change in structure here being from an octahedron for $[Cr(H_2O)_6]Cl_3$ to a tetragonally distorted octahedron for the $[Cr(H_2O)_4Cl_2]Cl$. It also apprears that the substitution of a chloride ion for a water molecule involves about the same energy as shown in a previous study. (3) . The entropy for the dehydration reaction of 15.33 e.u. $mole^{-1}$ is also in agreement with the previous study for the chloride-water exchange. (2)

It was noted from this study that the dehvration of $[Cr(H_2O)_4]Cl$

and $[Cr(H_2O)_4Cl_2]Cl \cdot 2H_2O$ can serve as a model system for testing the theory that structure changes can be indicated by thermochemistry. The $[Cr(H_2O)_4Cl_2]Cl \cdot 2H_2O$ hydration isomer is known to have water hydrogen bonded in the outer sphere and should give enthalpy and entropy values equal to the ice-vapor reaction at 25°C. The $[Cr(H_2O)_6]Cl_3$ involves the chloride and water exchange with a structure change while the $[Cr(H_2O)_4Cl_2]Cl \cdot 2H_2O$ involves no change in structure.

The spectra of $[Cr(H_2O)_4Cl_2]Cl$ was found to fit a tetragonally distorted octahecron with "z" axis elongation. An observed Dq value of 1643 cm^{-1} is in agreement with the calculated value obtained using the average field rule.

$$Dq_{[Cr(H_2O)_4Cl_2]Cl} = 4/6Dq_{[Cr(H_2O)_6]Cl_3} + 2/6Dq_{CrCl_3}$$

Using the Dq value found for $[Cr(H_2O)_6]Cl_3$ and a Dq value of 1380 cm^{-1} for $CrCl_3$ (12), a calculated value of 1647 cm^{-1} is obtained for $[Cr(H_2O)_4Cl_2]Cl$.

The spectrum of $[Cr(H_2O)_6]Cl_3$ was found to fit a near perfect octahedral model. An observed Dq value of 1780 cm^{-1} is in agreement with the 1740 cm^{-1} (37) reported for $KCr(SO_4)_2 \cdot 12H_2O$ which has chromimum (III) ions octahedrally surrounded by water molecules.

REFERENCES

1. H. Joy, Computer Program for Diagonalization of Secular Determinant (unpublished), Oak Ridge National Laboratoires, 1966.

2. W. K. Grindstaff, Ph.D. Dissertation, University of Oklahoma, 1966.

3. W. K. Grindstaff and N. Fogel, J.C.S. Dalton, 1476 (1972).

4. W. Rudorff, J. Kandler, G. Lincke, and D. Babel, Angew, Chem. 71, 672 (1959).

5. H. J. Seifert, Z. Anorg. Allg. Chem. 307, 137 (1961).

6. A. Benrath, Z. Anorg. Allg. Chem., 163, 396 (1927).

7. A Benrath and G. Ritter, J. Prakt. Chem., 154, 2 (1939).

8. Kinshino Hirakawa, Kazuyaski Hirakawa and T. Hashimato, J. Phys. Soc. Japan, 15 2063 (1960).

9. H. Soling, Acta. Chem. Scand. 22 (1) 2793 (1968).

10. J. Ferguson, D. L. Wood, and K. Knox, J. Chem. Phys., 39, 881 (1963).

11. F. Gilmore, Nucl. Sci. Abstr., 24 (1) 1088 (1970).

12. K. Knox, Acta. Cryst. 14, 583 (1961).

13. A. Engberg and H. Soling, Acta. Chem. Scand., 21, 168 (1967).

14. N. Thorup and H. Soling, Acta. Chem. Scand., 23 (8) 2933 (1969).

15. G. Schnarzenback and H. Flascka, Complexometric Titrations, Methuen and Co., LTD. New Fetter Lane, London, 1969.

16. D. Skoog and D. West, Fundamentals of Analytical Chemistry 2nd ed., Holt Rinehart and Winston, New York, 1969.

17. L. C. Lewis and N. Fogel, J. Chem. Soc., A, 1141 (1970).

18. S. Shchukaru, J. Vasil'kova and G. Barrinok, Ser. Fiz. i. Khim., No. 3, 145 (1965); Chem Abstr., 64 770 (1966).

19. "Handbook of Chemistry and Physics," 51st ed. R. Weast Ed. Chemical Rubber Co., Cleveland, (1970).

20. W. Latimer, Oxidation Potential, 2nd ed., Prentice-Hall, Inc. Englewood Cliffs, N.J., 1952.

21. F. Daniels and R. Alberty, Physical Chemistry, 3rd ed., John Wiley and Sons Inc., New York, 1967.

22. H. Bethe, Ann. Physik, (5) 3, 133 (1929).

23. C. J. Ballhausen, Introduction to Ligand Field Theory, McGraw-Hill Book Co., Inc., New York, 1968.

24. G. Racah, Phys. Rev., 34, 1293 (1929).

25. B. N. Figgis, Introduction to Ligand Fields, John Wiley and Sons, Inc., New York, 1966.

26. K. W. H. Stevens, Prac. of Roy. Soc., 26, 96 (1952).

27. J. H. Van Vleck, Disscussions Faraday Soc., 26, 96 (1958).

28. F. A. Cotton, Chemical Applications of Group Theory, John Wiley, New York, 1966.

29. C. J. Ballhausen and A. D. Liehr, Mol. Phys., 2, 123 (1959).

30. A Abragam and M. H. L. Pyrce, Proc. Roy. Soc. A205, 135 (1951).

31. A. Abragram and M. H. L. Pyrce, Proc. Roy. Soc. A206, 173 (1951).

32. W. Low, Phys. Rev., 109, 256 (1968).

33. N. Fogel, Article Submitted for Publication, (1974).

34. R. L. Carlin in "Transition Metal Chemistry," Vol. I. R. L. Carlin Ed. Marcel Dekker Inc., N.Y. 1965, Chap. 1.

35. D. Sutton, Electronic Spectra of Transition Metal Complexes, McGraw-Hill, London, 1968.

36. S. Kiode, Phil. Mag. 4, 243 (1959).

37. H. L. Schlafer and G. Glieman, Ligand Field Theory, Wiley-Interscience, New York, 1969.

38. R. Drago, Physical Methods in Inorganic Chemistry, Van Nostrand-Reinhold Co., New York, 1965.

39. B. N. Figgis, Trans. Faraday Soc., 56, 1553 (1960).

40. F. E. Mabbs and D. J. Machin, Magnetism and Transition Metal Complexes, Chapman and Hall Ltd., London, 1973.

41. B. N. Figgis and R. S. Nyholm, J. Chem. Soc. 4190 (158).

42. W. Jolly, The Syntheis and Characterization of Inorganic Compounds, Prentice-Hall Inc., Englewood Cliffs, 1970.

43. H. Latinen, Chemical Analysis, McGraw-Hill Book Co., New York, 1960.

44. W. K. Grindstaff and N. Fogel, Thermochemia Acta., 6 299 (1973).

45. N. Fogel, C. C. Lin, C. Ford, and W. K. Grindstaff, Inorg. Chem. 3, 720 (1964).

46. J. Mizuno, J. Phys. Soc. Japan, 15 1412 (1960).

47. R. D. Willett, C. Dwiggins, R. F. Kruh and R. E. Rundle, J. Chem. Phys. 38, 2429 (1963).

48. B. N. Figgis, M. Gerlock and R. Mason, Proc. Roy. Soc. 249A, 210 (1964).

49. M. Textor, E. Dubler and H. R. Oswald, Inorg. Chem. 1361 (1974).

50. A. F. Wells, Structural Inorganic Chemistry, Clarendon Press, 3rd ed., New York (1962).

51. R. E. Cathers and W. W. Wandlandt, J. Inorg. Nucl. Chem 27 1015 (1965).

52. I. G. Dance and H. C. Freeman, Inorg. Chem., 4 1555 (1965).

53. K. R. Andress and C. Carpenter, Z. Krist, 87, 446 (1934).

54. F. H. Spedding and G. C. Nutting, J. Chem. Phys. 2 421 (1934).

55. F. H. Spedding and G. C. Nutting, Ibid 3 369 (1935).

56. P. J. Elving and B. Zemel, J. Amer. Chem. Soc. 79, 1281 (1957).

57. E. L. King, Sr., M. J. M. Woods, and H. J. S. Gates, J. Amer. Chem. Soc. 80, 5015 (1958).

58. C. K. Jorgensen, Structure and Bonding, Vol 1, 3 (1966).